D4.21: State-of-the-art and implementation of design tools for floating structures

Edited by: José Azcona

With the contribution of:
J. Azcona, D. Bekiropoulos, H. Bredmose, N. F. Heilskov, A. Krieger, T. Lutz, A. Manjock, D. Manolas, D. Matha, K. Meister, R. Pereira, J. Rønby, F. Sandner and S. Voutsinas

Agreement n.:	308974
Duration	November 2012 – October 2017
Co-ordinator:	Mr Peter Hjuler Jensen

Support by:

Document information

Document Name:	State-of-the-art and implementation of design tools for floating structures
Confidentiality Class:	PU
Deliverable Number:	D4.21
Edited By:	José Azcona Armendáriz (CENER)
Contributing Authors:	J. Azcona, D. Bekiropoulos, H. Bredmose, N. F. Heilskov, A. Krieger, T. Lutz, A. Manjock, D. Manolas, D. Matha, K. Meister, R. Pereira, J. Rønby, F. Sandner and S. Voutsinas
Review:	A. Martinez (CENER), T. Fischer (RAMBOLL)
Date:	30 December 2013
WP:	WP4: Offshore Foundations and Support Structures
Task:	Task 4.2: Verification and validation of design methods for floating structures

INNWIND.EU, D4.21, State-of-the-art and implementation of design tools for floating structures

INNWIND.EU, D4.21, State-of-the-art and implementation of design tools for floating structures

INNWIND.EU, D4.21, State-of-the-art and implementation of design tools for floating structures

1 INTRODUCTION

Wind energy has grown at a good rate over the last few years. Most of this increase in wind capacity corresponds to onshore wind energy. Nevertheless, in some countries, many of the available onshore wind sites are already occupied. The remaining locations with high wind resource have a great natural value and can not host a wind farm due to environmental reasons or to the unacceptable visual impact. Offshore wind energy allows to expand the potential of wind energy, since wind resources over the seas are immense. In addition, offshore winds are usually very constant and with very adequate average speeds for the energy production. Furthermore, as noise impact in offshore locations is not critical, the rotor tip speed ratio can be increased with respect to an onshore design, improving the efficiency of the turbine. For these reasons, offshore wind power is considered one of the most promising energy sources of the future, and currently is increasing its relevance as energy source.

The design of a wind turbine in an offshore location represents an important technical challenge, since the combination of different phenomena as hydrodynamic and aerodynamic loading, control actions, mooring system dynamics, etc. generates a totally different scenary of operating conditions. The development of analysis codes specific for this new conditions and the verification and validation against experimental data of these tools is one of the keys to achieve a reduction on the risks and the uncertainties in the design process, that will allow to optimize the designs, decrease the cost of the energy and also reduce the time-to-market.

The participants in the task 4.2 of the InnWind project are developing very different codes for the analysis of floating offshore wind turbines. Some of these tools are integrated codes for the analysis of the whole floating wind turbine system, and others are focused on the mooring lines dynamics, the rotor aerodynamics or the platform hydrodynamics. The partners plan to validate these codes against experimental data that are publicly available and also with data coming from the test campaign that will be carried out within the task.

This report documents the state of development of the partner's codes, describing the methodology and background theory that has been applied, the current capabilities and the possible applications of the tools. The future lines of development are also discussed. The results of the codes are presented and verified through comparison with other software and data available. This comparison is a preliminary check on the reliability of the codes before future activities on the task 4.2 where the tools will be validated against experimental data.

The coupling of the physical subsystems – aerodynamics, structural dynamics, hydrodynamics and mooring dynamics – is a challenge for computational modeling of floating wind turbines. Existing coupled simulation codes for onshore wind turbines representing the structure as modally reduced elastic bodies in a global multibody approach and aerodynamics with the blade-element momentum theory (BEM) are state of the art in industry. At this point, the methodologies of marine engineering need to come into play, coupling with the already mentioned representation of the plant portion above sea level. A common practice to model the hydrodynamic part in a coupled simulation of a floating wind turbine (FWT) is to apply linear hydrodynamics, which means solving the radiation and diffraction problem separately with potential flow and linear wave theory in frequency domain. The solution to these problems is then superposed and transformed into time domain as three force and torque components, respectively, acting on a reference point of the platform. Other approach to the hydrodynamics of slender bodies is the use of the Morison Equation. This method can be applied to capture the full hydrodynamic loading or to calculate only the viscous forces, complementing the calculation provided by the potential theory, that neglects this effect. Besides these common approaches various more detailed models exist. On the aerodynamics side CFD or free wake vortex model can be used. CFD methods can also be used on the hydrodynamics calculation.

INNWIND.EU, D4.21, State-of-the-art and implementation of design tools for floating structures

The chapters 2, 3, 4 and 5 presents the contribution of the University of Stuttgart to the deliverable. Their tools are presented in these chapters in an increasing level of analysis complexity. For the conceptual design of floating wind turbines, as illustrated in Figure 1.1, numerical models with an adapted level of detail are necessary. At each stage, marked by concentric lines, different questions have to be answered by the simulation tools.
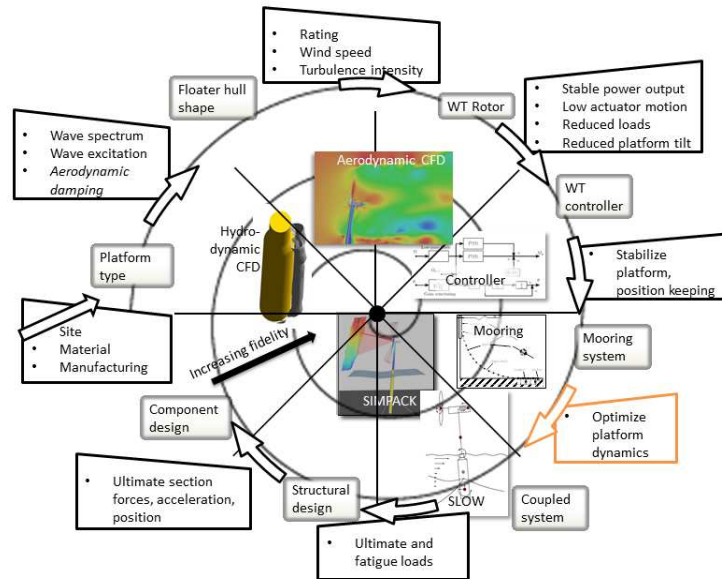
Figure 1.1 – Design spiral according to [1.1] with associated numerical tools.

The first method, described in chapter 2, is a simplified model that is suitable for considerably faster computations than the other coupled methods described above. This is very valuable during early conceptual design phases of a new FWT. The second method, described in chapter 3, applies linear hydrodynamic theory, as described above, but features a very flexible definition of the structural part of the wind turbine. It also includes an integrated dynamic mooring model. The third and fourth methods, on the other hand, are high-fidelity CFD methods, calculating the hydrodynamic and aerodynamic parts of a FWT with CFD and are described in chapters 4 and 5.

Chapter 6 describes the status of development and the capabilities of the *hydro_GAST* software, developed by NTUA for the integrated time domain simulations of wind turbines. The aerodynamics can be computed using Blade Element Momentum theory (BEM) or a free wake vortex model. The finite elements method (FEM) is applied to the structural dynamics and mooring lines and two different hydrodynamic models are implemented: linear potential theory and the Morison Equation.

In chapter 7, DHI's tool for the computation of the full nonlinear, viscous hydrodynamics coupled with large amplitude 6 degrees-of-freedom motion of a floating structure is presented. The tool is based in the CFD open source software OpenFOAM®. This software has been expanded to include movable meshes that allow capturing the non-linearities of the fluid-structure interaction in particular under rough sea states.

The development of a non-linear dynamic simulation code for the analysis of mooring lines is described in chapter 8. The code, developed by CENER is called OPASS (Offshore Platforms Anchoring System Simulator) and is based on finite elements. It considers the effect of inertia, hydrodynamic added mass, gravity, hydrostatics, water drag, axial elasticity, structural damping and cable-seabed interaction (contact and friction). The model implemented in the code is presented with detail together with the tool verification against other softwares.

In chapter 9, it is presented an extension of the aero-hydro-servo-elastic code Flex5 to fully nonlinear waves performed by DTU. A TLP (Tension Leg Platform) floating platform is modeled and a comparison of simulations with linear and non-linear waves is shown. In addition, the effect of aerodynamic damping is discussed.

Chapter 10 gives an overview of the codes used by the certification agency DNV GL. For the commercial development of floating wind energy certification will play a significant role. Load assumptions for offshore wind turbines are calculated at DNV GL with the fully integrated, elastic time domain simulation code GH_BLADED. The hydrodynamics of a floating structure and its anchoring systems are modelled at DNV GL with the code ANSYS AQWA. A description of the coupling approach between ANSYS AQWA and GH_BLADED and its validation is given. Furthermore the code SESAM, developed by DNV and widely used in the offshore industry, is presented with its features for simulating non-linear mooring systems.

The International Energy Agency (IEA) Wind Task 30 started in 2010 as a collaboration project of different companies, Universities and research institutes to investigate offshore wind turbine coupled simulations. This task was also known as OC4 (Offshore Code Comparison Collaboration Continuation) since it is a comparison between codes developed by the different participants. The second phase of the Task 30 was focused on the modelling and simulation of a floating platform and several of the participants in the InnWind Task 4.2 have also validated their code developments within this project. In chapter 11, we are present some of the results obtained within OC4 phase 2 by those InnWind partners that have participated, with the purpose of providing a more comprehensive view of the tools and the validation effort.

This report has been coordinated by José Azcona, with contributions from Frank Sandner, Denis Matha, Thorsten Lutz, Dimitrios Bekiropoulos and Konrad Meister (chapters 2, 3, 4 and 5), Spyros Voutsinas and Dimitris Manolas (chapter 6), Nicolai F. Heilskov and Johan Rønby (chapter 7), José Azcona (chapters 8, 11 and 12), Henrik Bredmose (chapter 9) and Ricardo Pereira, Antonia Krieger and Andreas Manjock (chapter 10).

1.1 References

[1.1] Evans, J., "Basic design concepts" Journal of the American Society of Naval Engineers, p. pp. 671–678, 1959.

2   REDUCED NONLINEAR MODEL FOR FLOATING WIND TURBINES (SLOW[1])

The simplified model of the floating wind turbine aims at a fast simulation of the overall nonlinear coupled dynamics. Such a fast computation allowing for numerous iterations at an early stage of development is not possible with state-of-the-art, commercially available software. Simulation outputs to focus on here are, e.g., the unconstrained 3D platform motion, rotor speed, blade pitch angle, tower top displacement and main internal forces. Load distributions or specific node deflections of certain bodies on the other hand are not sought to be covered by this model. The simplification also implies that higher frequency modes of the stiffer DOFs like the blades or generator shaft are not considered. From a numeric point of view focus is set on computational speed so that iterations, recursions, integrations, time-to-frequency domain conversions, excessive memory access, etc. is avoided wherever possible. In order to accomplish these goals the structure is modeled as a coupled multibody system of rigid bodies with only nine DOFs. The equations of motion (EQM) of the 3D model are set up by applying the Newton-Euler formalism. As a result the mathematical model is available in state-space formulation as a system of symbolic ordinary differential equations (ODE) which can be directly compiled, yielding a high computational efficiency. Aerodynamics as well as the mooring line model is based on an interpolation of look-up data that is gained in a pre-processing step. Aerodynamic coefficients allow the calculation of rotor torque and thrust with a scalar rotor-effective wind speed as input. Quasi-static fairlead forces from the mooring lines as a function of horizontal and vertical displacements are stored offline and interpolated during runtime. Hydrodynamic forces are computed by the reduced model through a potential flow approach. Morison's equation is the basis for the herein presented development of a wave load estimation which requires only the current wave height as input. Eventually, kinetics of wave-structure interaction can be calculated without a numerical integration over depth due to the applied deepwater approximation for linear waves. The next subsections will first introduce the set-up of the EQM of the structure and then addressing the aero- and hydrodynamic subsystems.

2.1   Wind turbine structural model

Figure 2.1 shows a sketch of the exemplary mechanical model of the OC3-Hywind FOWT, as defined in [2.2]. A setting with four rigid bodies and nine DOFs has been selected for the reduced model. The EQM are set up from a physical perspective following the Newton-Euler formalism. The thereby involved operations of matrix algebra are calculated with symbolic programming so that the EQM are finally available as ODEs in a symbolic formulation. The resulting code can then be compiled and thus allows for high flexibility since it can be simulated by standard integration schemes. The nonlinear EQM can be transformed into state space domain which means that it is solved for the first derivative of the state vector

$\mathbf{\dot{x}}$, which consists of the vector of the degrees of freedom $\mathbf{q}$ and its derivative $\mathbf{\dot{q}}$
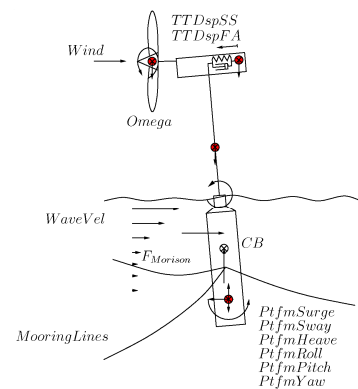
Figure 2.1: Sketch of reduced nonlinear model.

---

[1] Stuttgart Low Order Wind turbine

INNWIND.EU, D4.21, State-of-the-art and implementation of design tools for floating structures

$$x^{\cdot} = [\blacksquare(q^{\cdot} @ q^{-})] = [\blacksquare(q^{\cdot} @ M^{\intercal}(-1) \; (p(q, (q))^{\cdot} - k(q, (q,)^{\cdot} \; q^{\cdot}))]. \tag{2.1}$$

On the right hand side remains the generalized mass matrix M, the generalized vector of Coriolis, centrifugal, and gyroscopic forces p and the generalized vector of the applied forces k. A more detailed description of the structural model can be found in [2.7].

2.2   Aerodynamic Model

For this fast model BEM theory as industry standard which requires an iteration to find the induction factors, is avoided. The chosen procedure is to simulate a BEM model for various tip-speed ratios λ and blade pitch angles Θ until a steady state is reached as a pre-processing step. With the resulting two-dimensional look-up table for the thrust and torque coefficients c_T and c_P only the rotor effective wind speed is necessary to calculate the thrust force F_{aero} and torque M_{aero} on the rotor. In order to compute this representative wind speed at hub height first, a weighted average of the three-dimensional turbulent wind field on the whole rotor plane is needed, given by v_0. Second, a transformation of this estimation into the rotor coordinate system is necessary, so that the relative horizontal wind speed is computed. Finally, the relative rotor effective wind speed takes the form

$$v_{rel} = \dot{r}_{rotor,x} - v_0. \tag{2.2}$$

This is the scalar disturbance necessary to calculate the thrust force

$$F_{aero} = \frac{1}{2}\rho\pi R^2 c_T(\lambda, \Theta) v_{rel}^2 \tag{2.3}$$

and the external aerodynamic torque acting on the rotor body

$$M_{aero} = \frac{1}{2}\rho\pi R^3 \frac{c_P(\lambda, \Theta)}{\lambda} v_{rel}^2 \tag{2.4}$$

with air density ρ and rotor radius R. The described method has already been tested and successfully implemented for nonlinear model predictive control (NMPC) in [2.8].

2.3   Hydrodynamic model

For this simplified model no complex computations shall be required for pre-processing as is the case for the previously described linear hydrodynamics theory. Therefore, the implementation of Morison's formula has specific advantages: First, it is formulated in time-domain which is especially useful for real-time applications. Second, it is independent from multi-dimensional geometry-dependent input parameters and, lastly, there is a valuable means of simplification with the deepwater approximation as explained later in this section. Morison force in both horizontal directions results from an integration of velocity- and acceleration-dependent terms over depth z with water density ρ and cross-sectional area A_x as

$$F_{mor,i} = \rho A_x \int_0^{z_1} [(1 + C_A) a_{f,i}(t,z) + C_A \, a_{b,i} + \\ C_D (u_{f,i}(t,z) + u_{b,i}) | u_f - u_b | dz. \tag{2.5}$$

The coefficient of the added mass term is C_A and the damping coefficient is C_D. Velocities u_i and accelerations a_i have an index f if they refer to fluid particles and an index b if they refer to body velocities. This dependency on structure accelerations yields the implicit formulation of eqn. (2.1). The functions that describe fluid particle kinematics over depth derived from potential flow theory in both

INNWIND.EU, D4.21, State-of-the-art and implementation of design tools for floating structures

horizontal directions are hyperbolic. For the velocity potential Φ of the fluid over depth in x -direction remains with the free-surface elevation η and gravity constant g for draft length h

$$\Phi(z,\eta,\omega) = \frac{g}{\omega}\frac{\cosh[k(z+h)]}{\cosh(kh)}\eta.$$ (2.6)

This function depends on the wave angular frequency ω and the wavenumber k that is itself related to the wave frequency through the implicit dispersion relationship, see [2.6].

The frequency-dependency of the model is a challenge regarding a real-time implementation, since the wave frequency is not easily measurable. Another issue of eqn. (2.6) is that it cannot be integrated analytically over the water depth z and requires a numerical loop that would significantly slow down the code. In order to solve these issues the velocity potential Φ is rewritten using deepwater approximation so that the potential

$$\Phi^{dw}(z,\eta,\omega) = \frac{g}{\omega}e^{kz}\eta$$ (2.7)

remains according to [2.6] as a simple exponential function. This simplifies eqn. (2.5) considerably if its last term, the vectorial contribution is neglected. That term is a correction to Morison's original formula for differing spatial directions between fluid and structure motion. With the fluid kinematics described as exponentials rather than hyperbolic functions it is possible to integrate eqn. (2.5) over depth z analytically rather than through a numeric loop and therefore save computational time. If the wave angular frequency ω is additionally available further useful reduction of the wave disturbance model is achieved. This information might come from sensor measurements or an estimation, for example as the peak angular frequency ω_p of the wave spectrum. Thus, the fluid kinematics as input to Morison's equation (2.6) are no longer necessary but only the free-surface elevation η , which is easily measurable. Consequently, a method is presented to compute wave loads on the spar-buoy in real-time using deepwater approximation to the linear potential flow theory estimating a peak spectral wave frequency. For the external force from aerodynamics a similarly simple model with measurable inputs has been developed as given in the following.

2.3.1   Mooring line model

The floating platform is moored by three catenary lines that are anchored on the seabed. The differential equation for a stationary line is solved analytically. According to [2.3] the resulting nonlinear system of equations for the horizontal displacement x_F and the vertical displacement z_F of the fairleads with the corresponding horizontal force H_F and the vertical force V_F has the form

$$\begin{aligned} x_F &= f(H_F, V_F) \\ z_F &= f(H_F, V_F). \end{aligned}$$ (2.8)

Applying a numerical solver the forces on the fairleads can be obtained for various displacements x_F and z_F. Eventually, a function interpolates this data and returns the external forces on the platform body during runtime.

2.4   Verification

In order to estimate the validity of the model various simulations have been performed with the certified **FAST** code [2.4] and the reduced model. FAST is an aero-hydro-servo-elastic code with a modal reduction of the structure up to the 2nd modes and a total of 22 DOFs. The hydrodynamic model uses

linear potential flow theory with the radiation and diffraction solution and aerodynamics based on BEM theory. First evaluations from a free-decay test with constant wind from an upright platform position have returned good results in terms of frequency, ratio of decay and steady states.

Figure 2.2 shows the power spectral density function (PSD) of moment M_{yT} for the two models. The waves are irregular with Hs=6m and Tp=10s. The wind is turbulent (class 1a), with an average speed of 20m/s. The first peaks of the PSD, being the platform pitch eigenfrequency, the peak spectral wave frequency and the first tower eigenfrequency, coincide. Higher frequencies are not represented by the reduced model. The reliability and fidelity of the model for conceptual design purposes has been evaluated within a statistical study with FAST as reference for various IEC load cases, see [2.5].
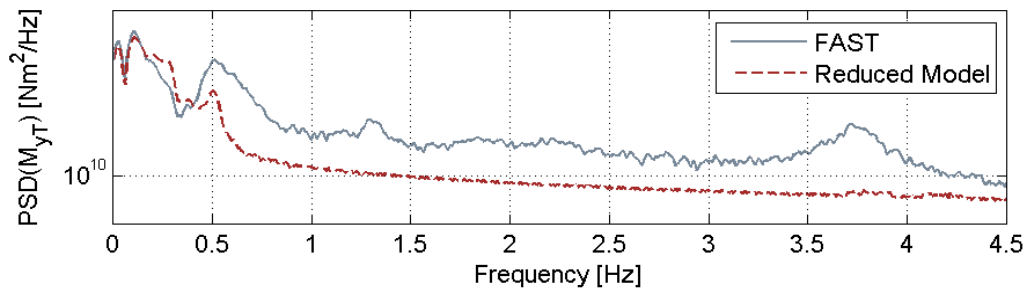
Figure 2.2: PSD of tower base moment; FAST vs. reduced model

Although higher frequencies are not represented in the reduced model, ultimate loads as well as the motion response of the tower top and the platform agrees quite well. In order to assess the fidelity of the simplified model and its range of applicability a comparison against FAST [2.5] with the OC3-Hywind model, see [2.7], has been performed. Figure 2.3 shows the tower base bending moment over wind speed bins with mean, extremes and standard deviation. It can be seen that the mean value coincides with the reference model for most wind speeds with slight deviations around rated wind speed and close to shut down. Also standard deviations and extreme values are comparable with a better correlation in the full load regime than in the partial load regime.

INNWIND.EU, D4.21, State-of-the-art and implementation of design tools for floating structures
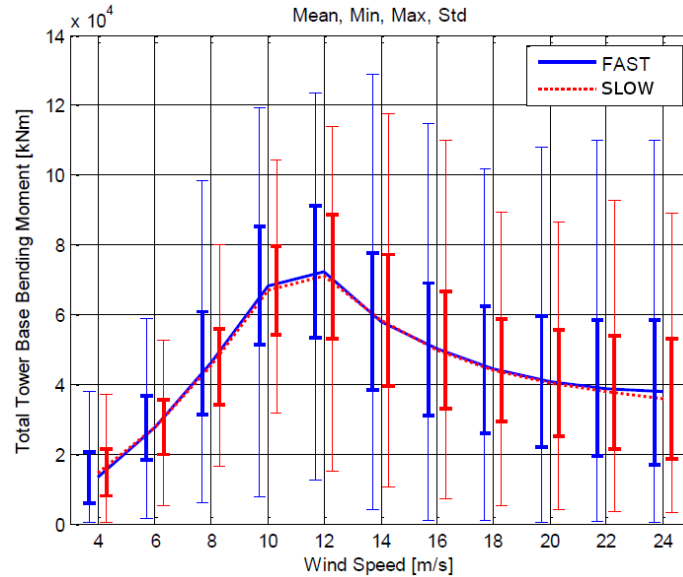
Figure 2.3 – Extreme load of total tower base bending moment over wind speed bins, [2.5].

Figure 2.4 provides an overview of the relative differences between the FAST model and the reduced model for selected extreme loads and displacements from production load cases 1.x. The bars show relative differences of generator power (GenPwr), generator torque (GenTq), tower top fore-aft and side-to-side displacement (TTDspFA-SS), floating platform surge and pitch (PtfmSurge-Pitch), and the tower base bending moments in fore-aft and side-to side direction, as well as the global moment (TwrBsMxt10, TwrBsMyt10, TwrBsMMxy1). The ratios all show values above zero, indicating that the FAST model predicts higher extreme loads. Most of the extreme loads occur for DLC1.6a, which is similarly predicted by both models. With the exception of platform surge and tower side to side displacement, the results are within 5% - 7%, which represents a good agreement given the differences between the models and the large amount of stochastic simulations (1362 single DLC 1.x runs) this comparison is based on. Even for loads and displacements in side-to-side direction, the results are close.
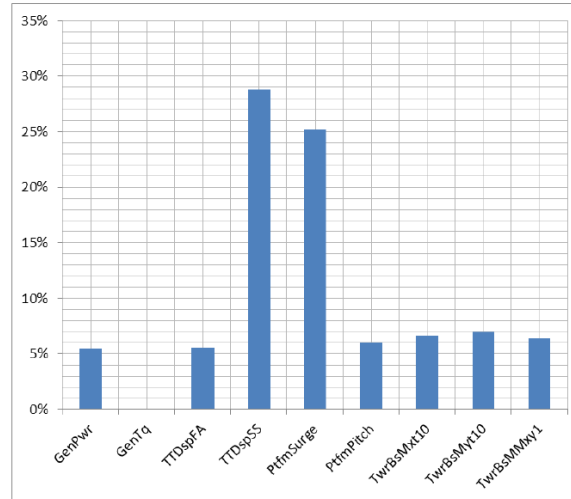
Figure 2.4 – Production load cases extreme value differences ([FAST-RM]/[FAST]) [2.5].

2.5   Application for Optimization

The tool has been applied for an optimization of a floating offshore wind turbine for load and cost reduction, see [2.1]. Besides various structural dimensions, including the floater hull shape the control system is considered within the integrated model. For the optimization task the floating wind turbine "OC3 spar-buoy", see [2.7] has been used. First the reduced model described in this chapter was applied inside the optimisation loop. Afterwards a model with a higher fidelity was used to further optimize the solution gained from the previous optimization run. The second model is the one described in chapter 3. With the aim of reducing cost and loads by reducing weight and section forces, several optimization problems are developed. These problems contain a target function, design variables and inequality constraints. They are solved by the local non-linear optimization method Sequential Quadratic Programming (SQP). In the process of this study it is shown that the definition of the target function and the constraints play a crucial role in the quality of the optimization results. The results show a great potential for structural and geometric optimization of the chosen floating wind turbine "OC3 spar-buoy".

2.6   Conclusions

The described tool is a standalone numerical model of a spar-mounted FOWT that reliably reproduces the overall nonlinear behavior of the system. A real-time factor of about 100 is achieved by simplifying physical models and avoiding numerical loops. Steady states, resonance frequencies up to the first tower mode and a statistical analysis of IEC load cases confirm the validity of the model. Thus, it is suitable for fast computations of the integrated system of a floating wind turbine for preliminary estimates of the system dynamics. This is necessary for conceptual design on one hand but also for controller design or model based control on the other hand.

This kind of simplification still keeping the physics of the interconnected subsystems has not been available so far. It is important to state, however, that there are various simplifications in each subsystem, which means that the application of the code must be limited to early assessments of a

INNWIND.EU, D4.21, State-of-the-art and implementation of design tools for floating structures

new development. The InnWind wave tank tests will make it possible to assess the validity of the applied simplifications. The flexibility of the tool and the availability of the code will allow for a simple adaptation of the model to compare it to the wave tank setting. It is the first time, such a validation with experimental data is possible.

2.7 Future work

Current and future work on the code addresses the aerodynamic and the hydrodynamic module. For the development of an individual blade-pitch controller (IPC) a simplified model for sheared and yawed inflow is being set up. On the hydrodynamics side an adaptation of Morison's Equation for various cylinders or "pontoons" as in the case of semi-submersibles and non-slender cylinders is being investigated. This will help to validate the tool with the InnWind wave tank test results.

For the analysis of the results of the wave tank test the reduced model allows to customize geometric parameters as well as specific external loads. This is especially useful when performing a parametric study in order to find the causes for deviations between measurements and simulations. Model imperfections, like, e.g., a slightly unbalanced rotor, differing moments of inertia or center of gravity can be easily modelled by the reduced model.

2.8 References

[2.1] Härer, A., Matha, D., Kucher D. and Sandner, F., *"Optimization of offshore wind turbine components in multi-body simulations for cost and load reduction"* In: Proceedings of the EWEA Offshore 2013, Frankfurt.

[2.2] Jonkman, J., *"Definition of the Floating System for Phase IV of OC3"* NREL, 2010.

[2.3] Jonkman, J., *"Dynamics Modeling and Loads Analysis of an Offshore Floating Wind Turbine"*, NREL, 2007.

[2.4] Jonkman J. and Buhl, M. *"Fast User's Guide"* NREL, 2005.

[2.5] Matha, D., Sandner F. and Schlipf, D., *"Efficient Critical Design Load Case Identification for Floating Offshore Wind Turbines with a Reduced Nonlinear Model"* The Science of Making Torque from Wind, 2012.

[2.6] McCormick, M. E., *Ocean Engineering Mechanics*, Oxford University Press, 2010.

[2.7] Sandner, F., Schlipf, D., Matha, D., Seifried R. and Cheng, P. W., *"Reduced Nonlinear Model of a Spar-Mounted Floating Wind Turbine"* In: DEWEK, Bremen, Germany, 2012.

[2.8] Schlipf, D., Sandner, F., Raach, S., Hocke, V., Matha D. and Cheng, P. W. *"Nonlinear Model Predictive Control of Floating Wind Turbines"* 2013.

INNWIND.EU, D4.21, State-of-the-art and implementation of design tools for floating structures

3 COUPLED FLEXIBLE MULTIBODY MODEL FOR FLOATING WIND TURBINES (SIMPACK)

SIMPACK is a commercially available general-purpose MBS code developed by SIMPACK AG. The code is used by the automotive, railway, aerospace, and robotics industries and allows integrated wind turbine simulation. SIMPACK functionality can be easily extended by user specific routines and scripts as performed by USTUTT by implementation of aerodynamics, hydrodynamics and load calculations modules allowing the simulation of FOWT. Figure 3.1 present a typical FOWT topology with different levels of detail for flexible bodies. Scripts defined by USTUTT, as well as a SIMPACK user interface (based on open SIMPACK scripts) for configuring, running and analyzing DLC simulation exist to enable efficient load case calculation and post-processing, for which either SIMPACK's internal post-processor is used or an interface to the NREL post-processing suite can be utilized.
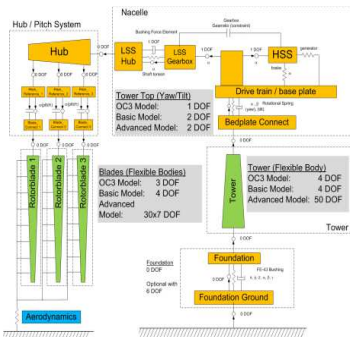
Figure 3.1: SIMPACK WT model topology
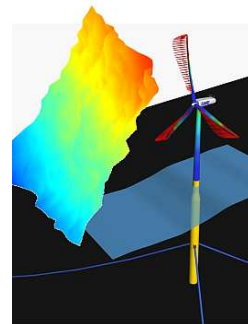
Figure 3.2: SIMPACK FOWT model

3.1 Short introduction

The SIMPACK code uses a multi-body system dynamics (MBS) representation with variable maximum number of degrees of freedom. Flexible bodies are integrated by a modal formulation with variable number of DOFs. Aerodynamics can be modeled in quasi-steady blade-element/momentum (BEM) theory, generalized dynamic inflow model with correction models, potential flow free wake free vortex lifting line theory or CFD. Wind inflow is either uniform or turbulent. Hydrodynamic forces are calculated with linear hydrodynamic theory and the mooring lines are modeled in a quasi-static manner or dynamically with MBS.

3.2 Structural dynamics

SIMPACK uses a flexible MBS formulation. The parts or bodies of the wind turbine structure are connected using complex joints with different types of force elements acting from the inertial system on the bodies (e.g., aerodynamics on the rotor, hydrodynamics on the support structure) and between bodies (e.g., spring-damper elements). The SIMPACK code is able to include flexible FEM bodies either with a built in FE beam module or from external FE codes for non-beam-like structures. With the built-in FE module, a blade model consisting of Euler-Bernoulli or Timoshenko beam elements in modal formulation is used, which is capable of considering bending in flap- and edgewise direction, torsional and tensional rigidity, and the relevant coupling effects. The relevant geometric stiffening effects are included representing a nonlinear model for medium displacements. The blade model also can be split into separate flexible bodies that are connected with zero DOF, representing a nonlinear blade model for large displacements. The validation for the nonlinear behavior was performed by a comparison with

the FEM code Abaqus. The flexible tower is modeled with the same approach. Single- and multi-torsional drivetrain models can be implemented and accounting for the flexibility of the bedplate and other components is possible. Drivetrain models for specific analysis, mainly for frequency domain analysis, also can include models for tooth contacts. The blades' and tower's eigenmodes usually are resolved up to 20Hz. The so-called split blade approach, which is fully geometric non-linear, is computationally much more demanding and only used for specific load cases where very accurate prediction of deflection and torsion is required. Figure 3.3 shows a comparison of blade deflections with the regular and advanced split SIMPACK structural blade model to FEM Abaqus linear and non-linear results, validating the accuracy of the advanced blade model in SIMPACK. Figure 3.4 in addition presents a comparison to OC3 results of 2nd tower and blade eigenfrequencies with basic and advanced SIMPACK structural representations. The influence of the full geometric nonlinear blade representation is clearly identifiable. This is particularly important for accurate predictions of e.g. blade tip deflections. Overall SIMPACK offers an arbitrary level of detail of the structure and thus has the advantage of being adaptable to any specific problem one is interested in analyzing. Models with a similar simulation depth as traditional codes such as NREL's FAST are possible, as well as much more detailed models for e.g. reliable blade tip deflection predictions or drive train resonance analysis.
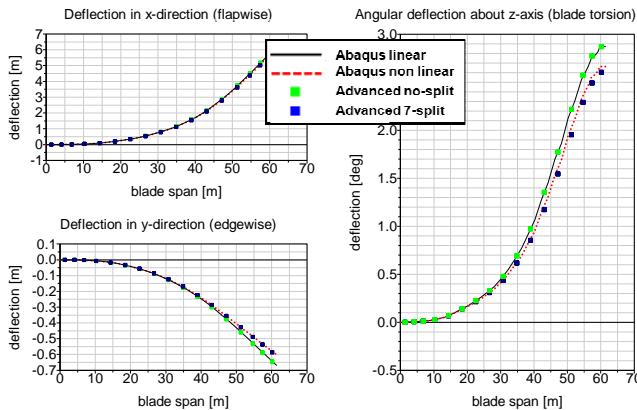
Figure 3.3 - Comparison of blade deflections with simple and advanced SIMPACK structural blade model to FEM Abaqus.
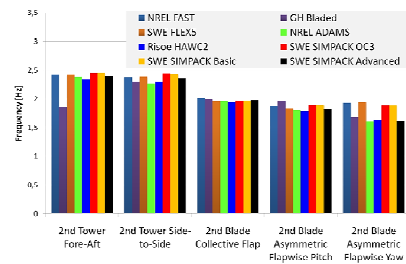
Figure 3.4 - Flexible tower and blade eigenmodes comparsion.

3.3 Aerodynamics

In SIMPACK a wide range of aerodynamic models is available. BEM can be used by application of NREL's *AeroDyn* (v12.58 as implemented by USTUTT and *AeroDyn* v13 as standard interface), as described above. In addition the Aeromodule, a BEM and lifting line free wake free vortex code AWSM developed by ECN, is coupled to SIMPACK. Finally, the CFD code FLOWer also is coupled to SIMPACK. While the two BEM options are equivalent or identical to FAST's AeroDyn, AWSM offers a physical model which intrinsically covers more effects than BEM; the same is true for CFD, which is even closer to representing the real physics at the rotor. Figure 3.5 shows a wake visualization during a floating platform pitch motion with ECN's AWSM code coupled to SIMPACK, where the significant influence of floating motion on wake development is clearly identifiable. SIMPACK has also implemented a FSI coupling with the CFD URANS code FLOWer, described in chapter 4. The coupling implemented currently is a staggered algorithm (often called loose coupling) with implicit time integration by the CFD solver and an explicit time integration scheme of the structure by SIMPACK. Further information is available e.g. in [3.2].
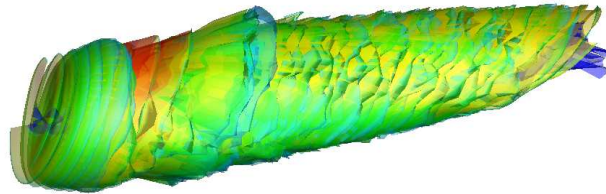
Figure 3.5 - Wake velocity visualization during a floating platform pitch motion with ECN's AWSM code coupled to SIMPACK.

3.4 Hydrodynamics and mooring line dynamics

Hydrodynamics in SIMPACK can either be modeled by a simple Morison force or by linear hydrodynamics. Here NREL's HydroDyn is interfaced where wave kinematics for irregular sea states are calculated using Airy wave theory. The hydrodynamic loading includes contributions from linear hydrostatic restoring, nonlinear viscous drag contributions from Morison's equation, added mass and damping contributions from linear wave radiation (including free-surface memory effects), and incident wave excitation from linear diffraction. The linearized radiation and diffraction problems are solved in the frequency domain for a platform of arbitrary shape using three-dimensional panel-based programs for computing wave loads and motions of offshore structures. AQWA and WAMIT are the most common commercial software packages used for the calculation of the hydrodynamic coefficients which can then be used in HydroDyn.

SIMPACK can model mooring lines two ways. One method is to solve the mooring-line tensions quasi-statically in a separate module and interface with the main code at each time step. Here the same formulation as implemented in *HydroDyn* is used. The other way is to use an integrated dynamic nonlinear MBS mooring line model, in which each line is discretized into separate rigid or flexible bodies connected by spring-damper elements. The hydrodynamic forces on each line element are calculated using the Morison equation in its relative formulation.

Figure 3.6 and Figure 3.7 show the topology and principle of the MBS dynamic mooring line model. For fast load case simulations usually HydroDyn and the quasi-static mooring line model are used.
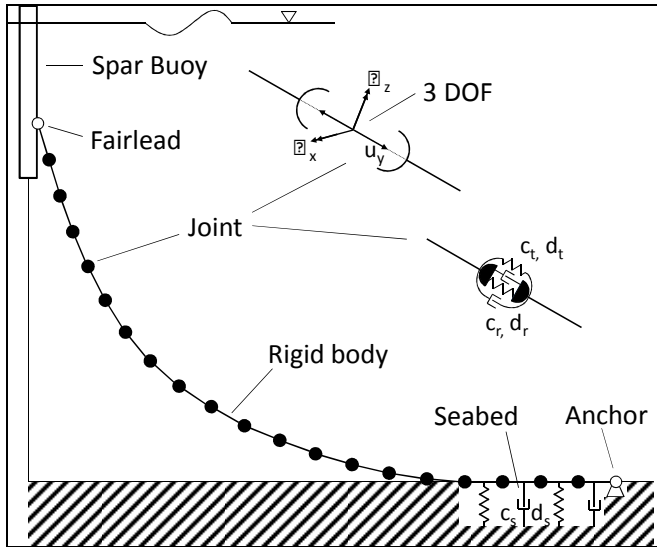
Figure 3.6 - Schematic diagram of the MBS mooring line model.
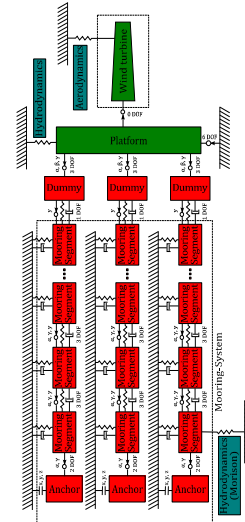
Figure 3.7 - MBS mooring line topology.

3.5   Validation and future work

SIMPACK was validated during the OC3 project [3.1] and is used within the OC4 project phase 2 during the writing of this report. Though in Chapter 11 an overview of the validation of the different tools described in this document is provided, by comparison of their results, we will show here some particular results relating our multibody tool for the simulation of floating wind turbines that we feel of special interest. Figure 3.8 shows the estimated RAOs of the platform pitch angle about the horizontal axis perpendicular to the wind speed for the OC4-semi submersible, see [3.4]. These "effective RAOs" are generated by introducing a white noise wave spectrum and a transformation of the results into frequency domain. The results shown here are extracted from the collected results of the OC4 study, see also [3.3]. Figure 3.9 shows the magnitude of the tower base bending moment as response to the same white noise wave excitation. Looking at the platform pitch response it can be seen that the SIMPACK code (marked in bold red as "SWE") performs comparably to other codes that use linear hydrodynamics theory augmented with viscous drag forces from Morison Equation. SIMPACK does not include second order hydrodynamics or nonlinear waves. The mooring lines are modelled in a quasi-static manner which is common for most industry-standard tools. Figure 3.10 and Figure 3.11 show the magnitude of the eigenfrequencies of the floater degrees of freedom as well as selected structural degrees of freedom. It can be seen that the first shows, again, comparable results to other linear hydrodynamics codes. The structural dynamics model in SIMPACK consists of modally reduced bodies up to the second order. Differences in Figure 3.11 might also come from the different aerodynamic models which can introduce fluctuating loads at frequencies where others don't. SIMPACK uses the aerodynamic module AeroDyn as does FAST. This explains the aligned results.

INNWIND.EU, D4.21, State-of-the-art and implementation of design tools for floating structures
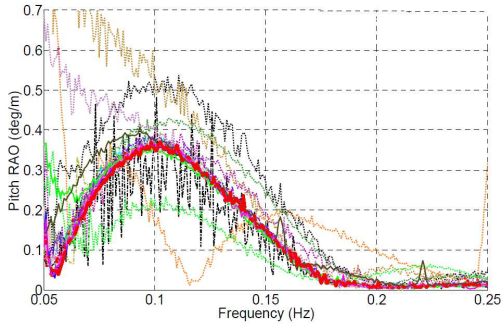
Figure 3.8 – Pitch RAO estimation, no wind. Time-series generated "effective RAOs" [3.3].
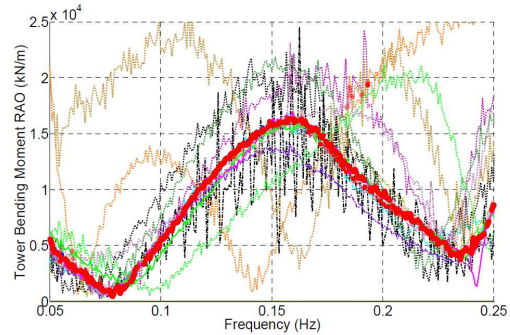
Figure 3.9 - Tower base bending moment RAO estimation, no wind. "Effective RAOs" [3.3].
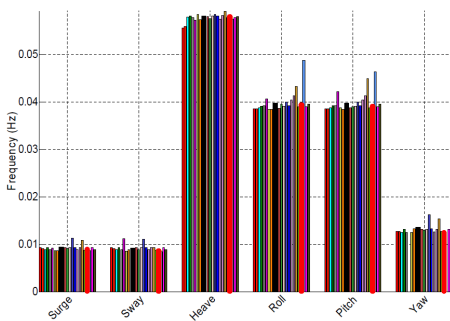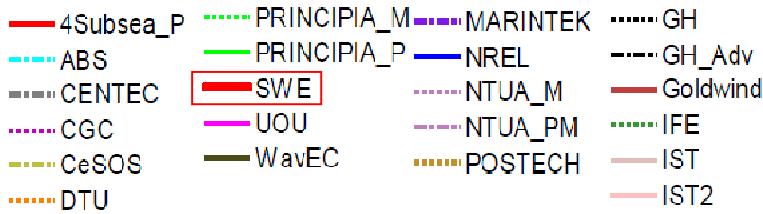
Figure 3.10 – Eigenfrequencies in the degrees of freedom of the floating platform [3.3].
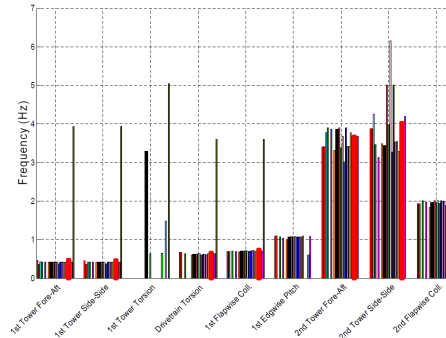
Figure 3.11 – Eigenfrequencies of selected structural degrees of freedom [3.3].

A recently finished validation exercise for the dynamic mooring system was performed using OC4 load cases and selected forced oscillation cases. Figure 3.12 shows the OC4 setup with the dynamic mooring line model and Figure 3.13 provides fairlead tension results from a forced sinusoidal oscillation of the OC3 platform about its equilibrium position. The significant difference of tension predictions of a quasi-static and a dynamic mooring line model, which shows an oscillation of tension depending on the forced motion direction and history, can be clearly identified. The advantage of this dynamic mooring line model implemented in SIMPACK is that the MBS formulation of the mooring lines are directly part of the DAE system of equations of motion of the wind turbine system, therefore avoiding any coupling issues. The results (not shown here for brevity) of the dynamic mooring model are also in good agreement with other dynamic mooring line codes used in OC4.

INNWIND.EU, D4.21, State-of-the-art and implementation of design tools for floating structures

Figure 3.12: SIMPACK OC4 model with dynamic mooring lines
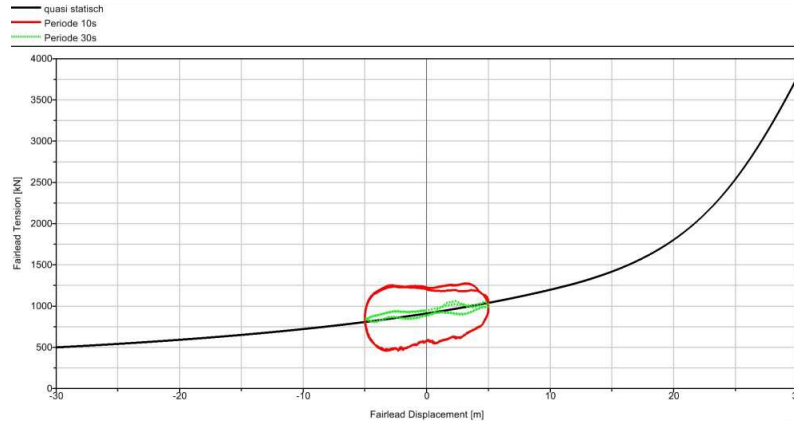
Figure 3.13: Dynamic mooring fairlead tension hysteresis curve during forced oscillation with the dynamic SIMPACK MBS mooring system model

Current developments include:

- Mixing of Morison and linear Hydrodynamic forces to be applied to the floating platform, also allowing for floating platform flexibility
- Full linearization capabilities of aerodynamics and hydrodynamics (e.g. including whirling modes, aerodynamic/hydrodynamic damping etc.)
- Coupling to CFD hydrodynamic code for distributed hydrodynamic force computation on the platform surface and comparison with simpler models

3.6 References

[3.1] Jonkman J. and Musial, W., *"Offshore Code Comparison Collaboration (OC3) for IEA Task 23 Offshore Wind Technology and Development"* NREL, 2010.

[3.2] Matha, D., Lutz, t., Wendt, F., Werner M. and Cheng, P. W., *"Aerodynamic Inflow Conditions on Floating Offshore Wind Turbine Blades for Airfoil Design Purposes"* ISOPE, 2012.

[3.3] Robertson, A., Jonkman, J., Musial, W., Vorpahl F. and Popko, W., *"Offshore Code Comparison Collaboration, Continuation: Phase II Results of a Floating Semisubmersible Wind System"* In: Proceedings of the EWEA Offshore 2013, Frankfurt.

[3.4] Robertson, A., Jonkman, J., Song, M. M. H., Goupee, A., Coulling A. and Luan, C., *"Definition of the Semisubmersible Floating System for Phase II of OC4"* NREL, 2013.

INNWIND.EU, D4.21, State-of-the-art and implementation of design tools for floating structures

4 COUPLED CFD MODEL FOR HYDRODYAMIC ANALYSIS OF FLOATING WIND TURBINES (CFX)

Flow-induced hydrodynamic loads are simulated at USTUTT-SWE with the commercially available CFD code ANSYS CFX [4.3]. It uses the Finite-Volume Method to solve the Reynolds-Averaged Navier-Stokes (RANS) equations on structured and unstructured grids and is coupled to the MBS tool SIMPACK. The interface between the liquid (water) and gas (air) represents a free surface that is modeled via the Volume of Fluid (VOF) approach. It computes the shape and location of the free surface on the basis of a fractional volume function [4.1].

The coupling between CFX and SIMPACK has been developed by [4.2] for the simulation of fluid-structure-interaction on tidal current turbines. Arnold demonstrates the validity of the coupling based on a code-to-code comparison of the simulation of a bisymmetric rotor blade of a tidal current turbine. Besides the incorporation of higher-order effects and the consideration of steep and breaking waves on offshore structures the proposed approach inherently provides a detailed pressure and loads distribution on the hull of the floating platform. Computation of the pressure field using common linear or non-linear hydrodynamics modeling techniques is complicated. Especially complex floater geometries for example with several columns and pontoons, can be analyzed with the presented technique to a higher level of detail and thus benefit the design process.

4.1 Structure of the MBS-CFD Coupling

Several aspects motivate the application of the coupling between CFX and SIMPACK. First of all, CFX is only able to implement rigid bodies in a standalone simulation. Applying a Fluid-Structure-Interaction (FSI) using FEM and CFD for complex structures requires unreasonable high computational resources. However, the dynamics of modally reduced flexible FEM bodies of the floating platform should be investigated in future analyses based on this research. The flexible bodies can be implemented within the MBS simulation environment. Secondly, the complexity of the rigid body in CFX is limited and only simple elements using spring-damper properties are possible. Thirdly and most important, an integrated aero-servo-hydro-elastic analysis of a floating offshore wind turbines cannot be performed in CFX standalone. The coupling to the MBS tool, however, enables the consideration of the mooring system, aerodynamic forces on the rotor and tower, the effect of the control system etc.

The coupling is controlled by means of a moderator script that on the one hand directs CFX to send loads/receive motion information to/from SIMPACK and on the other hand commands SIMPACK to send motion/receive loads information to/from CFX (see Figure 4.1). A fully implicit iteration scheme is incorporated within the coupling for transient simulations.

Within SIMPACK, a user force element written in Fortran is implemented. This interface is named CFX2SPCK and used to read and transform loads and to measure and send deformations during a coupled simulation.
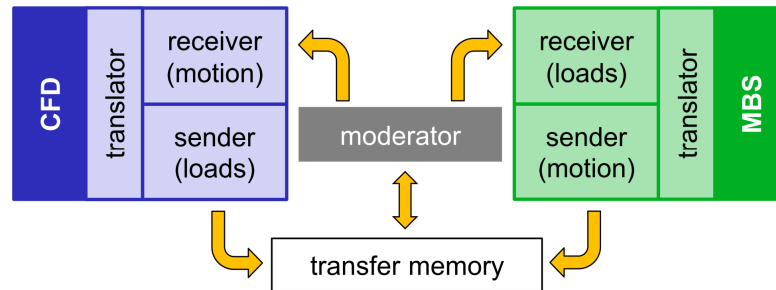
Figure 4.1 – Methodology and structure of the MBS-CFD coupling

4.2 Verification

The wind turbine is mounted to the conceptual floating platform OC3-Hywind spar-buoy for Phase IV of the IEA Annex 23 Offshore Code Comparison Collaboration (OC3) project [4.4]. A simple free-decay test in platform surge in still water without wind that is derived from load case specification 1.4 in the OC3 project Phase IV [4.5] has been chosen. All translational (surge, sway) and rotational (roll, pitch, yaw) platform DOFs are enabled except for the heave motion due to numerical instabilities during the first iterations of the coupled simulation. The instabilities have already been resolved at a later stage.

Excitation of platform surge and pitch motion is predominant in this load case and results are shown in Figure 4.2. Solid lines (black) refer to the coupled simulation (MBS+CFD), dashed lines (blue, green, red) to MBS standalone interfaced with HydroDyn (MBS+HydroDyn) and dash-dot lines (cyan) to NREL's wind turbine design tool FAST. The latter is used to simulate the fully integrated model of the OC3-Hywind spar-buoy according to the specifications.

The mesh at the boundary layer of the platform is resolved sufficiently to include viscous damping in CFD. The rigid body used for simple modeling of the rotor-nacelle assembly and the tower does not influence the surge motion if results of MBS+HydroDyn+AddDamping are compared to FAST. Applying linear hydrodynamics (MBS+HydroDyn) additional linear damping (AddDamping) is added to the linear radiation damping from potential flow theory and the nonlinear viscous-drag from Morison's equation to match with measurement data of the Hywind system. Results of platform surge almost converge for MBS+CFD and MBS+HydroDyn if the additional damping is reduced. The deviation can be decreased further by reduction of the empirical hydrodynamic viscous drag coefficient (PtfmCD) from 0.6 to 0.5 used for calculation of viscous drag from Morison's equation. Results of MBS+CFD and MBS+HydroDyn (reduced PtfmCD) show a good agreement in terms of amplitude and damping. However, the frequency of the damped oscillation in surge (approximately 0.008 Hz) is higher using coupled MBS and CFD. Thus, CFD predicts less added-mass contributions than linear hydrodynamics.
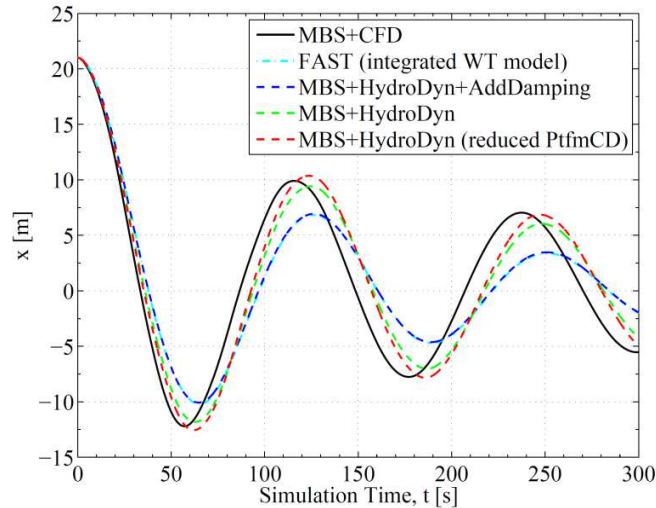
Figure 4.2 – Platform surge motion of the OC3-Hywind system compared between different hydrodynamic approaches

The influence of friction between the fluid and the structure in the boundary layer is ignored in hydrodynamics based on potential flow theory. It may be introduced by the additional linear damping. A reason for differences between methods may be the application of the simplified wind turbine model that does not account for aerodynamic damping of the rotor-nacelle-assembly and tower. This effect in turn is included in the measurement data of the Hywind system and the resulting additional linear damping. However, the influence of aerodynamic drag is assumed to be small due to the low platform velocities during the free-decay.

Separated flow and resulting vortices can be found at the platform as highlighted in black in Figure 4.3 by the vorticity. The back flow regions are demonstrated by the tangential velocity vectors (red). At t = 57 s the platform surge reaches a turning point and the floating system reverses the direction of motion. As time progresses the platform interacts with its wake while the vortices move around the platform.

HydroDyn accounts for flow separation by means of velocity-dependent damping from Morison's equation (nonlinear viscous drag). It is driven by parameters that are determined empirically and thus represent a potential cause for differences between methods. However, dynamic effects due to three-dimensional flow around the platform and fluid-structure-interactions cannot be captured with linear hydrodynamics but by CFD.

INNWIND.EU, D4.21, State-of-the-art and implementation of design tools for floating structures
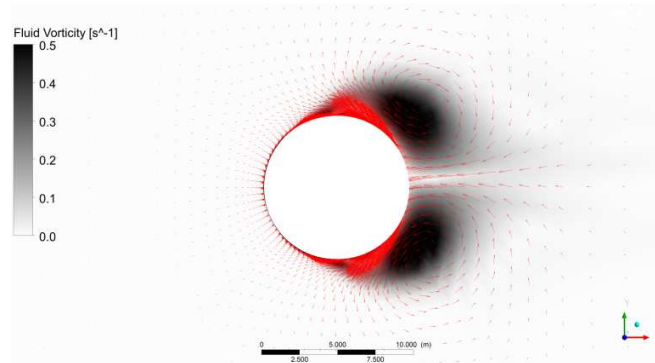
Figure 4.3 – Vorticity (black) and tangential velocity vector (red) demonstrating flow separation and vortex generation along the spar-buoy

4.3   Future Work

The mutual influence of rigid body modes-of-motion of the floating system may be studied with additional simulations, for example, free-decay response in pitch. More complex platform geometries need to be simulated like the OC4-DeepCwind semisubmersible IV [4.6] consisting of several columns and pontoons. The proposed approach shall also be used to analyze the effect of steep and breaking waves on the dynamics of floating offshore wind turbines. A design optimization may be performed with detailed loads on the platform hull.

4.4   References

[4.1] ANSYS, „Ansys 14.5 Theory Manuel," 2013.

[4.2] Arnold, M., Biskup, F. and Cheng, P.W. "Simulation of Fluid-Structure-Interaction on Tidal Current Turbines based on coupled Multibody and CFD Methods" In 23rd International Offshore and Polar Engineering Conference, Anchorage, USA, 2013.

[4.3] Beyer F. and Cheng, P. W. "Analysis of Floating Offshore Wind Turbine Hydrodynamics using coupled CFD and Multibody Methods" In: 23rd International Ocean and Polar Engineering Conference, Anchorage, USA, 2013.

[4.4] Jonkman, J. "Definition of the Floating System for Phase IV of OC3," 2010.

[4.5] Jonkman J. and Musial, W. "Offshore Code Comparison Collaboration (OC3) for IEA Task 23 Offshore Wind Technology and Development," Golden, CO/USA, 2010.

[4.6] Robertson, A., Jonkman, J., Song, M.M., Goupee, A., Coulling A. and Luan, C. "Definition of the Semisubmersible Floating System for Phase II of OC4," NREL, 2013.

INNWIND.EU, D4.21, State-of-the-art and implementation of design tools for floating structures

5 TOOL FOR CFD BASED SIMULATION OF FLOATING WIND TURBINES

To analyze the complex aerodynamics of offshore floating wind turbines the University of Stuttgart (Institute of Aerodynamics and Gas Dynamics) uses a sophisticated high fidelity process chain, which is based on the CFD flow solver FLOWer. The code, which was developed by the German Aerospace Centre (DLR), was formerly used for aircraft and helicopter simulations and contains wind turbine specific extensions. FLOWer the incompressible Reynolds-averaged Navier-Stokes equations in integral form. The numerical procedure is based on block structured meshes and uses a central cell-cell-vertex or cell-centered or AUSM finite volume formulation for the spatial discretisation. FLOWer is of second order in space (central difference scheme) and time. The time integration is done by an explicit hybrid multi stage Runge-Kutta scheme, which is embedded in a dual time stepping algorithm. The turbulence terms can be calculated by choosing a turbulence models like the Spalart Allmaras or Wilcox k-omega for instance. To speed up convergence the solution procedure is embedded into a sophisticated multigrid algorithm. The simulation uses overlapping grids, which is supported by CHIMERA technique

5.1 Improvement for Simulation of Offshore Floating Wind Turbines

To simulate floating platform structures the standard implementation of FLOWer was extended. In the original formulation FLOWer uses either a Fourier series or a polynomial function in order to prescribe a general movement. Anyhow, for a realistic description of the wind turbine platform motion one single function is not sufficient. Therefore, FLOWer was extended to use piecewise defined polynomials as movement description.

5.2 Description of a typical turbine model

A typical setup of a wind turbine simulation performed at the University of Stuttgart (IAG) considers all turbine blades in detail, spinner, hub, tower and ground. In case of the floating simulations an auxiliary structure at the ground is used, which allows the 6-DOF motion of the turbine. The ground is defined as planar, so the wave characteristics are not considered. The blades and the other structures of the model are linked to each other by using the CHIMERA technique for overlapping grids. The CHIMERA technique, which is also implemented for unsteady simulations, allows performing rotor motions like pitch and rotation while hub and tower remain steady. In case of floating offshore simulations the whole turbine is moved time dependent via predefined translation and rotation to consider the 6-DOF motion (see Figure 5.1). To avoid gaps in the numerical setup while the turbine is floating an additional sphere is created between the ground and the tower. During floating operation the tower and the whole turbine slides on the sphere surface to guarantee a connection to the ground. The sensitivity of the CFD chain for the simulation of floating turbines has been demonstrated within the KIC InnoEnergy project OFFWINDTECH [5.2], [5.3].

Figure 5.1: Schematic view of different turbine motions [5.3]

5.2.1 Needed Input Data

The simulations of a turbine in floating state need several input parameters which need to be defined. As the pressure distribution is computed directly in the simulation and not read from a database the real shape of the blade is needed. Besides this the geometry of tower, spinner and hub is needed as

well. To achieve the correct flow state detailed information has to be provided about the inflow. Currently it is possible to use the whole range from simple uniform inflow to turbulent unsteady atmospheric inflow in the simulations. The more complex the inflow is, the more information about the inflow is needed. As the simulation does not include a turbine controller rotational speed pitch and yaw angle need to be defined prior to the simulation. If a change of one of these motions during the simulation needs to be considered, a function describing the motion can be defined. Regarding the 6-DOF motion additional functions have to be defined for the whole turbine. The information about the motions describing the three rotational movements pitch, roll and yaw and the three translatory movements surge, sway and heave have to be extracted from an external code, as FLOWer has no hydrodynamic model implemented. The input of the rotational motions have to be defined in the Eulerian angle definition. Nevertheless if the rotational movements are described within a fixed coordinate system, the Cartesian angles have to be transformed into Eulerian angles, by using a MATLAB tool which is available at the Institute of Aerodynamics and Gas Dynamics.

5.2.2   Provided Output Data

The CFD based floating offshore wind turbine simulations provide detailed unsteady information of the whole flow field around the turbine and flow state on the turbine, while 3d viscous unsteady and rotational effects are considered. In a post processing step, loads, torque and power of the turbine can be evaluated. Besides the global turbine characteristics a detailed view into the blade aerodynamics is possible. This covers spanwise unsteady pressure distributions and extraction of flow separation lines. Regarding the turbine wake the simulation provides information about the unsteady wake deficit, radial and axial velocity distribution, the blade tower interaction, the tip and inboard vortex distribution and the overall wake development. In case of floating turbine simulations, the interaction of the turbine with its own wake, which leads to a highly dynamic load state, can be analyzed. Moreover, information about unsteady aerodynamic effects like phase shifting and dynamic stall effects can be received.

5.3   Prior Use of Tool

Till now the described process chain was and still is used in numerous national and European projects to analyse wind turbines focusing on unsteady aerodynamic effects, load and noise control and wake aerodynamics. The simulation of floating offshore wind turbines using this tool was first performed during the OFFWINDTECH project [5.2]. In this project a modified NREL/UpWind 5MW wind turbine in combination with the HYWIND spar boy was analyzed in floating state under various inflow conditions. The simulations were compared to floating simulations of identical turbine configuration (motions and inflow conditions) using the MBS-code SIMPACK that makes use of the ECN Aero-Module tool for BEM based aerodynamic analysis. Regarding the global rotor loads SIMPACK and FLOWer showed good agreement in the non floating state. After the beginning of floating motion the CFD tool, showed a slight increase of the loads and a phase shift (see Figure 5.2). Moreover, for the test cases considered, there was a tendency that the amplitudes of the load spectra provided by CFD were somewhat higher compared to the SIMPACK results.
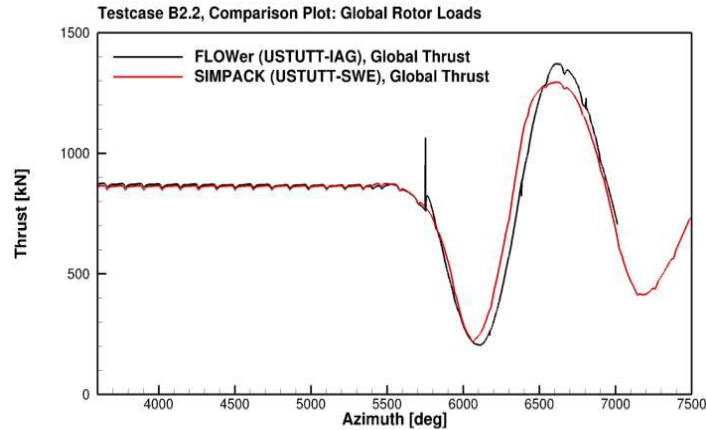
Figure 5.2: Global thrust of the OFFWINDTECH turbine in (non)floating state [5.1]

Besides the global loads an analysis of the spanwise load distribution along the blade during non floating operation showed a good agreement, too, while the biggest deviations could be determined in the inboard blade section and the tip region of the blade (see Figure 5.3).
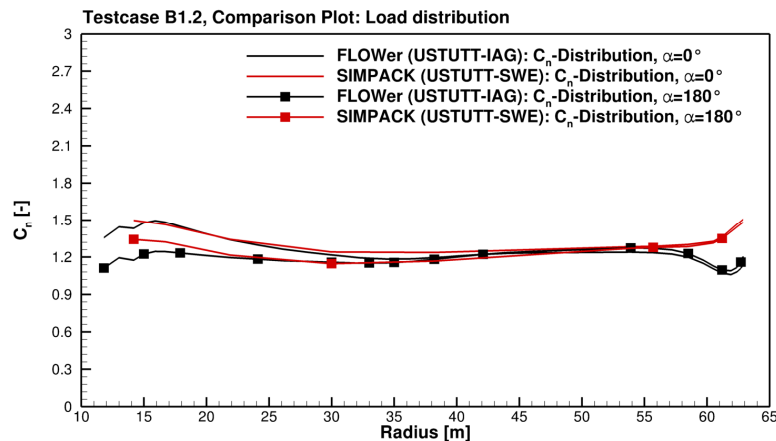
Figure 5.3: Spanwise distribution of normal and tangential force coefficients along the turbine blade during non floating state [5.1]

5.4   Conclusion

The CFD based tool provides detailed time and space resolved information of the whole aerodynamic flow state of a floating wind turbine. Compared to models based on Blade-Element-Momentum theory CFD uses less modeling and thus represents physical effects more accurately. As the blade pressure distribution is calculated based on the 3d viscous flow characteristics no corrections reducing accuracy are needed. The gain of accuracy and information has to be paid by high computational costs. Today it takes more than 100,000 CPU hours to perform an analysis of an offshore floating wind turbine just for one inflow state to receive one minute real time operation.. Another point is that FLOWer does not include a hydrodynamic model. Due to the excessive CPU demands for a coupled simulation it is not planned to implement such a model into FLOWer.

This all leads to the fact, that CFD at the current state should be used for analysis of specific, high complex flow situations, to provide results covering more physical effects as faster tools do. The results than can be used for verifying or tuning the aerodynamic of faster, simpler engineering models in analyzing high complex flow situations.

5.5   References

[5.1] Sandner, F., Schlipf, D., Matha, D., Seifried R. and Cheng, P. W. *"Reduced Nonlinear Model of a Spar-Mounted Floating Wind Turbine"*, DEWEK, Bremen, Germany, 2012.

[5.2] Bekiropoulos D. and Lutz, T. *"OFFWINDTECH Deliverable D2013-3.1: Comparison of benchmark results from CFD-simulation"* 2013.

[5.3] Bekiropoulos D. and Lutz, T., OFFWINDTECH WP 3 Symposium on Offshore Wind Technologies, Barcelona, June 20th, 2013.

INNWIND.EU, D4.21, State-of-the-art and implementation of design tools for floating structures

6 HYDRO_GAST INTEGRATED ANALYSIS TOOL FOR FLOATING WIND TURBINES

6.1 Overview of hydro_GAST

NTUA is participating in WP4 with *hydro_GAST* an in-house developed software designed to perform time domain simulations for the complete wind turbine system. *hydro_GAST* is modular comprising:
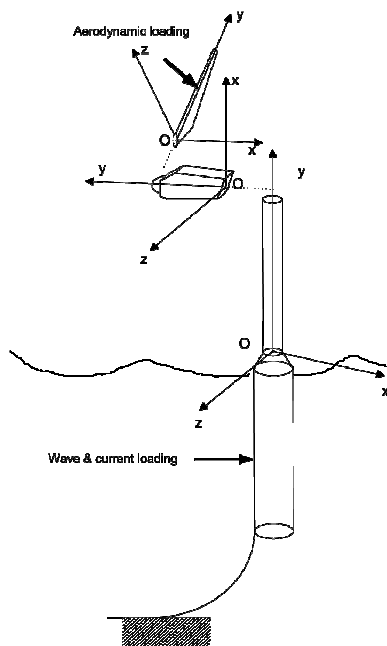
Figure 6.1: physical modeling in hydro_GAST

- The "aerodynamic module" that provides the aerodynamic loads along the rotor blades

- The "structural module" that provides the deformed shape and the associated kinematics defined for each separate solid component of the machine

- The "hydrodynamic module" which provides the wave & current loading on the support structure (floater or jacket)

- The "mooring module" which provides the geometry of the mooring line as well as the associated loads

- The 'dynamic module" that defines the dynamics of the whole system

The modular definition in *hydro_GAST* accommodates various options for the physical modelling associated to a specific module. A brief description of the available options is given next.

6.2 Modelling Options in *hydro_GAST*

6.2.1 Options in the "aerodynamic module":

The following options are included:

a) BEM modelling, accounting for dynamic inflow based on the ONERA model (RAFT).
   RAFT follows the usual guidelines of BEM modelling. It contains: tip and/or tip losses, 3D correction of the 2D polars (if not included already in the tables), yaw misalignment corrections.

b) A free-wake 3D modelling using vortex particle dynamics (GENUVP).
   GENUVP combines a panel representation of the solid surfaces with a vortex particle approximation of the wake. Solid surfaces can take one of the following representations: non-lifting bodies represented by sources (the tower), open lifting surfaces carrying dipoles and shedding vorticity along their edges (blades, tower of downwind machines), closed lifting surfaces carrying sources and dipoles (thick blades). The evolution of the wake is followed in the Lagrangian formulation of the vorticity including convection and deformation.

The code runs unsteady and steady state results are obtained upon time convergence.

Loads are calculating using the pressure distribution obtained directly from the flow solver. An a posteriori viscous correction is applied using 2D tabulated polars. The correction is based on the estimation of an effective angle of attack and an effective relative velocity. The effective angle of attach is obtained from the potential load calculation assuming that the potential force per strip corresponds to lift. The effective relative velocity is taken as the average per strip relative surface velocity.

End of time step:
• non-entry b.c.
• Kutta condition

Convect wake vorticity

Near-wake is transformed into vortex blobs
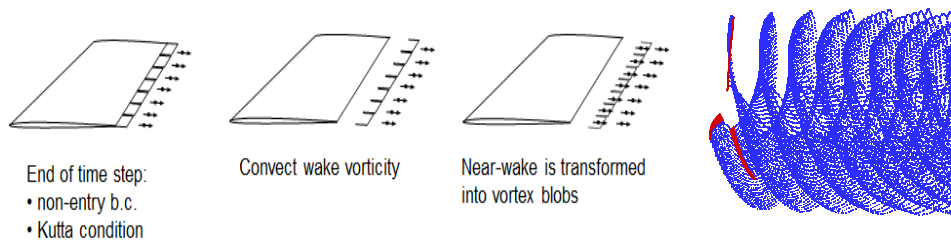
Figure 6.2: The surface singularity intensities are determined using the non-entry boundary conditions and the pressure Kutta along the emission lines. Upon convection, the surface vorticity of the recently released wake is transformed into vortex particles which are subsequently followed as fluid particles (as shown in the last plot),

GENUVP is also using the ONERA model for correcting the potential loads with the following particularity: instead of the so called "attached" part in the ONERA model, the potential loads are retained. So the correction is restricted to the "separated" part which corresponds to the purely viscous contribution.

Flow simulations with GENUVP, cost a lot more compared to RAFT. In order to reduce the cost, the following techniques have been developed and implemented:

- o In addition to the serial version, GENUVP has been implemented in Open MP and in MPI
- o The velocity due to the solid boundaries is calculated using tree-algorithms which take advantage of the $1/r^2$ behaviour of the kernel

A sequence of three grids is introduced

We define a piecewise constant approximation for all singularities over the dense grid, on which we also place the control points.

control point

$R/d < a$ $\begin{cases} \text{Yes proceed to the next level} \\ \text{No proceed with point calculation} \end{cases}$

$$\int_{S_i}(...)dS = \sum_{i=1}^{n}\frac{S_i}{S}\int_{S}(...)dS \qquad S = \bigcup_{i=1}^{n}S_i$$
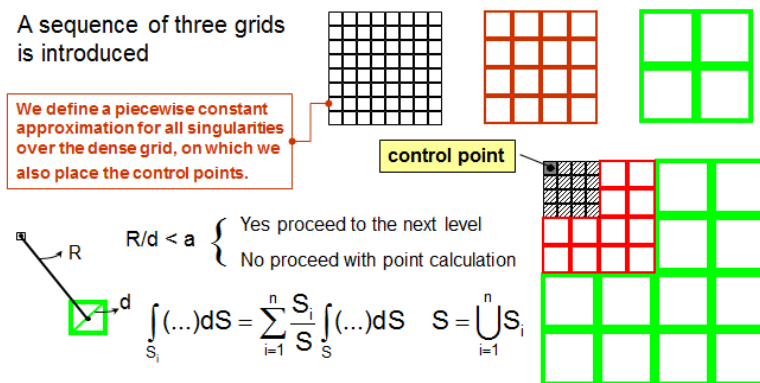
Figure 6.3: Tree-algorithm is used evaluating panel integrals. To this end a sequence of surface grids are introduced. Each grid level is produced by that of the previous level by regular partitioning. The choice of level is decided based on the ration of the distance over the panel surface. As the evaluation point approaches the solid surface the tree algorithm move from coarser to finer grids. The saving achieved decreases the cost from being $\sim N^2$ to $N.logN$. In this way very large surface grids can be accommodated which in cases of wave-hydrodynamics is important

o The evolution of the wake is performed using the PM (Particle-Mesh) method

1. Projection step:

$$\vec{\omega}_{i,j,k} = \frac{\sum_p \vec{\omega}_p V_p f(\vec{x}_{ijk} - \vec{Z}_p)}{\sum_p V_p f(\vec{x}_{ijk} - \vec{Z}_p)}$$

2. Solution step (FD): $\nabla^2 \vec{\psi} = -\vec{\omega} \Rightarrow \vec{\psi}_{i,j,k}, \vec{u}_{i,j,k}, (\vec{\omega}\nabla)\vec{u}\big|_{i,j,k}$

3. Interpolation step: $W_p = \sum_{ijk} W_{ijk} f(\vec{x}_{ijk} - \vec{Z}_p):\quad W_p = \vec{u}_p \text{ or } (\vec{\omega}\nabla)\vec{u}\big|_p$
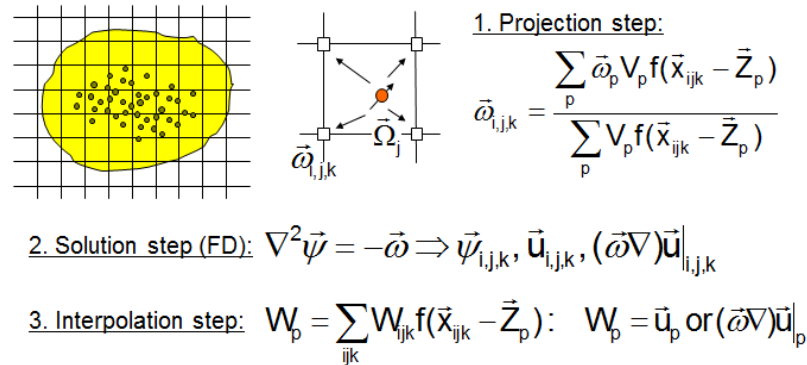
Figure 6.4: Outline of the PM method. The PM method is used instead of the Biot-Savart law and concerns the particle-to-particle interactions. Using a fast Poisson solver it is possible to obtain the velocity and deformation induced by the wake over the entire flow field. The Poisson equation for the vector potential is solved with exponentially decaying far field conditions. To this end the vorticity carried by the particles is projected on a Cartesian grid. The projection functions are constructed to conserve all moments of vorticity up to a certain order which also defines the accuracy of the approximation. In GENUVP up to 3rd order projection functions are available. The flow information from the grid is back interpolated to the particles using the same functions

o The contribution of the far-far wake is taken into account using the so called hybrid approximation.
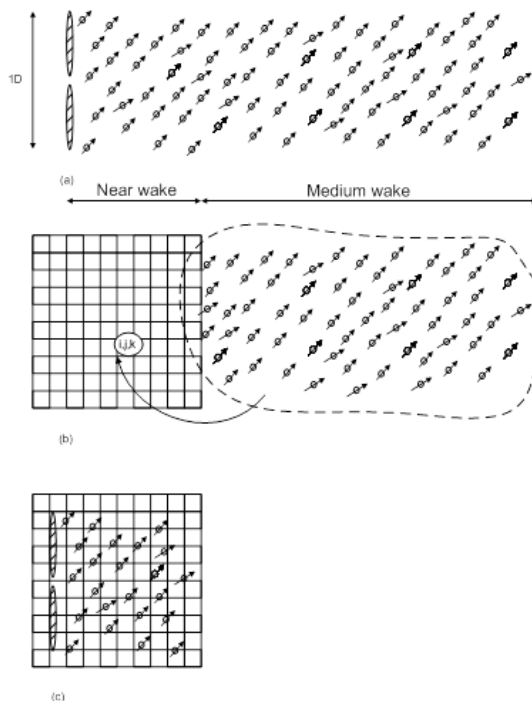
Figure 6.5: Schematic description of the hybrid wake approximation.

The hybrid wake is suitable when the main interest is in the rotor region. The basic idea is that the medium wake region contains the starting vortex its further evolution in time, its effect in the rotor and near wake regions will remain the same and at most periodic. This has been verified with numerical tests. The near wake covers a space of 1-2 D in length while the medium wake extends another 2-3 D. Once the space specified for the medium wake is covered by the wake, the effect of this part on the PM grid covering the rotor and near wake region is calculated and stored. All subsequent computations are restricted up to the near wake. As the simulation proceeds, the particles that exit the near wake region are discarded. In this way the cost of the wake evolution is kept to a reasonable level. In fact the application of the hybrid wake approximation allows performing long full aeroelastic simulation with turbulent wind inflow as defined in the IEC.

INNWIND.EU, D4.21, State-of-the-art and implementation of design tools for floating structures

6.2.2   Options in the "structural module":

All structural modelling is based on beam theory and the FEM approximation. All components are modelled by one or several beams with appropriate connections.
- Timoshenko beam modelling (for the blades, the drive train, the tower, the members of the support structure either floater or jacket)
- 2nd order Euler Bernoulli (mainly used for the blades)
- Truss element modelling (for the mooring lines)

Bending in two directions, tension and torsion are included as degrees of freedom. In the case of Timoshenko beam elements also shear is taken into account.
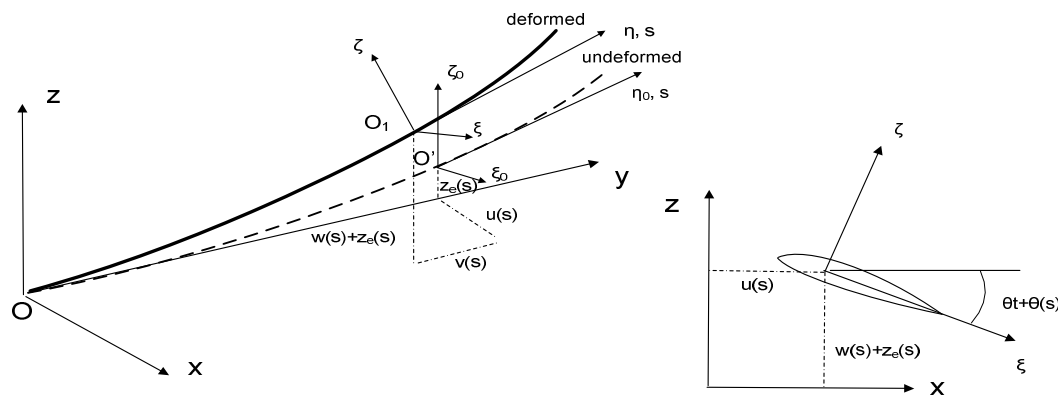
Figure 6.6: 2nd order beam theory is formulated in the deformed state modeling introducing kinematic -geometric non-linearities in the equilibrium equations.
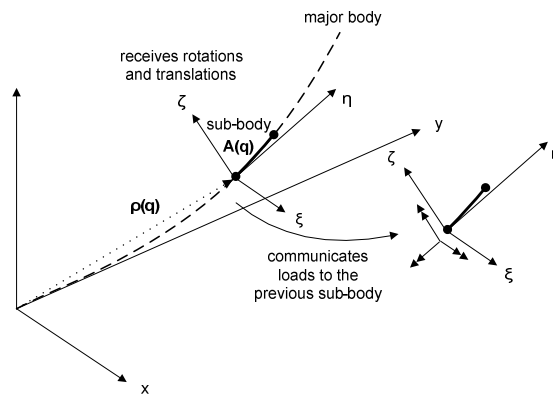
Figure 6.7: In the sub-body partitioning of a true component (e.g. the blade), every sub-body is introduced within the context of multi-body dynamics. At the connection points between sub-bodies kinematic and dynamic continuity act as boundary conditions. Thus a specific sub-body by cumulatively receiving the deformations of the previous sub-bodies, will have in its dynamic equations the terms that correspond to large displacements and rotations.

Note: Large displacements and rotations are taken into account by sub-body partitioning which consists of dividing a component in a number of beam parts non-linearly connected.

6.2.3 Options in the "hydrodynamic module":

There are two options for calculating the wave and current loading:
- Linear wave theory. The default option in this case is to solve the diffraction/radiation problem in the frequency domain and thereby obtain the mass, stiffness and damping operators needed in the dynamic equations of the floater rigid body degrees of freedom. The problem is solved in integral form and uses surface grids on which piecewise constant source distributions are defined. Alternatively the linear hydrodynamic equations can be solved in the time domain in coupled mode with the rest of the wind turbine configuration. This option is part of the developments carried out in Task 4.2.3 and is needed in case the floater is assumed to also shed vorticity as for example in the case of plates acting as damping devices.
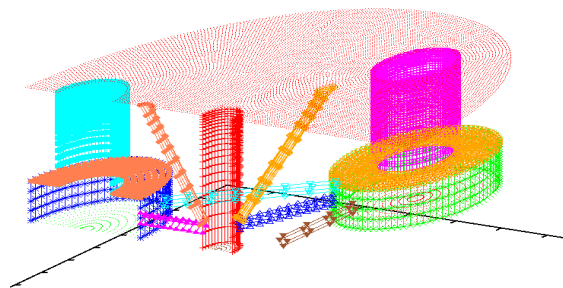
Figure 6.8: Surface grid for the semi-submersible floater defined within IEC Annex 30

- Using Morison's equation. Application of Morison's equation provides a fast way to include the effect of wakes. It is the default option when the support structure is a jacket but also when non-linear waves are considered. The option of solving the non-linear wave equations is not available.

6.2.4 The "mooring module":

The moorings are modelled by the so called "dynamic mooring line model" combined with sea-bed interaction. The mooring line is modelled as a series of truss elements (i.e. 1D structural elements only transferring axial loads) with the possibility to also accommodate buoys as lumped masses. The interaction with the sea bed is modelled by a series of springs which are activated once the mooring line approaches the sea-bed surface.

6.2.5 The "dynamic module":

The dynamics of the complete system is formulated in the framework of multi-body dynamics. Within this context, the control equations together with their associated degrees of freedom are included in fully coupled mode. At points of connection (junctions), the constrains or connection conditions of the relevant numerical bodies (which correspond to either a physical component of the wind turbine or part of its division in sub-bodies as done for example for the blades) correspond to kinematic and loading matching. .
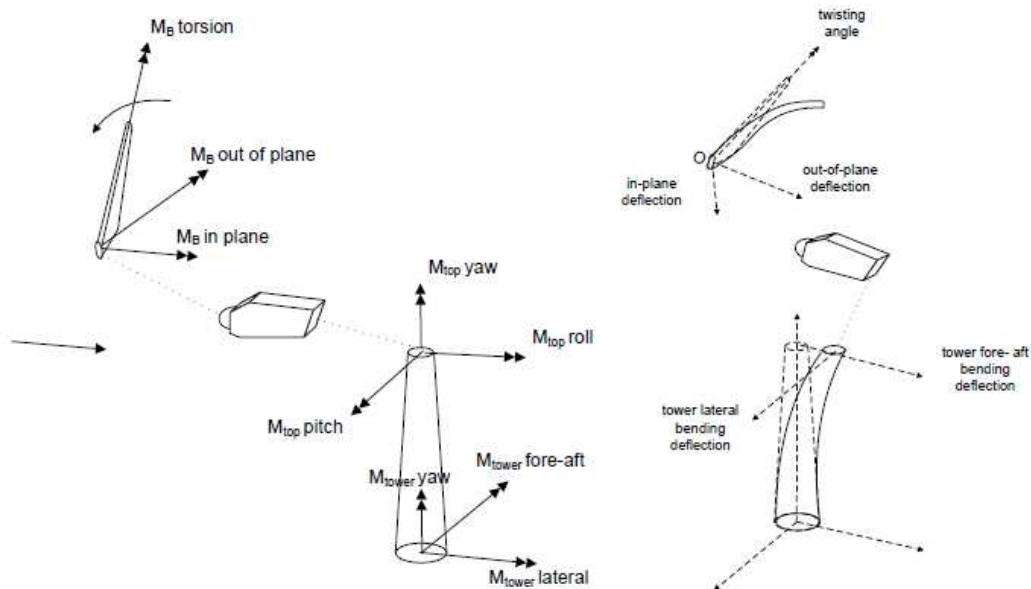
Figure 6.9: The multi-body definition of a wind turbine and the coupling principle. Each main component is modeled separately. At the connection points (e.g. the tower top, the blade roots) amongst the connected bodies one is defined as the component providing displacements and rotations while all others provide back the loads. The "dynamics" module in *hydro_GAST* accommodates rigid body motions as well control equations either in dll form or as a code.

6.2.6 Other possibilities

Time integration in *hydro_GAST* is carried out in the so-called incremental context. The equations are linearized with respect to the most current solution and solved for the incremental correction. In each time step an iterative procedure is followed until the incremental correction converges to a predefined error bound.

Linearization is part of the software and besides assisting in time integration, offers the possibility to perform linear stability analysis in combination with Coleman's transformation.

In non-symmetric but still periodic cases, Floquet's theory should be applied. Due to its high computational cost, in this case the analysis is carried out with respect to a reduced order model. The activities concerning the development of reduced order models are part of Task 4.2.3 and are described in the relevant deliverable.

6.3 Recent developments

The particular focus of NTUA's contribution to Task 4.2 concerns the assessment of free-wake modeling for floating wind turbines. In this connection,
   o   GENUVP has been successfully connected to *hydro_GAST*
   o   A series of tests have been carried out and comparisons between BEM and Free_wake based aeroelastic simulations have been compared in view of quantifying the relevant implications on the response of the machine.

INNWIND.EU, D4.21, State-of-the-art and implementation of design tools for floating structures
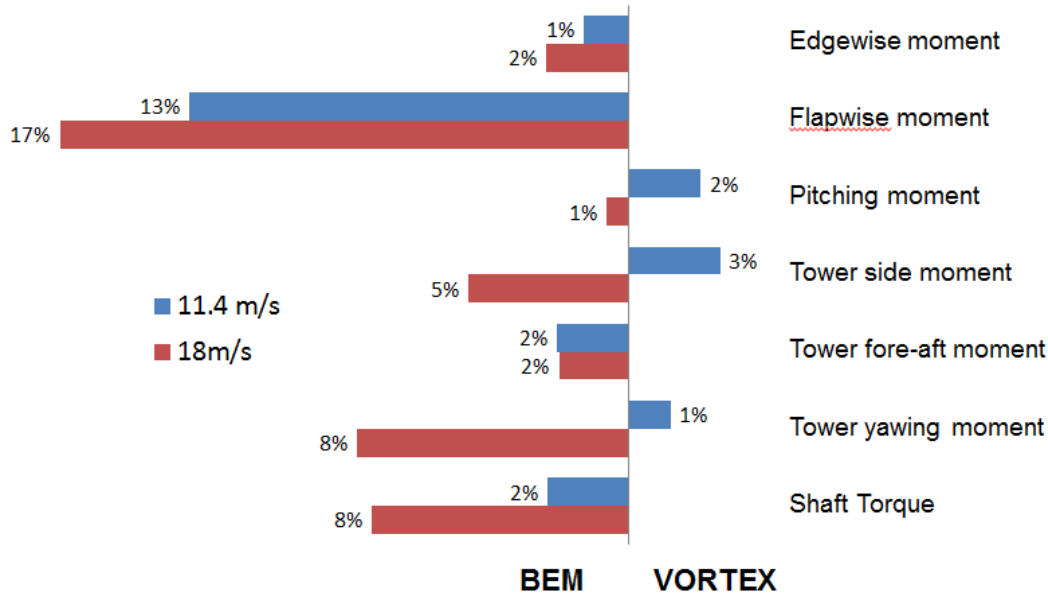
Figure 6.10: Comparison of the fatigue loads predicted with the BEM (RAFT) based and VORTEX(GENUVP) based versions of *hydro_GAS*. for two mean wind speeds 11 and 18m/s for the spar-buoy version of the NREL 5MW machine defined in IEA Annex OC3. This comparison which is here included as an indication, as well as the rest of the comparisons showed that in general terms the specific BEM based simulations lead to higher loads and by that they are regarded to be on the safe side. In certain cases, as for example in yaw for which it is expected that BEM based aerodynamics is prone to errors, significant differences appear when results are compared with VORTEX based computations.

6.4 Verification and Validation

The on-shore version of *hydro_GAST* has been validated/verified in [6.1] for the most recent validation work. With respect to the full *hydro_GAST* there has been no validation so far due to lack of available measured data. However the full *hydro_GAST* version has been compared to other state-of-art codes within the activities of IEA Annexes OC3 and OC4. Relevant to floating concepts is the work on the spar-buoy concept (OC3) performed with both the BEM and the GENUVP options, and the work on the semi-submersible floater of OC4 performed with the BEM option.

6.5 Future work

The main code modifications and adaptations related to Task 4.2 have been completed and therefore the rest of the Task duration will be given to tests. These tests will primarily concern the semi-submersible floater of OC4 which has been already simulated with the BEM based version.
Further developments in *hydro_GAST* are however in progress in relation to the activities of WP4. They refer to including wake generation from the floater and the coupled solution of the hydrodynamic problem in time.

6.6 References

[6.1] Riziotis, V.A., Voutsinas, S.G., Politis, E.S., Chaviaropoulos, P.K. (2010) "Stability analysis of parked wind turbine blades using a vortex model," Proceedings of the Science of Making Torque from the Wind Conference, Heraklion, Greece, June 28-30, 2010.

INNWIND.EU, D4.21, State-of-the-art and implementation of design tools for floating structures

7 COMPUTATIONAL FLUID DYNAMICS FOR FLOATING WIND TURBINES IN ROUGH SEAS (DHI)

7.1 Scope

The aim of DHI's work is to develop and validate a CFD tool accurately capturing the detailed motion of a floating structure in realistic irregular wave fields. Flexibility of the structure will be ignored yielding 6 degrees of freedom to represent the body state. Focus is on the 2-way coupling between structure and water including the full nonlinearity and viscous effects in the hydrodynamic CFD calculations. The role of wind will be represented only via a simple model adding a force term to the body equations of motion. Mooring lines are also included as external body forces calculated from the instantaneous floater position and orientation. The substructure geometry will be accurately modelled whereas the only information needed about the superstructure is its contributions to the structure mass, center of mass and inertia tensor.

7.2 Background

As described in [7.2] (section 2.3.3 and 5.2) the current state-of-the-art approach for hydrodynamic load calculations on floating structures is to use linear potential theory with Boussinesq-type or statistical wave fields as input. Typically the sea state is treated as a linear superposition of independent Airy wave components and the force that each of these exerts on the body is separated into independent contributions from wave radiation, wave diffraction and a hydrostatic pressure term. WAMSIM is an example of a code adopting this "divide-and-conquer" approach. It is very efficient and accurate whenever the assumptions of small wave amplitude, small body displacements and motion, and negligible viscous effects apply.

However, non-linear hydrodynamic effects play a significant role when a floating wind turbine is subjected to extreme wave conditions. It is well known that fluid viscosity influences hydrodynamic forces on the floating body when the motion amplitude is large and the body is of a bluff shape. The absence of viscosity in potential theory not only alters fluid damping but also, to some extent, the added-inertia characteristics. The shortfall of viscous effects in codes based on potential flow theory like WAMSIM is sometimes compensated by introducing an external empirical viscosity term in the body equations of motion [7.3]. Although theories based on the potential flow assumption are able to reproduce the heave motions reasonably well, they are less accurate in the prediction of roll motion. This is owing to the highly nonlinear nature of the roll motion due to the roll-damping effect. At wave frequencies near a natural frequency of the floater system flow separation is likely to occur. Viscous damping effects caused by flow separation are known to heavily influence especially the roll motion and hence the stability of the floating wind turbine.

To date there has been no widely available and well validated tool for numerically testing of floater designs in more extreme sea conditions involving steep-sided and breaking waves or strong currents. In order to speed up the optimization of floating wind turbine concepts in view of combined hydrodynamic stability and structural survivability, a numerical test bed to test structures in more extreme conditions is paramount.

The OpenFOAM® software is a strong candidate for such a tool. It is an extensive code library containing tools for all aspects of CFD. It is written in C++ and includes many specialised CFD solvers for various flow situations [7.10, 7.14]. It was originally developed at Imperial College in the 1990'ies and has since gained a large momentum during the past decades with a huge international user and developer community now contributing to its validation and development. Today the code is

maintained and freely distributed by the OpenFOAM Foundation which is sponsored by the ESI Group also holding the trademark to the name.

The code includes all components necessary to calculate the full nonlinear, viscous hydrodynamics coupled with large amplitude 6 degrees-of-freedom (6 DOF) motion of a floating structure. The main components are described below.

7.3 The OpenFOAM® free surface solver

OpenFOAM® includes a solver for the Navier-Stokes equations for two immiscible and incompressible fluids – in our case air and water. It captures the air-water interface using a variation of the Volume-of-Fluid (VOF) method [7.1, 7.4, 7.12, 7.13] originally developed by [7.7]. The advantage of the VOF method is its ability to cope with arbitrary interfacial shapes, including the complex patterns of breaking waves. It also has favorable mass conservation properties compared to other surface capturing techniques (e.g. the level set method). The pressure-velocity coupling is solved using the PIMPLE algorithm (a merge of the PISO and SIMPLE algorithms). PIMPLE allows the use of outer correctors and under-relaxation with multiple momentum correctors. In case of turbulent flows, the Navier-Stokes model allows coupling with a number of turbulence models available in OpenFOAM® (RANS and LES). The solver is parallelised and has been demonstrated to scale well up to many hundreds of cores.

7.4 Dynamic mesh method

OpenFOAM® operates with meshes consisting of general polyhedral cells allowing the mesh to fit exactly around complex structures. In order to handle a floating marine structure a dynamic mesh approach is adopted. Thus, at each time step of the solution algorithm the fluid-structure boundary surface is displaced and reoriented in accordance with the total hydrodynamic plus external forces and torques on the structure. An algorithm to redistribute mesh points inside the fluid domain is also executed at each time step to ensure the mesh quality. On the fluid-structure interface a moving wall boundary condition is applied for the fluid velocity field in order to ensure the no-slip condition. The time integration of the 6 DOF body motion ordinary differential equations (ODE) is performed using a special symplectic integrator. This has lower order than traditional ODE solvers but was chosen for its favorable energy conservation properties in contrast to traditional schemes where numerical dissipation of energy can be an issue for long simulations [7.5]. Once the body boundary position and boundary condition have been updated from the 6 DOF calculation the surrounding flow is calculated for the new time with the updated boundary data. This ensures the correct two-way coupling between the body motion and the transient solution of the flow equations [7.9, 7.11].

7.5 Wave generation

Non-linear wave interaction with floating marine structures involves wave breaking under harsh sea conditions, which adds to the complexity of the non-linear forcing. There are several options for generating irregular sea states at one or more walls of the fluid domain. One option is to impose a precalculated velocity field at the wave generator wall(s) synthesized as a linear superposition of Airy waves with different amplitudes, periods, phases and directions to produce e.g. a realisation of the JONSWAP spectrum. Even though the wave field is synthesized from linear theory its propagation through the computational domain is governed by the full nonlienar Navier-Stokes equations. Another alternative method for wave generation recently developed at DHI is to let a wave generator wall move as a piston type wave maker with the cells in front of the wall deforming to accommodate the wall motion. This ensures accurate representation of the input waves generated in physical wave tank tests.

7.6 Wave damping

The motion of a floater in the ocean is damped primarily via the energy carried away with the radiated waves. When such radiated waves meet the external domain walls in a CFD calculation they will be reflected back into the domain thus polluting the target sea state and altering the body motion. Several methods are available to reduce this reflection problem: One approach referred to as a numerical beach is to artificially increase the water viscosity in a region near the external domain walls. This results in strong dissipation of wave energy in those regions. Another approach is the relaxation method where an artificial force is included in the Navier-Stokes equations in regions close to the domain walls [7.8]. This force "pulls" the velocity field in those regions towards a predefined value e.g. from an analytical solution (typically simply zero velocity). Finally in the active absorption method the wave energy is extracted directly on the domain walls. The approach here is to apply shallow water theory and information about the velocity field in the cells touching the domain boundary to calculate and impose an instantaneous boundary velocity field corresponding to full wave transmission through the wall [7.6]. Active absorption applying digital filters allows a significantly smaller fluid domain around the floating structure as compared to the numerical beach and relaxation methods. It does, however rely on shallow water theory and so is not adequate for all situations.

7.7 Mooring lines

A floating wind turbine requires a mooring system to ensure station keeping and avoid impact with other structures. Wave impact forces due to non-linear wave interaction with the floating wind turbine are transferred to the mooring system which then responds with a constraint to the motion of the floating structure. Mooring lines can be represented in OpenFOAM® simulations as linear damped springs attached to the hull fitting and to anchor points. In the near future this will be replaced by a more realistic representation with a spring working curve.

7.8 Results in irregular waves

This section presents an outline of the capabilities of the OpenFOAM CFD model. The TLP concept of a floating wind turbine has been chosen for demonstration. The TLP floater is represented by a floating rectangular box with height, h = 30 m, extending 6 m x 6 m and draft T =20 m in water of density rho = 1025 kg/m³. The moment of inertia is that of a rectangular box where center of gravity is located in bottom parts the body, to render a more stable roll and pitch response.

Initially the floater is at rest in the center of the computational domain with a center of mass position at [37.5; 37.5 ; 40] m, see Figure 7.1. The computational domain extend in the x-direction [0; 75] m, y-direction [0; 75] m and z -direction [0; 75]m with the still water level being at z = 50 m.

A simple mooring system consisting of four tension legs is used. Each tension leg-mooring line is modelled with a linear spring including damping. The unstretched length is 35.1 m and axial stiffness EA = 0.35 MN. The hydrodynamic forces on the mooring lines are neglected. Each cable is attached a corner of the bottom part of the floater. From the attachment point on the device the tension leg is vertically anchored at the sea bed, leaving the total footprint of the mooring system to be contained within the horizontal extend of the floater. The equilibrium condition of the moored body is equal that of the free floating case.

INNWIND.EU, D4.21, State-of-the-art and implementation of design tools for floating structures
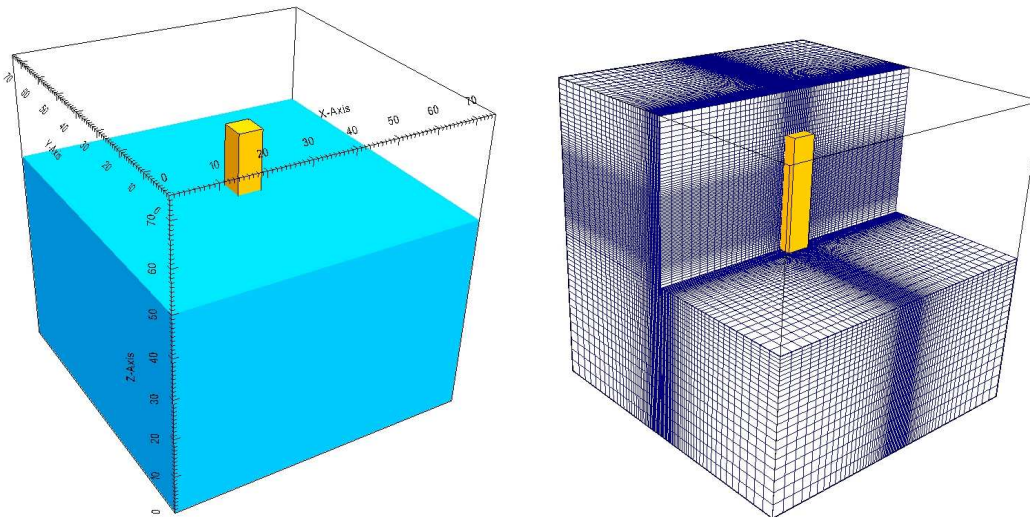
Figure 7.1: Left: Computational model domain and Right: Computational mesh

The computational mesh of the fluid domain is a structured hexahedral mesh. A narrow band of high resolution in the z-direction surrounding the still water level is made in order to better capture the motion of the generated waves. The structure of the global mesh can be seen in Figure 7.1. The total number of cells in the mesh is roughly 0.7 million. Close to the surface of floater the resolution is increased in order model the effect of the boundary layer. The small cells attached to the body are prone to high skewness during large displacements of the body during excessive pitch, roll and yaw motion.

Turbulence is modelled with k-epsilon model in combination with standard wall functions [7.15] for modelling the surface of the TLP and seabed. Hence by placing the near-wall cell at a distance of $30 < y^+ < 100$, the flow in this cell may then described by wall function.

Active absorption is applied on all vertical boundaries of the computational domain, hence removing the necessity of extending of the domain in the wave direction (x-direction).

The wave conditions at the imagined site are represented by a JONSWAP spectrum [DNV-RP-C205] with a peak enhancement parameter of 3.3, significant wave height $H_s = 3.6$ m and peak wave period $T_p = 5.4$ s. Only unidirectional waves were considered. The spectrum is modelled by a series of sinusoidal wave components as outlined in section 3.3.2 in [7.16].

A minimum number of sinusoidal wave components needed to represent the theoretical spectrum is computed, hence reducing the resolution. Due to the large computational demand of the present complex model, the simulation time had to be limited to relatively short time series. The time series were selected to 600s (10 min). The time series were chosen which best reproduced the wave spectra, and included one or more extreme events within the 600s. In other words, the wave spectra for the short time series do not differ significantly from the corresponding spectra for full 3-hour time series. The spectra applied in the CFD simulations are shown in Figure 7.2 together with the corresponding time signal of the surface elevation. Figure 7.2 compares the CFD results of the free wave fields to the

INNWIND.EU, D4.21, State-of-the-art and implementation of design tools for floating structures

analytically derived spectra based on linear theory. The input signals and the simulated signals are in good agreement.
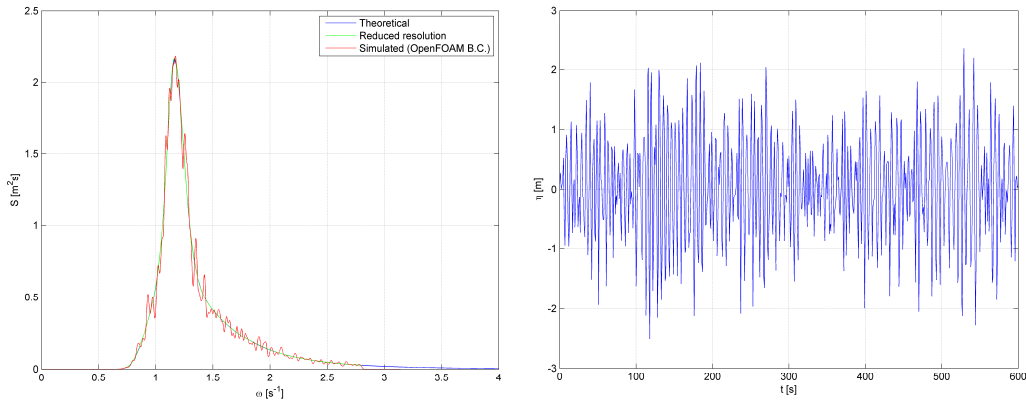
Figure 7.2: The JONSWAP wave spectra used as input to the CFD simulations; H_s=3.6m, T_p=5.4 s and gamma = 3.3. Right: Corresponding time signals of the surface elevation.

Figure 7.3 shows a snapshot of the simulation in the crest of the wave at 37s. The distortion of the mesh due to motion of the TLP is evident.
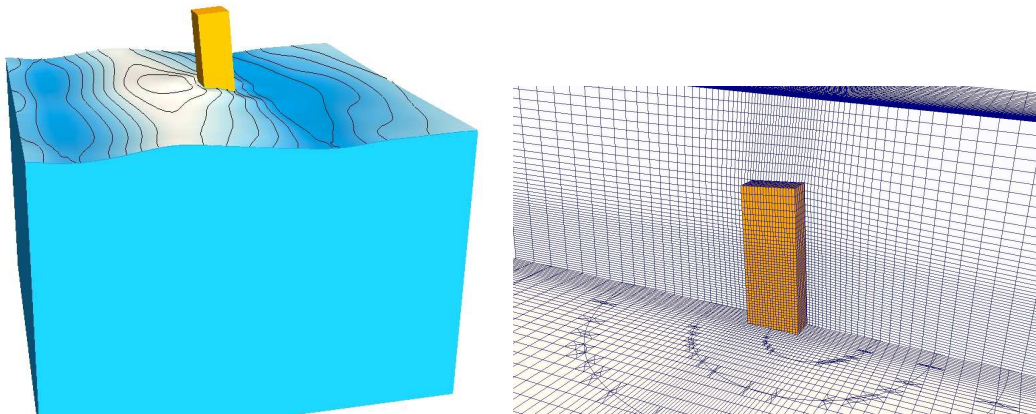
Figure 7.3: Snap shot of the solution state after 37 s. The iso-surface of the volume-fraction variable in the VOF approach equal 0.5 is used to illustrate the free surface. The surface is colored such that maximum wave height is colored white minimum is colored blue. To the right is a close up of the mesh surrounding the TLP.

INNWIND.EU, D4.21, State-of-the-art and implementation of design tools for floating structures

Figure 7.4 depicts the motion response of the TLP. It can be observed that in case of the current TLP configuration the floater is most sensitive to surge motion. As expected the heave motion is of less dominant nature.
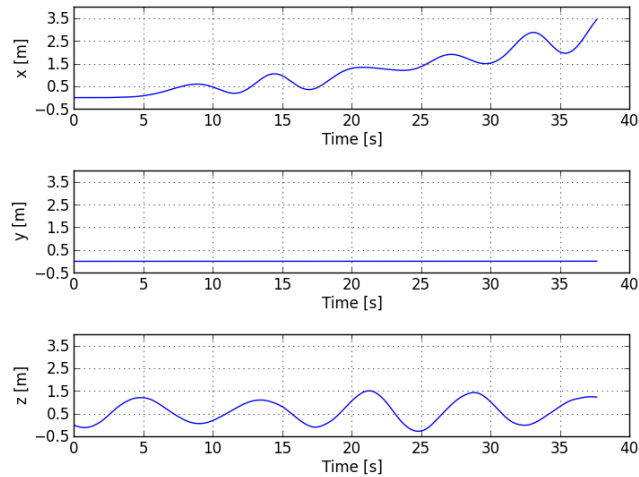
Figure 7.4: The surge, sway and heave motions of the floater moving in irregular waves.

Figure 7.5 illustrates the tension forces in the mooring lines at the attachment point. Mooring line no. 1 and 2 are attached to the upstream corners of the floater and are exposed to the largest forces as expected.
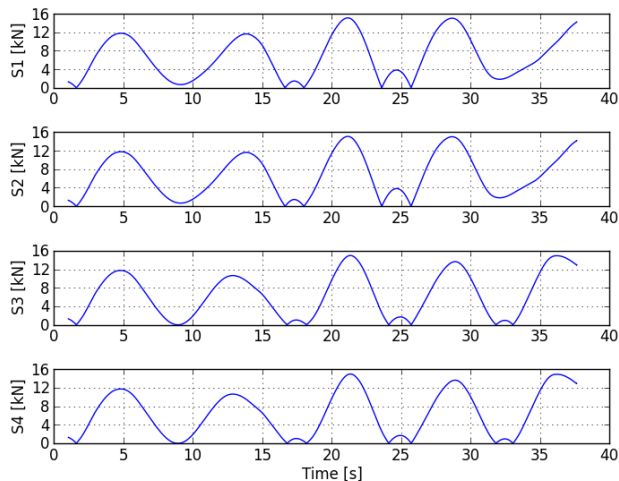
Figure 7.5: Left: The tension force magnitude at the attachment point to the floater in each of the four mooring cable.

INNWIND.EU, D4.21, State-of-the-art and implementation of design tools for floating structures

7.9 Status and further developments

A methodology for performing coupled analysis of floating wind turbines was presented. The coupling of the free-surface Navier-Stokes solver and active wave boundary strategy has been tested. The floater was subjected to a real sea state. Albeit no conclusion should be drawn from the present test case, it served to demonstrate that the 2-way coupling approach between structure and water including the full nonlinearity and viscous effects can capture the complex interaction between the mooring system and the floating structure.

As described above the key OpenFOAM® components for advanced simulation of the 2-way coupling between a floating structure and the surrounding sea are readily available. Their specific application in this context is, however, only very scarcely validated. Building up confidence in the code and possibly identify components that need to be improved is the main objective of DHI's activities under INNWIND task 4.2. Validations performed including heave tests for simple structures as well as convergence tests with respect to spatial mesh resolution and time step size. As part of the validation the sensitivity of the solver to very large body displacements will be investigated. For large body displacements and rotations the mesh quality degrades - eventually to a level where the solver crashes. Gaining experience with the solver robustness for large mesh deformations is an important part of mapping the application envelope of the tool, including enhancing the model by including mesh with sliding mesh motion on the top, bottom and side patches of the domain to allow for large surge displacements with minimum mesh skewness. An extension of mooring line description library is invariable in order to include detail description of a mooring system, which needless to say have a significant impact on the motion response of the floating wind turbine.

In deliverable 4.25 the code will ultimately be validated against the physical test data produced in deliverable 4.24. Other data that could be used for validation is the data from the Hydralab project "Dynamic Response of Floating offshore Structures under Random Waves and Wind Action" performed at DHI in 2012 (by partners from University of Salento in Italy, Instituto Superior Técnico in Portugal, RWTH Aachen in Germany, National Technical University Athens in Greece and Cores in Bulgaria). This might be done at a later time but will not be done as part of deliverable 4.21. For code validation against physical wave tank tests our recently developed wave maker based on moving meshes will be very useful as it can accurate reproduce waves generated in the real physical test facilities.

The main drawback of the CFD approach compared to codes such as WAMSIM is the significantly increased computational times. Both within the INNWIND project and other research projects DHI is working continuously on optimizing the code performance. Nevertheless in the years to come it is not realistic that CFD will replace potential codes. Rather it will serve as an invaluable supplement extending the scope of numerical floater design testing to more extreme sea states and viscously dominated situations. Its true potential is to gradually replace expensive full and small scale physical tests.

A particular challenge with OpenFOAM® is the high complexity of the code and the daily work with it. Even though the code is freely available and easy to get started with the efforts required to get to a point where it can be applied to real world engineering problems are tremendous. DHI is currently conducting a project aiming at making OpenFOAM® more easily accessible to non-CFD experts by documenting the code, developing standard setups for marine and offshore applications as well as streamlining installation process and the workflow with the code. These efforts will also be valuable to the INNWIND project.

Finally it should be mentioned that the OpenFOAM® surface capturing algorithm often causes high artificial velocities parallel to the water surface in both the air and water phase.

INNWIND.EU, D4.21, State-of-the-art and implementation of design tools for floating structures

Furthermore the current VOF implementation requires a very regular mesh near the free surface or it will become unstable. DHI In a new research project DHI is investing heavily in eliminating these problems by improving the VOF algorithm and its implementation in OpenFOAM®. The improved stability and flexibility of the OpenFOAM® free surface solver family derived from this project will feed directly into the INNWIND project.

7.10 References

[7.1] Berberovic E, Van Hinsberg NP, Jakirli´c S, Roisman IV, Tropea C., *"Drop impact onto a liquid layer of finite thickness: dynamics of the cavity evolution"* Physical Review E Statistical, Nonlinear, and Soft Matter Physics 79(3):1–15. Art.no: 036 306, 2009.

[7.2] Cordle, C., *"State-of-the-art in design tools for floating offshore wind turbines"* Upwind deliverable D4.3.5

[7.3] Christensen, E.D., Jensen, B., Mortensen, S., Hansen, H.F. and Kirkegaard, J., *"Numerical Simulation of Ship Motion in Offshore and Harbour Areas"* The 27th International Conference on Offshore Mechanics and Arctic Engineering (OMAE 2008)

[7.4] Deshpande, S.S., Anumolu , L. and Trujillo , M.F., *"Evaluating the performance of the two-phase flow solver interFoam"* Computational Science & Discovery 5, 2012.

[7.5] Dullweber A., Leimkuhler B., McLachlan R., *"Symplectic splitting methods for rigid body molecular dynamics"* J. Chem. Phys. 107 (15), 1997.

[7.6] Higuera, P., Lara, J.L. and Losada, I.J., *"Realistic wave generation and active wave absorption for Navier–Stokes models"* Application to OpenFOAM. Coastal Engineering, 2013.

[7.7] Hirt C.W, Nichols B.D., *"Volume of fluid (VOF) method for the dynamics of free boundaries"* Journal of Computational Physics 39(1):201–225, 1981.

[7.8] Jacobsen, N.G., Fuhrman, D.R., Fredsøe, J., *"A wave generation toolbox for the open-source CFD library: OpenFoam®"* Int. J. Numer. Meth. Fluids 70(9): 1073–1088, 2012.

[7.9] Jasak, H., *"Dynamic Mesh Handling in OpenFOAM"* 48th AIAA Aerospace Sciences Meeting, Orlando, Florida, 2009.

[7.10] Jasak, H. *"Error Analysis and Estimation for the Finite Volume Method with Applications to Fluid Flows"* PhD thesis submitted to the Department of Mechanical Engineering, Imperial College of Science, Technology and Medicine, June 1996.

[7.11] Jasak, H. and Tukovic, Z., *"Dynamic mesh handling in OpenFOAM applied to fluid-structure interaction simulations* V European Conference on Computational Fluid Dynamics" ECCOMAS CFD, Lisbon, 14-17 June, 2010.

[7.12] Rusche, H., *"Computational fluid dynamics of dispersed two-phase flows at high phase fractions"* PHD Thesis, Imperial College of Science, Technology and Medicine, UK, 2002.

[7.13] Weller, H.G., *"Derivation, modelling and solution of the conditionally averaged two-phase flow equations"* Technical Report TR/HGW/02, Nabla Ltd, 2002.

[7.14] Weller HG, Tabor G, Jasak H and Fureby C, *"A tensorial approach to computational continuum mechanics using object oriented techniques"* Comput. Phys. 12, 620, 1998.

[7.15] Wilcox, D.C., *"Turbulence Modeling for CFD"* Third Edition, DCW Industries, Inc., La Canada, CA, 2010.

[7.16] *"Environmental conditions and environmental loads"* DNV-RP-C205. Recommended Practice prepared by Det Norske Veritas, DNV, October 2010.

INNWIND.EU, D4.21, State-of-the-art and implementation of design tools for floating structures

8 OPASS CODE FOR DYNAMIC ANALYSIS OF MOORING LINES ATTACHED TO FLOATING WIND TURBINES

8.1 Offshore floating wind turbines

Average water depth of offshore wind farms has been increasing over the last few years. This increment in depth also means an increment in the cost of the monopiles and gravity based structures that currently are used as foundations. For this reason, as depth increases, floating platforms surges as an feasible and economically efficient alternative for supporting wind turbines at high depths.
When a floating wind turbine is installed, the mooring system holds the structure in the desired location (station keeping) and for some platform types, as TLP's, provides a restoring moment that contributes to counteract the overturning moment due to the rotor aerodynamic thrust and the hydrodynamic loading. The mooring system is made of several cables attached to the platform in a point called fairlead, and with the lower ends anchored to the seabed.

Depending on how the system stability is achieved, there are three main typologies of floating wind turbines. The first one is the ballast stabilized, where mass is concentrated in the lower part of a spar-type platform. Thus, the center of gravity of the system is positioned below the center of buoyancy and this way, a restoring moment will appear when the platform is displaced from his vertical position. The second stabilization method consist on increasing the surface of the platform at the water surface level, using the buoyancy force to obtain the restoring moment. Finally, stability can be also obtained designing a relatively light platform with respect to its volume, so that the excess in buoyancy force is compensated by the tension in the mooring lines. These kind of platforms are called TLP (Tension Leg Platforms) and unlike the other two designs mentioned before, where the mooring lines form a catenary, in TLP's, the lines are taut.

8.2 State of the art in simulation codes for mooring lines of floating wind turbines

A reliable simulation of the dynamics of the different concepts of floating wind turbine has to integrate all the phenomena that can influence the behavior of the system as aerodynamics, hydrodynamics, control, structural dynamics, mooring lines dynamics, etc. Each of these effects can have an influence over the rest, so the calculation has to consider them in a coupled, integrated manner. This kind of codes are usually called "integrated codes".

The influence of mooring lines over the global dynamics of the different typologies of floating wind turbines is very important and therefore, an accurate simulation of the mooring system within the coupled code can be fundamental for a precise description of the floating wind turbine behavior and for the loads calculation in the different components of the system [8.13].

Most of the programs with capabilities for the modeling of mooring lines dynamics do not allow to represent with accuracy the integrated dynamic simulation of the whole floating wind turbine system [8.15]. On the other hand, many of the codes developed within the wind energy sector for the simulation of floating wind turbines use simplified models for the representation of the mooring lines.

In the following paragraphs, the different modeling approaches for the mooring system will be presented and the codes for the simulation of cables and for the simulation of floating wind turbines will be reviewed discussing their capabilities for the integrated analysis of the floating wind turbines.

INNWIND.EU, D4.21, State-of-the-art and implementation of design tools for floating structures

8.2.1 Mooring lines modeling approaches

The equations of motion of a submerged line are, by nature, non-linear. As they are rather complex, they can not be solved analytically. Instead, numerical methods have to be applied. The codes for the simulation of floating wind turbines use several different approaches to describe the mooring system behavior coupled with the platform motions. Some of them are simplified methods as the quasi-static approach or the force-displacements relationships. Other models represent the full dynamics equations of the lines, though this means a much higher computational effort. The following bullet points summarize the main approaches for the modeling of the mooring lines:

- **Quasi-static**
The quasi-static approach consists on the resolution of the static equations of the catenary at every time step of the simulation, given the position of the line fairlead that is attached to the platform. This method neglects the inertial effects and also the hydrodynamic drag produced by waves, currents or the movements of the line.

- **Force-displacement relationship**
In this model, non-linear spring stiffnesses are applied to the translational and rotational degrees of freedom of the platform point where the fairlead of the line is connected. The force-displacement relationship has to be derived using a dynamic line analysis code and the results obtained would be similar to the quasi-static approach.

- **Finite Element model**
In the Finite Element Method (FEM), the dynamic equations of motion of the mooring line are solved by dividing the model into a set of non overlapping elements (bars or beams) that are connected by nodes at their ends. The behavior of the element is expressed by a finite number of degrees of freedom at the element nodes that are the value at the corresponding node of a function (or functions) defined at the element. These functions are called interpolation functions. The response of the whole system is assumed to be obtained from connecting (assembling) all the discrete elements.

- **Finite Difference Method**
In this method, the domain is discretized as in the FEM method, and the derivatives in the system of equations are substituted by finite difference schemes based in Taylor series expansion. In contrast with FEM, the model is discretized not only in the space, but also in time. The Finite Difference Method is considered less stable than FEM.

- **Multi-Body models**
In a Multi-Body model, the system is modeled as a set of rigid or flexible bodies with joints that can allow or constraint the relative displacements between two bodies, or introduce a stiffness or damping. In the case of cable modeling, the elements have to be flexible at least in the axial direction to capture the cable dynamics.

8.2.2 Codes for the simulation of floating wind turbines with simplified mooring lines models

BLADED is one of the most popular commercial codes for the simulation of wind turbines [8.2]. It has been developed by Garrad Hassan, originally for the simulation of onshore wind turbines with a cantilevered tower base. It has been extended to model floating structures using Morison equation for the computation of the hydrodynamic loading. Sea states can be user-defined varying from linear sea-states using Airy theory to irregular sea states defined by JONSWAP (or user-defined) wave energy

spectra. Wave diffraction can be accounted for using a time-domain MacCamy-Fuchs approximation. Non-linear waves' particle kinematics are calculated using stream function theory. The order can be chosen based on wave height, wave period and water depth. In BLADED, the mooring lines are included through non-linear force-displacement relationships applied to the platform degrees of freedom. The aerodynamics of the rotor are based on BEM theory and, for the structural dynamics, a modal approach has been implemented. The modes of tower and blades are calculated internally, before the simulation, using a multi-body model. Additionally, a dynamic wake model and dynamic stall is accounted for.

HAWC2 is a code developed by Risœ-DTU. It also applies the BEM theory for the aerodynamics and the Morison equation for the hydrodynamics. A multi-body formulation is used for the structural dynamics and the mooring lines are represented by a force-displacement relationship.

The code FAST is an open-source and free publicly available software developed by NREL [8.9]. FAST allows the integrated simulation of onshore wind turbines and also offshore wind turbines both with a monopile or a floating substructure. The structural dynamics are modeled using a combined modal and multi-body approach. The aerodynamics are based on the the BEM theory and are solved by a module called AeroDyn. The hydrodynamics of floating platforms are calculated by the module HydroDyn using potential theory. Quadratic drag based on the Morison equation can be added to take into account for the viscous forces. A drag coefficient along the vertical centreline of the platform has to be defined.

8.2.3 Codes for the simulation of floating wind turbines with dynamic mooring lines models

Table 8.1 summarize the codes that currently allow the dynamic simulation of mooring lines and are integrated or have been coupled with a comprehensive offshore floating wind turbine dynamic simulator. Most of the tools included in the table are the result of coupling of different codes with capabilities for the simulation of different domains of the problem, but there are also some tools that have been developed specifically for the simulation of floating wind turbines.

INNWIND.EU, D4.21, State-of-the-art and implementation of design tools for floating structures

Code Name	Code Developer	Moorings Dynamics	Coupled Code for Hydrodynamics	Hydrodynamics Formulation	Coupled Code for Aerodynamics	Aerodynamics Formulation	Dynamic Stall	Coupled Code for WT Structural Dynamics	WT Structural Dynamics	Coupling Developer	References
OrcaFlex	Orcina	FEM (LM)	-	PF+QD/ PF+ME/ME	FAST	BEM/GDW	yes	FAST	Modal-MBS	Orcina	[8.13]
CHARM3D	Texas A&M University & Offshore Dynamics Inc.	FEM	-	PF+ME	FAST	BEM/GDW	yes	FAST	Modal-MBS	Texas A&M University & Offshore Dynamics Inc.	[8.22]
SIMO/RIFLEX	Marintek	FEM	-	PF+ME	HAWC2	BEM	yes	HAWC2	MBS	Risœ & Hydro Oil & Energy	[8.11], [8.23]
SIMO/RIFLEX	Marintek	FEM	-	PF+ME		BEM	yes	-	MBS	-	[8.5]
SIMO/RIFLEX	Marintek	FEM	-	PF+ME	AeroDyn	BEM/GDW	yes	-	MBS	CeSOS/NTNU	[8.19]
ANSYS Aqwa	ANSYS, Inc.	FEM	-	PF+ME	FLEX5	BEM	yes	FLEX5	Modal-MBS	ANSYS, Inc.	-
DeepLines	Principia	FEM	-	PF+QD/ME	Internal DLL	BEM	yes	-	FEM	IFPEN	-
aNySimPHATASpro	MARIN	MBS	-	PF+ME	PHATAS	BEM	yes	PHATAS	Modal-MBS	MARIN & ECN	-

INNWIND.EU, D4.21, State-of-the-art and implementation of design tools for floating structures

SIMPACK	SIMPACK AG	MBS	HydroDyn	PF+QD	AeroDyn	BEM/GDW	yes	-	MBS	University of Stuttgart	[8.14]
ProteusDs	University of Victoria & Dynamic Systems Analysis Ltd.	FEM(LM)	FAST (HydroDyn)	PF+QD	FAST (AeroDyn)	BEM/GDW	yes	FAST	Modal-MBS	University of Victoria	-
3DFloat	IFE	FEM	-	ME	-	BEM	no	-	FEM	-	[8.17]
Hydro-GAST	NTUA	FEM	-	PF+ME	-	BEM/FWV	yes	-	FEM	-	-
FEM: Finite Elements Method *LM: Lumped Mass* *MBS: Multi-Body System*			*PF: Potencial Flow* *QD: Quadratic Drag* *ME: Morison Elements*				*BEM: Blade Element Theory* *GDW: Generalized Dynamic Wake* *FWV: Free Wake Vortex*				

Table 8.1: Summary of floating wind turbines simulation tools including mooring dynamics

INNWIND.EU, D4.21, State-of-the-art and implementation of design tools for floating structures

Many of the codes for the analysis of offshore floating moored platform have been developed during years for the industry of the oil & gas, but these codes do not have the capability of simulating the aerodynamics and structural dynamics of the wind turbine installed on the platform. On the other hand, most of the aeroelastic tools for the simulation of wind turbines do not have capabilities for the computation of floating turbines yet, since the development of offshore floating wind turbines is taking place in the last few years. This is the reason why many of the advanced codes for the hydrodynamic analysis of floating platforms coming from the oil & gas industry have been coupled with aeroelastic codes from the wind energy sector.

This is the case of OrcaFlex, a commercial software developed by Orcina for the dynamic analysis of offshore structures, including catenary systems as mooring lines, flexible risers or umbilical cables [8.18]. Orcina has coupled OrcaFlex with the FAST code [8.13]. In the resulting tool, FAST is responsible for the simulation of aerodynamics, the control system and the structural dynamics of flexible elements as the rotor and the tower. OrcaFlex computes the hydrodynamics of the platform and the dynamics of the mooring system.

A similar coupling involving FAST for the representation of the wind turbine aerodynamics and structural dynamics has been implemented with the CHARM3D code that is in charge of the computation of the floating body and the mooring system dynamics [8.22]. CHARM3D is a code for purchase developed by Texas A&M and Offshore Dynamics, Inc. for the simulation of moored floating structures, but it is not able to include a wind turbine model taking into account the effects of coupled aerodynamics, structural dynamics or the control actions.

SIMO/RIFLEX is one of the leading software for the analysis of offshore structures. Historically has been widely used in the oil & gas industry. RIFLEX is a finite element module for the dynamic analysis of mooring lines and SIMO is the module that performs the time domain hydrodynamic analysis of the floating platform, using potential theory. Morison elements can also be included. Marintek has developed a module for the calculation of the aerodynamic forces on the wind turbine rotor based on the BEM theory [8.5]. These forces are implemented in the code as a user-specified external force. The forces obtained at each of the blade elements are integrated and the resulting 3 forces and 3 moments are applied to the SIMO model as an external load.

The SIMO/RIFLEX code has also been coupled with HAWC2 for the inclusion of the wind turbine's aerodynamic loading. This coupling has been implemented by Risœ and Hydro Oil & Energy [8.11], [8.23]. HAWC2 is an aeroelastic code specific for the simulation of bottom fixed wind turbines developed by Risœ National Laboratory [8.10]. It uses the BEM theory for the aerodynamics and a Multi-Body formulation for the structural dynamics.

ANSYS Aqwa is a general purpose software for the analysis of offshore structures. The mooring system can be modeled using Finite Elements theory. ANSYS, Inc. has coupled his software with the code FLEX5 but neither the tool nor the documentation are publicly available. FLEX5 is a code created by DTU for the aeroelastic computation of onshore wind turbines. It is based on the BEM theory and uses a modal representation of the flexible bodies.

DeepLines is a general code for the simulation of offshore structures based on the potential theory or, alternatively, the Morison equation. It includes the dynamic analysis of the mooring system. Currently, PRINCIPIA, the company owner of the code, is collaborating with IFPEN (Institut Français du Pétrole - Energies Nouvelles) adding to the code capabilities for the simulation of floating wind turbines. The rotor aerodynamics model is based on the BEM theory and is coupled with the DeepLines code through a DLL generated by IFPEN. A preliminary verification of the tool has been performed within the IEA Annex 30 (OC4).

The integrated tool aNySimPHATAS*pro*, developed by MARIN, is the result of the coupling of the code aNySim*pro* and PHATAS. aNySim has been developed by MARIN for the analysis of offshore structures and is able to consider the mooring dynamics using a Multi-Body formulation. PHATAS is a code developed by ECN for the aeroelastic simulation of onshore wind turbines.

SIMPACK is another commercial software for the dynamic simulation of mechanisms widely used in many different industrial sectors. It is a general purpose program that has been used to model the structural dynamics of a floating wind turbine, including the mooring lines. The aerodynamics and hydrodynamics have been introduced in the model by coupling with SIMPACK the NREL's AeroDyn and HydroDyn codes [8.14].

ProteusDS is a specific software for the dynamic analysis of mooring lines, that uses a finite elements formulation with the cable mass lumped at the nodes. It has been developed by the University of Victoria and Dynamic Systems Analysis Ltd. ProteusDS has been compiled as a DLL and then coupled with the FAST code, providing a tool for the integrated simulation of floating wind turbines, including the dynamics of the mooring system.

There are also a few codes specialized for the simulation of offshore floating wind turbines that include the mooring dynamics.

3DFloat is an specific code for the integrated analysis of onshore and offshore wind turbines, including mooring system dynamics. It has been developed by IFE [8.17] and uses the BEM theory for the aerodynamics, the Finite Element Method for the structural and mooring lines dynamics and the Morison equation for the hydrodynamics.

Hydro-GAST is another integrated code developed by NTUA that uses potential theory for the hydrodynamics, the BEM theory or the Free Wake Vortex theory for the aerodynamics and a Finite Elements formulation for the mooring lines and structural dynamics.

8.2.4 Other specific codes for the dynamic analysis of mooring lines

Many other programs specific for the simulation of the dynamics of mooring lines exist, but they do not have capabilities for the simulation of the rest of components of a floating wind turbine and they have neither been coupled with other tools for this purpose though this could be done in the future. Some examples of specific codes for mooring lines based on the Finite Elements method are: MDD (Mooring Design and Dynamics) (Centre for Earth and Ocean Research, University of Victoria) [8.3], Ariane7 (VeriSTAR) [8.1], CABLE3D (Texas A&M), Flexcom V8 (MCS Kenny), HYBER (USFOS) [8.8] and SeaDyn (US Navy) [8.24]. The code LINES, developed by the Massachusetts Institute of Technology (MIT) is based in a Multi-Body formulation. The Massachusetts Institute of Technology, together with Woods Hole Oceanographic Institute has also developed the WHOIcable code [8.6], that is based in the Finite Difference method. This code is publicly available.

8.2.5 Summary on codes for mooring line dynamics

Many codes for the dynamic analysis of mooring lines exist, but few of them have been specifically developed for the simulation of offshore wind turbines. The wind energy industry has its own particular requirements and challenges: for instance, a reliable simulation of the dynamics of a floating wind turbine requires the coupled simulation in the time domain of many different phenomena as the aerodynamics, the hydrodynamics, the structural dynamics, the mooring lines dynamics or the control actions.

Some of the codes previosuly mentioned are specialized software for the analysis of cable dynamics and others are general codes for the modeling of offshore structures, mainly for the naval or oil & gas industries. Among the few comprehensive tools that can compute an integrated simulation of the whole system, most of them are the result of the coupling of different existing software. This kind of coupled tools can present several drawbacks. Simulation programs coming from different industrial sector as naval or oil & gas, may be too specialized in some of the parts of the problem and too simplified in the rotor aerodynamics representation. In addition, the coupling between codes can suppose a loose on the computational efficiency or on the robustness of the simulations. These are important aspects when you need to integrate in your design process the

simulation of a huge battery of load cases: the loads calculation of a floating wind turbine according to the certification guidelines requires the simulation of several thousands of load cases. Specialized tools in wind energy usually represent the wind turbine using a reduced number of degrees of freedom. These type of tools can have advantages in computational cost over other software for general purpose. The introduction of a dynamic model for the mooring lines implies the inclusion of a high number of additional degrees of freedom, and therefore represents a challenge in terms of computational effort.

8.2.6   OPASS code capabilities

CENER's code for the dynamic simulation of mooring lines has been called OPASS (Offshore Platforms Anchoring System Simulator). OPASS formulation is based on finite elements, with three translational degrees of freedom defined at each node. The code considers the effect of inertia, hydrodynamic added mass, gravity, hydrostatics, water drag, axial elasticity and structural damping. The code is able to simulate the dynamics of mooring lines. These components are usually built with chains and wires: thus, the bending stiffness is low and can be neglected. The contact of the line with the seabed are also included. The line-seabed static and dynamic friction are modelled through a springs model.

The OPASS code has been coupled with the FAST code, whose original mooring lines model is a quasi-static approach. The new coupled code provides an integrated tool for the simulation of floating wind turbines considering the aerodynamics, hydrodynamics, structural dynamics, mooring system dynamics and control in a coupled computation. The validation of this tool is being performed in the IEA Annex30 (OC4).

OPASS programming has been optimized to achieve a computer efficient code. The loads calculation of a floating wind turbine according to guidelines as IEC 61400-3 requires the simulation of several thousands of load cases. Tools for the computation of offshore wind turbines as Bladed or FAST have a very limited number of degrees of freedom. The inclusion of a dynamic mooring lines model means the introduction of several hundreds of new degrees of freedom which is a challenge from the point of view of computational effort. For this reason, a efficient programming of a tool as OPASS, that has been specifically developed for the wind energy sector is a critical issue.

Three different time integration schemes are available in the OPASS code: a simple explicit scheme based in the central difference formula [8.12], the Runge-Kutta-Nyström scheme [8.7] and the Adams-Moulton-Bashforth [8.4].

8.2.7   OPASS code current and future developments

Currently, the inclusion of new rotational degrees of freedom on the OPASS code is under development. This new feature will allow to apply the code for the simulation of slender structures where bending can not be neglected as dynamic cables for the energy evacuation of the floating platform. The new capability will allow to evaluate the effect of the dynamic cable over the platform dynamics and also will be a useful tool for the design and integrated loads calculation of dynamic cables.

In addition, it is planned to include a new integration "stiff" scheme for the equations of motion as the Generalized -α method. It is expected that this method will allow to increase the calculation time step improving the computational simulation time.

A preliminar verification against other codes as Simo-Riflex of the cable-seabed friction model has already been performed with success. Nevertheless, it is expected to perform a more extensive validation of the cable-seabed friction model in the future.

INNWIND.EU, D4.21, State-of-the-art and implementation of design tools for floating structures

8.3 Equations of Motion Implemented in OPASS

8.3.1 Basic Dynamic Equations

A mooring line has one of his ends fixed to the seabed by an anchor and the other end, called fairlead, is attached to the floating platform. Part of the line can be in contact with the seabed. A coordinate system l_0 is defined in the cable as the distance along the unstretched length of the cable, from the anchor to the cable section to be considered, as it is shown in **Figure 8.1**.
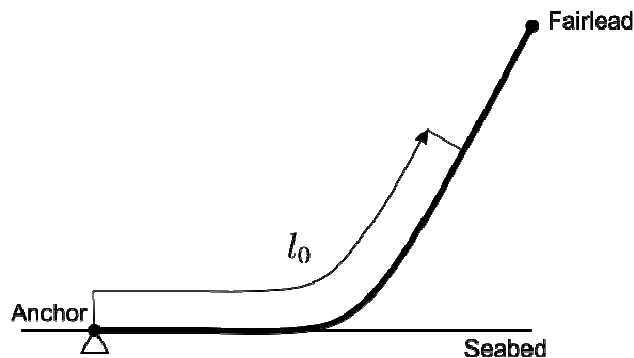
Figure 8.1: Cable line and reference length along the cable

As the cable is a very slender structure, shear forces can be neglected. If the bending and torsion stiffness are low enough to also be neglected, the only internal forces are the tension T and the structural damping F_D. Both internal forces are always tangential to the cable. The external forces acting on the cable are the gravity, the buoyancy and the hydrodynamic drag forces. There is also and additional inertial force due to the volume of water displaced by the line in movement (added mass).

We are going to consider an infinitesimal length of cable dl, at point P, that is located at a distance l_0 along the unstretched length of the cable. The forces acting on this portion of the cable are showed in Figure 8.2 . The resultant force from hydrostatic pressure and gravity $\vec{F}_1$, is vertical. The hydrodynamic drag force is split into two components: normal and tangential to the cable. The tangential component is $\vec{F}_2$ and the normal component is $\vec{F}_3$. The inertial force coming from the added mass, $\vec{F}_4$ is supposed to have only a component normal to the cable. All these forces are expressed per unit of unstretched length and in the global reference system.
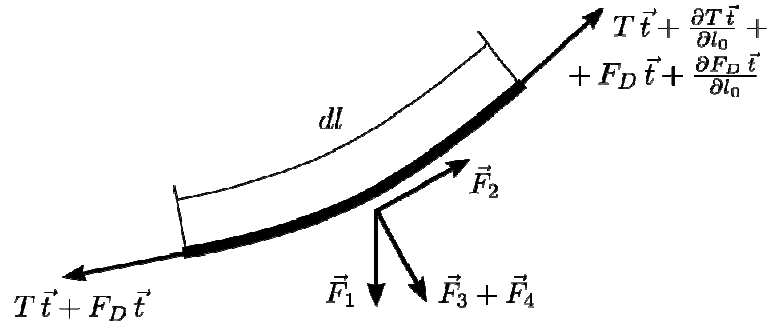
Figure 8.2: Forces acting on an infinitesimal length of cable

According to Figure 8.2, and considering the inertial forces in the balance of forces, we can write the following equation in the global coordinate system:

$$\gamma \ddot{\vec{R}} - \frac{\partial (T \vec{t})}{\partial l_0} - \frac{\partial (F_D \vec{t})}{\partial l_0} - (\vec{F}_1 + \vec{F}_2 + \vec{F}_3 + \vec{F}_4) = 0 \qquad (8.1)$$

Where γ is the line mass per unit of cable unstretched length, $\ddot{\vec{R}}$ is the acceleration of point P in the global reference system and, $\vec{t}$ is the vector tangential to the cable at point P in the global reference system.

If we relate the displacements of the cable to an initial reference cable configuration R, then the current position vector $\vec{R}$ of point P can be expressed in the global reference system as:

$$\vec{R} = \vec{R}_0 + \vec{U} \qquad (8.2)$$

Where $\vec{R}_0$ is the initial position vector of point P at the reference line configuration R, and $\vec{U}$ is the displacement vector. The vector tangential to the line at point P in equation (8.1) can be calculated as:

$$\vec{t} = \frac{\dfrac{\partial \vec{R}}{\partial l_0}}{\left| \dfrac{\partial \vec{R}}{\partial l_0} \right|} \qquad (8.3)$$

8.3.1.1 Elastic force

For the infinitesimal element that we are considering, the axial deformation ε is defined as:

$$\varepsilon = \frac{\partial l}{\partial l_0} - 1 = \left| \frac{\partial \vec{R}}{\partial l_0} \right| - 1 \qquad (8.4)$$

Where l is the distance along the stretched length of the cable.

The tension at point P can be obtained from the constitutive equation:

INNWIND.EU, D4.21, State-of-the-art and implementation of design tools for floating structures

$$T = EA\varepsilon \tag{8.5}$$

Where E is the material Young's modulus and A is the section area of the cable.

8.3.1.2 Structural damping force

The structural damping is based on the Rayleigh model. In general, Rayleigh model assumes the damping to be proportional to the mass and the stiffness. But in our model, we are going to neglect the term of the mass and we are going to assume the damping force F_D at point P proportional only to the stiffness EA. The proportionality coefficient is β. Thus, we can formulate:

$$F_D = \beta EA\dot{\varepsilon} \tag{8.6}$$

Where $\dot{\varepsilon}$ is the deformation velocity.

8.3.1.3 Gravity and hydrostatic forces

The gravity force is a body force: it acts throughout the volume of the cable. By contrast, the hydrostatic force is not a body force: it is produced by the integration of the hydrostatic pressure over the element. Nevertheless, it can be treated as a volume force if the element considered is totally surrounded by water and can be calculated according to Archimedes' Principle. For a cable this is not strictly true, but as the diameter of the section is small in comparison with the length, the error induced by this assumption is neglectable. The resultant force from hydrostatic pressure and gravity per unit of unstretched length, expressed by $\vec{F}_1$, is the weight of the cable minus the weight of the displaced volume of water per unit of unstretched length. The direction of the force is vertical. Thus:

$$\vec{F}_1 = \begin{bmatrix} 0 \\ 0 \\ -\gamma_r g \end{bmatrix} \tag{8.7}$$

and

$$\gamma_r = \frac{\rho_c - \rho_w}{\rho_c}\gamma \tag{8.8}$$

Where g is the gravity constant, γ_r is the equivalent mass per unit length of the cable submerged in water, ρ_c is the density of the cable and ρ_w is the density of the water.

8.3.1.4 Hydrodynamic forces

The hydrodynamic forces considered equation (8.1) are the tangential drag $\vec{F}_2$, the normal drag $\vec{F}_3$ and the hydrodynamic inertial force $\vec{F}_4$, that is also normal to the cable. These hydrodynamic forces are represented in Figure 8.3.

INNWIND.EU, D4.21, State-of-the-art and implementation of design tools for floating structures
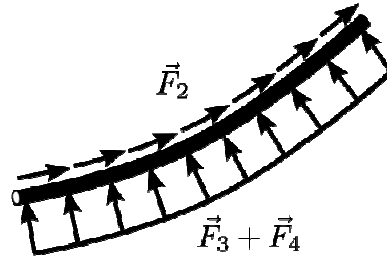
Figure 8.3: Tangential drag, normal drag and added mass force along the cable

Using the Morison equation for slender cylinders [8.16], the value of the tangential drag force per unit length of the unstretched cable can be calculated as:

$$\vec{F}_2 = C_2 \, | \vec{V}_t | \, \vec{V}_t (1+\varepsilon) = C_2 \left(| \vec{V} \cdot \vec{t} | \vec{V} \cdot \vec{t} \right) (1+\varepsilon) \vec{t}$$

$$C_2 = \frac{1}{2} C_{dt} D \rho_w$$

(8.9)

Where C_{dt} is the tangential drag coefficient and D is the diameter of the cable. The vector $\vec{V}$ is the relative velocity between the water and the cable and $\vec{V}_t$ is the component tangential to the element, both expressed in the global reference system.

In a similar way can be obtained the drag force normal to the cable per unit length:

$$\vec{F}_3 = C_3 \, | \vec{V}_n | \, \vec{V}_n (1+\varepsilon) = C_3 \left[\vec{V} \cdot \vec{V} - \left(\vec{V} \cdot \vec{t} \right)^2 \right]^{\frac{1}{2}} \left[\vec{V} - \left(\vec{V} \cdot \vec{t} \right) \vec{t} \right] (1+\varepsilon)$$

$$C_3 = \frac{1}{2} C_{dn} D \rho_w$$

(8.10)

Where C_{dn} is the normal drag coefficient and $\vec{V}_n$ is the component normal to the element of the relative velocity between the water and the cable.

The hydrodynamic inertial force per unit of unstretched cable length is:

$$\vec{F}_4 = -C_4 (1+\varepsilon) \left[\ddot{\vec{R}} - (\ddot{\vec{R}} \cdot \vec{t}) \vec{t} \right]$$

$$C_4 = C_{mn} \frac{\pi D^2}{4} \rho_w$$

(8.11)

Where C_{mn} is the normal added mass coefficient.

Substituting equations (8.5), (8.6) and (8.11) into (8.1) finally results in:

INNWIND.EU, D4.21, State-of-the-art and implementation of design tools for floating structures

$$\gamma\ddot{\vec{R}} + C_4(1+\varepsilon)\left[\ddot{\vec{R}} - (\ddot{\vec{R}} \cdot \vec{t})\vec{t}\right] - \frac{\partial(EA\varepsilon\vec{t})}{\partial l_0} - \frac{\partial(\beta EA\dot{\varepsilon}\vec{t})}{\partial l_0} - \vec{F}_1 - \vec{F}_2 - \vec{F}_3 = 0$$

(8.12)

8.3.2 The Finite Elements Equations

8.3.2.1 Virtual Works principle

According to the Virtual Works Principle, the path followed by a system is the one for which the difference between the work performed by the forces along this path and other nearby paths is zero. If we apply a small (virtual) displacement that satisfies the boundary conditions $\delta\vec{U}$ with respect to a certain configuration at time t, the virtual work W_V done by the forces along the cable length must be zero. The virtual work can be obtained by multipliying equation (8.12) by the virtual displacement $\delta\vec{U}$ and integrating along the cable length:

$$W_V = \int_0^L \left\{ \left(\gamma\ddot{\vec{R}} + C_4(1+\varepsilon)\left[\ddot{\vec{R}} - (\ddot{\vec{R}} \cdot \vec{t})\vec{t}\right] \right) \cdot \delta\vec{U} - \left(\vec{F}_1 + \vec{F}_2 + \vec{F}_3 \right) \cdot \delta\vec{U} + \right.$$
$$\left. + EA\varepsilon\frac{\partial\delta\vec{U}}{\partial l_0} \cdot \vec{t} + \beta EA\dot{\varepsilon}\frac{\partial\delta\vec{U}}{\partial l_0} \cdot \vec{t} \right\} dl_0 - [EA\varepsilon\vec{t} \cdot \delta\vec{U}]_0^L - [\beta EA\dot{\varepsilon}\vec{t} \cdot \delta\vec{U}]_0^L = 0$$

(8.13)

Where L is the total cable length. The last two terms represent the work performed by the end forces at the initial and final faces of the cable. If the anchor and the fairlead of the cable are fixed or their displacements are prescribed, these terms are zero. Considering the boundary conditions of our problem, the anchor will remain fixed and the fairlead position will be determined by the platform displacements, thus, these terms are neglected in the following discussion.

8.3.2.2 Interpolation by shape functions

The mooring line is discretized into n finite elements using straight bar members. A bar has two main characteristics:

- The axial direction is much larger than the transversal directions.
- The bar resists an internal force in the axial direction

A local coordinate ξ_i is defined for each element i. ξ_i is 0 at the beginning of the element and it is 1 at the end as is described in Figure 8.4.
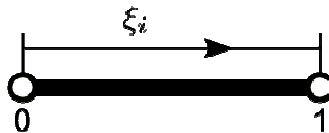
Figure 8.4: Element *I* local coordinate

Thus, the position of a point P along the unstreched length of the cable, l_0, can be expressed as:

INNWIND.EU, D4.21, State-of-the-art and implementation of design tools for floating structures

$$l_0 \approx l_{0i} + \xi_i L_i \tag{8.16}$$

Where L_i is the length of the element i and l_{0i} is the unstretched length to the initial node of the element i:

$$l_{0i} = \sum_{j=1}^{i-1} L_j \tag{8.17}$$

These parameters are shown in Figure 8.5.
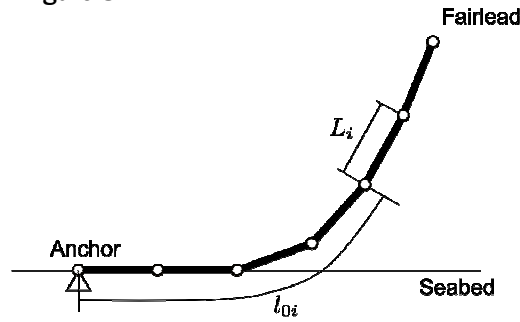
Figure 8.5: Discretized cable

All the magnitudes are assumed to be continuous along the finite element and they are approximated by interpolation of the values at the element nodes based in the following linear shape functions:

$$\begin{aligned} N_1 &= \xi_i \\ N_2 &= 1 - \xi_i \end{aligned} \tag{8.18}$$

The interpolations of these magnitudes can be expressed in a compact way by means of the shape functions matrix N :

$$N = \begin{bmatrix} 1-\xi_i & 0 & 0 & \xi_i & 0 & 0 \\ 0 & 1-\xi_i & 0 & 0 & \xi_i & 0 \\ 0 & 0 & 1-\xi_i & 0 & 0 & \xi_i \end{bmatrix} \tag{8.19}$$

Then, for the element i, we can write:

$$\vec{r}(\xi_i, t) \approx N(\xi_i) \vec{x}_i(t) \tag{8.20}$$

$$\vec{u}(\xi_i, t) \approx N(\xi_i) \vec{p}_i(t) \tag{8.21}$$

$$\delta\vec{u}(\xi_i, t) \approx N(\xi_i) \delta\vec{p}_i(t) \tag{8.22}$$

INNWIND.EU, D4.21, State-of-the-art and implementation of design tools for floating structures

$$\vec{r}(\xi_i, t) \approx N(\xi_i)\vec{x}_i(t) \tag{8.23}$$

$$\vec{v}(\xi_i, t) \approx N(\xi_i)\vec{v}_i(t) \tag{8.24}$$

Where $\vec{r}$ and $\dot{\vec{r}}$ are the 3 x 1 position and velocity vectors in the element reference system and $\vec{x}_i$ and $\dot{\vec{x}}_i$ are the 6 x 1 element nodal position and element nodal velocity vectors, both in the element reference system. $\vec{u}$ and $\delta\vec{u}$ are the 3 x 1 displacement and virtual displacement vectors and $\vec{p}_i$ and $\delta\vec{p}_i$ are the respective 6 x 1 element i nodal displacement and element i nodal virtual displacement vectors, all in the element reference system. Finally, $\vec{v}$ is the relative velocity of the water and $\vec{v}_i$ is the element i nodal vector for the relative water velocity in the local reference system.

In the case of the accelerations, different shape functions are chosen. Instead of linear shape functions, discontinuous step functions are defined. The reason is that with this election, we will obtain a mass matrix composed by 3 x 3 submatrices located at the diagonal. This is an important advantage for the inversion of the matrix that can be done with less computational effort.

$$N' = \begin{bmatrix} \psi_1 & 0 & 0 & \psi_2 & 0 & 0 \\ 0 & \psi_1 & 0 & 0 & \psi_2 & 0 \\ 0 & 0 & \psi_1 & 0 & 0 & \psi_2 \end{bmatrix} \tag{8.25}$$

Where:

$$\begin{aligned} \left. \begin{array}{l} \psi_1 = 1 \\ \psi_2 = 0 \end{array} \right\} \xi_i \in [0, 0.5] \\[2em] \left. \begin{array}{l} \psi_1 = 0 \\ \psi_2 = 1 \end{array} \right\} \xi_i \in [0.5, 1] \end{aligned} \tag{8.26}$$

So, the accelerations within element i are approximated as:

$$\ddot{\vec{r}}(\xi_i, t) \approx N'(\xi_i)\ddot{\vec{x}}_i(t) \tag{8.27}$$

Where $\ddot{\vec{r}}$ is the acceleration vector and $\ddot{\vec{x}}_i$ is the 6 x 1 element vector with the nodal accelerations, both in the local element system.

Finally, the matrix B is defined as the derivative of N:

$$B = \frac{\partial N}{\partial \xi_i} = \begin{bmatrix} -1 & 0 & 0 & 1 & 0 & 0 \\ 0 & -1 & 0 & 0 & 1 & 0 \\ 0 & 0 & -1 & 0 & 0 & 1 \end{bmatrix} \tag{8.28}$$

8.3.2.3 Local to global transformation matrix

The magnitudes in the local reference system of the i element and in the global reference system can be related through the 3 x 3 local to global transformation matrix T_i. To find the unit direction vectors, $\vec{e}_{1i}$, $\vec{e}_{2i}$ and $\vec{e}_{3i}$, that compose the local reference system attached to the bar element i, together with the element initial node (node 1) and final node (node 2), an additional node has to be defined. The position of this third node is arbitrary, though it has to be located out of the element, to define the plane containing the $\vec{e}_{2i}$ unit vector. The element i local reference system is illustrated in Figure 8.6.
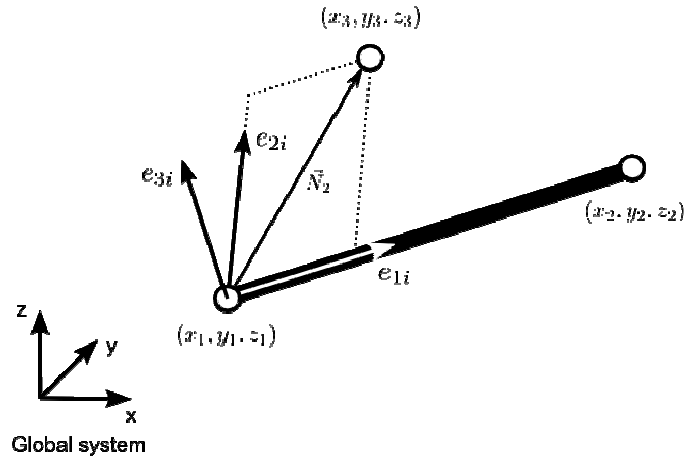
Figure 8.6: Global and element local reference systems

If (x_1, y_1, z_1), (x_2, y_2, z_2) and (x_3, y_3, z_3) are the coordinates of the node 1, node 2 and node 3 of the element i, the following vectors can be obtained:

$$\vec{n}_1 = \begin{bmatrix} x_2 - x_1 \\ y_2 - y_1 \\ z_2 - z_1 \end{bmatrix} \qquad \vec{N}_2 = \begin{bmatrix} x_3 - x_1 \\ y_3 - y_1 \\ z_3 - z_1 \end{bmatrix} \qquad \vec{n}_3 = \vec{n}_1 \wedge \vec{N}_2 \qquad \vec{n}_2 = \vec{n}_3 \wedge \vec{n}_1 \quad \textbf{(8.29)}$$

Then, the unit vectors of the local reference system for the i element can be calculated as:

$$\vec{e}_{1i} = \frac{\vec{n}_1}{|\vec{n}_1|} \qquad \vec{e}_{2i} = \frac{\vec{n}_2}{|\vec{n}_2|} \qquad \vec{e}_{3i} = \frac{\vec{n}_3}{|\vec{n}_3|} \qquad \textbf{(8.30)}$$

And then, the local to global transformation matrix is just:

$$T_i = \begin{bmatrix} \vec{e}_{1i} & \vec{e}_{2i} & \vec{e}_{3i} \end{bmatrix} \qquad \textbf{(8.31)}$$

INNWIND.EU, D4.21, State-of-the-art and implementation of design tools for floating structures

In the case of the element nodal vectors, we define a 6 x 6 transformation matrix, T_I as:

$$T_I = \begin{bmatrix} & & & 0 & 0 & 0 \\ & T_i & & 0 & 0 & 0 \\ & & & 0 & 0 & 0 \\ 0 & 0 & 0 & & & \\ 0 & 0 & 0 & & T_i & \\ 0 & 0 & 0 & & & \end{bmatrix}$$

(8.32)

The matrices N and N' interpolate the nodal magnitudes in the element local reference system. By means of the transformation matrices, we can define new matrices N_{gi}, N'_{gi} and B_{gi} to operate with the magnitudes at element i in the global system:

$$N_{gi} = T_i N T_I^T$$

(8.33)

$$N_{gi}' = T_i N' T_I^T$$

(8.34)

$$B_{gi} = T_i B T_I^T$$

(8.35)

Thus:

$$\vec{R}(\xi_i, t) \approx N_{gi}(\xi_i)\vec{X}_i(t)$$

(8.36)

$$\vec{U}(\xi_i, t) \approx N_{gi}(\xi_i)\vec{P}_i(t)$$

(8.37)

$$\delta\vec{U}(\xi_i, t) \approx N_{gi}(\xi_i)\delta\vec{P}_i(t)$$

(8.38)

$$\dot{\vec{R}}(\xi_i, t) \approx N_{gi}(\xi_i)\dot{\vec{X}}_i(t)$$

(8.39)

$$\ddot{\vec{R}}(\xi_i, t) \approx N'_{gi}(\xi_i)\ddot{\vec{X}}_i(t)$$

(8.40)

$$\vec{V}(\xi_i, t) \approx N_{gi}(\xi_i)\vec{V}_i(t)$$

(8.41)

Where $\dot{\vec{R}}$ is the 3 x 1 velocity vector, and $\vec{X}_i$, $\dot{\vec{X}}_i$ and $\ddot{\vec{X}}_i$ are the 6 x 1 element i nodal position, velocity and acceleration vectors, all in the global reference system. $\vec{P}_i$ and $\delta\vec{P}_i$ are the element nodal displacement and virtual displacement vectors, also in the global system. Finally, $\vec{V}_i$ is the element nodal relative water velocity in the global reference system.

INNWIND.EU, D4.21, State-of-the-art and implementation of design tools for floating structures

8.3.2.4 Definition of the adjacency matrix

We define for each element i an adjacency matrix A_i, composed by elements with value 0 or 1, that relates the 6 x 1 element i nodal vectors with the whole 6(n+1) x 1 discretized system global vector. So, the dimension of A_i is 6 x 6(n+1). If the nodes are numbered consecutively, then the adjacency matrix of the element i has the following structure:

$$\begin{bmatrix} 0 & & 0 & 1 & 0 & 0 & 0 & 0 & 0 & 0 & & 0 \\ 0 & & 0 & 0 & 1 & 0 & 0 & 0 & 0 & 0 & & 0 \\ 0 & \dots & 0 & 0 & 0 & 1 & 0 & 0 & 0 & 0 & \dots & 0 \\ 0 & & 0 & 0 & 0 & 0 & 1 & 0 & 0 & 0 & & 0 \\ 0 & & 0 & 0 & 0 & 0 & 0 & 1 & 0 & 0 & & 0 \\ 0 & & 0 & 0 & 0 & 0 & 0 & 0 & 1 & 0 & & 0 \\ \\ Index: & 1 & \dots & i-1 & i & i+2 & i+3 & i+4 & i+5 & i+6 & i+7 & \dots & 6n+6 \end{bmatrix} \quad (8.42)$$

And then:

$$\vec{X}_i = A_i \vec{X} \tag{8.43}$$

$$\dot{\vec{X}}_i = A_i \dot{\vec{X}} \tag{8.44}$$

$$\ddot{\vec{X}}_i = A_i \ddot{\vec{X}} \tag{8.45}$$

$$\delta\vec{P}_i = A_i \delta\vec{P} \tag{8.46}$$

This is a mathematical way to express the assembly of the discretized matrices implemented in the code.

8.3.2.5 Discretization of elastic forces

As we have neglected the elastic forces acting at the end sections of the cable, the term for the work produced by the elastic forces $W_{elastic}$ in the equation (8.13) is:

$$W_{elastic} = \int_0^L EA\varepsilon \frac{\partial \delta\vec{U}}{\partial l_0} \cdot \vec{t}\, dl_0 \tag{8.47}$$

The discretized element deformation ε_i is obtained deriving the expression (8.36) and introducing it into equation (8.4):

INNWIND.EU, D4.21, State-of-the-art and implementation of design tools for floating structures

$$\varepsilon = \left| \frac{\partial \vec{R}}{\partial l_0} \right| - 1; \varepsilon_i = \sqrt{\frac{B_{gi} \vec{X}_i}{L_i} \cdot \frac{B_{gi} \vec{X}_i}{L_i}} - 1 = \frac{\sqrt{\vec{X}_i^T B_{gi}^T B_{gi} \vec{X}_i}}{L_i} - 1 \qquad \text{(8.48)}$$

$$\sum_{j=1}^{i-1} jL_j < l_0 \le \sum_{j=1}^{i} jL_j$$

On the other hand, from derivation of equation (8.38) we have:

$$\frac{\partial \delta \vec{U}}{\partial l_0} \approx B_{gi} \frac{\delta \vec{P}_i}{L_i} \qquad \sum_{j=1}^{i-1} jL_j < l_0 \le \sum_{j=1}^{i} jL_j \qquad \text{(8.49)}$$

And the tangential vector $\vec{t}$ can be expressed introducing into (8.3) the derivative of the expression (8.36):

$$\vec{t} = \frac{\dfrac{\partial \vec{R}}{\partial l_0}}{\left| \dfrac{\partial \vec{R}}{\partial l_0} \right|} \approx \frac{B_{gi} \vec{X}_i}{|B_{gi} \vec{X}_i|} = \frac{B_{gi} \vec{X}_i}{L_i(1 + \varepsilon_i)} \qquad \sum_{j=1}^{i-1} jL_j < l_0 \le \sum_{j=1}^{i} jL_j \qquad \text{(8.50)}$$

Introducing into (8.47) the expressions (8.43), (8.46), (8.49) and (8.50), we have:

$$W_{elastic} \approx \sum_{i=1}^{n} \int_0^1 EA\varepsilon_i \frac{\delta \vec{P}^T A_i^T B_{gi}^T B_{gi} A_i \vec{X}}{L_i(1 + \varepsilon_i)} d\xi \qquad \text{(8.51)}$$

8.3.2.6 Discretization of structural damping

The term in equation (8.13) for the work produced by the structural damping forces W_{damp} is:

$$W_{damp} = \int_0^L \beta EA\dot{\varepsilon} \frac{\partial \delta \vec{U}}{\partial l_0} \cdot \vec{t} \, dl_0 \qquad \text{(8.52)}$$

The element deformation velocity can be obtained by the time derivation of the expression (8.48):

$$\dot{\varepsilon} \approx \dot{\varepsilon}_i = \frac{d\varepsilon_i}{dt} = \frac{\vec{X}_i^T B_{gi}^T B_{gi} \dot{\vec{X}}_i}{L_i^2(1 + \varepsilon_i)} \qquad \sum_{j=1}^{i-1} jL_j < l_0 \le \sum_{j=1}^{i} jL_j \qquad \text{(8.53)}$$

If we follow a parallel reasoning as to discretize the work of the elastic forces, we obtain the following expression:

$$W_{damp} \approx \sum_{i=1}^{n} \int_0^1 \beta EA\dot{\varepsilon}_i \frac{\delta \vec{P}^T A_i^T B_{gi}^T B_{gi} \vec{X}_i}{L_i(1 + \varepsilon_i)} d\xi \qquad \text{(8.54)}$$

And using (8.44) and (8.53), we have:

INNWIND.EU, D4.21, State-of-the-art and implementation of design tools for floating structures

$$W_{damp} = \sum_{i=1}^{n} \int_0^1 \beta EA \frac{\delta \vec{P}^T A_i^T B_{gi}^T B_{gi} \vec{X}_i \vec{X}_i^T B_{gi}^T B_{gi} A_i \ddot{\vec{X}}}{L_i^3 (1 + \varepsilon_i)^2} d\xi \qquad (8.55)$$

8.3.2.7 Discretization of external forces

The external forces considered are the gravity and the buoyancy $\vec{F}_1$, the tangential hydrodynamic force $\vec{F}_2$ and the normal hydrodynamic drag $\vec{F}_3$. The force produced by the hydrodynamic added mass is studied separately, as an inertial force.

Thus, the work due to these external forces in equation (8.13), $W_{external}$, is:

$$W_{external} = \int_0^L -\left(\vec{F}_1 + \vec{F}_2 + \vec{F}_3\right) \cdot \delta \vec{U} \, dl_0 \qquad (8.56)$$

The discretization of the distributed external forces $\vec{F}_1$, $\vec{F}_2$ and $\vec{F}_3$ respectively results in the resultant gravity and buoyancy elemental force: $\vec{F}_{1i}$; the tangential drag elemental force: $\vec{F}_{2i}$ and the normal drag elemental force: $\vec{F}_{3i}$.

The expression for $\vec{F}_{1i}$ can be easily obtained since $\vec{F}_1$ is constant and does not depend on the element local coordinate ξ. Thus, the discretized gravity and buoyancy force for the element i is just:

$$\vec{F}_1 \approx \vec{F}_{1i} = \begin{bmatrix} 0 \\ -\gamma_r g \\ 0 \end{bmatrix} \qquad (8.57)$$

$\vec{F}_{2i}$ is calculated from expression (8.9), using (8.41) and (8.50):

$$\vec{F}_2 \approx \vec{F}_{2i} = \frac{C_2}{L_i^3 (1 + \varepsilon_i)^2} | \vec{V}_i^T N_{gi}^T B_{gi} \vec{X}_i | \left(\vec{V}_i^T N_{gi}^T B_{gi} \vec{X}_i \right) B_{gi} \vec{X}_i$$

$$\sum_{j=1}^{i-1} j L_j < l_0 \leq \sum_{j=1}^{i} j L_j \qquad (8.58)$$

And in the same way, $\vec{F}_{3i}$ is obtained introducing (8.41) and (8.50) in the expression (8.10):

INNWIND.EU, D4.21, State-of-the-art and implementation of design tools for floating structures

$$\vec{F_3} \approx \vec{F}_{3i} = C_3(1+\varepsilon_i)\left[\vec{V}_i^T N_{gi}^T N_{gi}\vec{V}_i - \frac{\left(\vec{V}_i^T N_{gi}^T B_{gi}\vec{X}_i\right)^2}{(1+\varepsilon_i)^2 L_i^2}\right]^{\frac{1}{2}}$$

$$\left[N_{gi}\vec{V}_i - \frac{\left(\vec{V}_i^T N_{gi}^T B_{gi}\vec{X}_i\right)B_{gi}\vec{X}_i}{(1+\varepsilon_i)^2 L_i^2}\right] \qquad \sum_{j=1}^{i-1}jL_j < l_0 \leq \sum_{j=1}^{i}jL_j$$

(8.59)

Including into (8.56) the expressions (8.38), (8.46), (8.57), (8.58) and (8.57) we have:

$$W_{external} \approx \sum_{j=1}^{i-1}\int_0^1 -\delta\vec{P}^T A_i^T N_{gi}^T\left(\vec{F}_{1i} + \vec{F}_{2i} + \vec{F}_{3i}\right)L_i d\xi$$

(8.60)

8.3.2.8 Discretization of inertial forces

Finally, the term for the work produced by the inertial forces $W_{inertial}$ in equation (8.13) is:

$$W_{inertia} = \int_0^L\left(\gamma\ddot{\vec{R}} + C_4(1+\varepsilon)\left[\ddot{\vec{R}} - (\ddot{\vec{R}}\cdot\vec{t})\vec{t}\right]\right)\cdot\delta\vec{U}dl_0$$

(8.61)

If we substitute into (8.61) the expressions (8.38), (8.40), (8.45), (8.46) and (8.50), we have:

$$W_{inertia} \approx \sum_{j=1}^{i-1}\int_0^1\delta\vec{P}_i^T A_i^T N_{gi}'^T\left(\gamma L_i N_{gi}'A_i + C_4\left[L_i(1+\varepsilon_i)N_{gi}'A_i - \frac{B_{gi}\vec{X}_i\vec{X}_i^T B_{gi}^T N_{gi}'A_i}{L_i(1+\varepsilon_i)}\right]\right)\ddot{\vec{X}}d\xi$$

(8.62)

8.3.2.9 Discretized equations of motion

Once we have obtained the discretized expressions for the different terms of work within the equation (8.13) (expressions (8.51), (8.54), (8.60) and (8.62)), we can built the following equation for the total virtual work:

$$W_V \approx \delta\vec{P}^T\sum_{i=1}^{n}\int_0^1\left(\gamma L_i A_i^T N_{gi}'^T N_{gi}'A_i\ddot{\vec{X}} + C_4\left[L_i(1+\varepsilon_i)A_i^T N_{gi}'^T N_{gi}'A_i - \frac{A_i^T N_{gi}'^T B_{gi}\vec{X}_i\vec{X}_i^T B_{gi}^T N_{gi}'A_i}{L_i(1+\varepsilon_i)}\right]\ddot{\vec{X}} - L_i A_i^T N_{gi}^T\left(\vec{F}_{1i} + \vec{F}_{2i} + \vec{F}_{3i}\right) + \right.$$

$$\left. + \beta EA\frac{A_i^T B_{gi}^T B_{gi}\vec{X}_i\vec{X}_i^T B_{gi}^T B_{gi}A_i}{L_i^3(1+\varepsilon_i)^2}\vec{X} + EA\varepsilon_i\frac{A_i^T B_{gi}^T B_{gi}A_i}{L_i(1+\varepsilon_i)}\vec{X}\right)d\xi = 0$$

(8.63)

The virtual displacement $\delta\vec{P}$ can be eliminated from the expression (8.63) since it is an arbitrary displacement. This allow us to finally find the equations of motion of the system in the following form:

INNWIND.EU, D4.21, State-of-the-art and implementation of design tools for floating structures

$$M \ddot{\vec{X}} + C \dot{\vec{X}} + K \vec{X} - \vec{F} = 0 \qquad (8.64)$$

Where M is the mass matrix of the system:

$$M = \sum_{i=1}^{n} A_i^T \int_0^1 \left(\gamma L_i N_{gi}'^T N_{gi}' + C_4 \left[L_i (1 + \varepsilon_i) N_{gi}'^T N_{gi}' - \frac{N_{gi}'^T B_{gi} \vec{X}_i \vec{X}_i^T B_{gi}^T N_{gi}'}{L_i (1 + \varepsilon_i)} \right] \right) d\xi_i \, A_i \qquad (8.65)$$

C is the structural damping matrix of the system:

$$C = \sum_{i=1}^{n} A_i^T \int_0^1 \beta EA \frac{B_{gi}^T B_{gi} \vec{X}_i \vec{X}_i^T B_{gi}^T B_{gi}}{L_i^3 (1 + \varepsilon_i)^2} d\xi_i \, A_i \qquad (8.66)$$

The stiffness matrix of the system, K is:

$$K = \sum_{i=1}^{n} A_i^T \int_0^1 EA \varepsilon_i \frac{B_{gi}^T B_{gi}}{L_i (1 + \varepsilon_i)} d\xi_i \, A_i \qquad (8.67)$$

And $\vec{F}$ are the external forces of the discretized system:

$$\vec{F} = \sum_{i=1}^{n} A_i^T \int_0^1 L_i N_{gi}^T \left(\vec{F}_{1i} + \vec{F}_{2i} + \vec{F}_{3i} \right) d\xi_i \qquad (8.68)$$

8.3.2.10   *Elemental matrices and force vector*

The equations (8.65), (8.66), (8.67) and (8.68) provide the expressions to build the mass matrix, the structural damping matrix, the stiffness matrix and the external force vector of the complete system in the global reference system. These global matrices and vectors are the result of the assembly of the elemental matrices and forces. This assembly procedure is expressed mathematically by the products with the adjacency matrix A_i.

It is trivial to derive from these equations the expressions for the elemental mass matrix M_i, the structural damping matrix C_i, the structural stiffness matrix K_i and the force vector $\vec{F}_i$ in the global reference system:

$$M_i = \int_0^1 \left(\gamma L_i N_{gi}'^T N_{gi}' + C_4 \left[L_i (1 + \varepsilon_i) N_{gi}'^T N_{gi}' - \frac{N_{gi}'^T B_{gi} \vec{X}_i \vec{X}_i^T B_{gi}^T N_{gi}'}{L_i (1 + \varepsilon_i)} \right] \right) d\xi_i \qquad (8.69)$$

INNWIND.EU, D4.21, State-of-the-art and implementation of design tools for floating structures

$$C_i = \int_0^1 \beta EA \frac{B_{gi}^T B_{gi} \vec{X}_i \vec{X}_i^T B_{gi}^T B_{gi}}{L_i^3 (1 + \varepsilon_i)^2} d\xi_i \tag{8.70}$$

$$K_i = \int_0^1 EA \varepsilon_i \frac{B_{gi}^T B_{gi}}{L_i (1 + \varepsilon_i)} d\xi_i \tag{8.71}$$

$$\vec{F}_i = \int_0^1 L_i N_{gi}^T \left(\vec{F}_{1i} + \vec{F}_{2i} + \vec{F}_{3i} \right) d\xi_i \tag{8.72}$$

These elemental matrices and forces can also be expressed in the elemental reference system:

$$m_i = \int_0^1 \left(\gamma L_i N'^T N' + C_4 \left[L_i (1 + \varepsilon_i) N'^T N' - \frac{N'^T B \vec{X}_i \vec{X}_i^T B^T N'}{L_i (1 + \varepsilon_i)} \right] \right) d\xi_i \tag{8.73}$$

$$c_i = \int_0^1 \beta EA \frac{B^T B \vec{X}_i \vec{X}_i^T B^T B}{L_i^3 (1 + \varepsilon_i)^2} d\xi_i \tag{8.74}$$

$$k_i = \int_0^1 EA \varepsilon_i \frac{B^T B}{L_i (1 + \varepsilon_i)} d\xi_i \tag{8.75}$$

$$\vec{f}_i = \int_0^1 L_i N^T \left(\vec{f}_{1i} + \vec{f}_{2i} + \vec{f}_{3i} \right) d\xi_i \tag{8.76}$$

Where:

$$\vec{f}_{1i} = T_i^T \begin{bmatrix} 0 \\ -\gamma_r g \\ 0 \end{bmatrix} \tag{8.77}$$

$$\vec{f}_{2i} = \frac{C_2}{L_i^3 (1 + \varepsilon_i)^2} | \vec{v}_i^T N^T B \vec{x}_i | \left(\vec{v}_i^T N^T B \vec{x}_i \right) B \vec{x}_i \tag{8.78}$$

INNWIND.EU, D4.21, State-of-the-art and implementation of design tools for floating structures

$$\vec{f}_{3i} = C_3(1+\varepsilon_i)\left[\vec{v}_i^T N^T N\vec{v}_i - \frac{(\vec{v}_i^T N^T B\vec{x}_i)^2}{(1+\varepsilon_i)^2 L_i^2}\right]^{\frac{1}{2}}\left[N\vec{v}_i - \frac{(\vec{v}_i^T N^T B\vec{x}_i)B\vec{x}_i}{(1+\varepsilon_i)^2 L_i^2}\right] \qquad (8.79)$$

8.4 Code Implementation of the Cable Dynamics

The OPASS code has been programmed in Fortran 90 based on the theoretical development described in section 2, has been developed with the capability of simulating the dynamics of a mooring line submerged in water, under the action of waves and in contact with the seabed.

8.4.1 Implementation of the Finite Elements Method

The equation of motion of the system, (8.64), are built according to the classical steps of the Finite Elements Method:

1. Discretize the cable in a certain number of bar elements.
2. Built the elemental mass, damping and stiffness matrices using equations (8.73), (8.74), (8.75) and the external force vectors according to (8.76).
3. Transform the elemental matrices and force vectors into the global coordinate system using the local to global transformation matrix (8.32).
4. Assembly the global mass, damping and stiffness matrices and the global external forces vector using the adjacency matrices (8.42).

The resultant equations of motion are ordinary differential equations.

Alternatively, the steps 2 and 3 can be performed in only one step using the equations (8.69), (8.70), (8.71) and (8.72). These are the expressions that have been implemented in the code because they provide a better computational efficiency.

As has been explained in subsection 2.2, the interpolation function chosen for the inertial forces are step functions instead of linear functions. This results in a mass matrix composed by 3 x 3 submatrices around the diagonal. Thus, the assembly of the matrices and force vector (step 4) can be simplified and the inversion of the mass matrix is performed with much lower computational cost.

8.4.2 Initial configuration

The static solution of the catenary formed by the mooring line hanging between the fairlead and the anchor is used as the initial reference cable configuration R. This shape is calculated within the code using the analytical formulation for a cable suspended between two points that is described in [8.9]. This formulation considers the elastic stiffness of the mooring line, the cable weight and the buoyancy, the contact between the cable and the horizontal seabed and the tangential static seabed friction. The resulting system of equations has not an explicit solution and a Newton-Raphson iteration scheme has to be applied to solve it.

8.4.3 Seabed contact model

A contact model of the line with the seabed has been implemented using bi-linear springs. When a node is in contact with the seabed, a spring with stiffness K_{sc} provides the floor reaction force per indentation depth and per unit of line length. A damping D_{sc} is also included in the model. Indentation of the line into the seabed due to self-weight is:

INNWIND.EU, D4.21, State-of-the-art and implementation of design tools for floating structures

$$\delta S_0 = \frac{\gamma_r g}{K_{sc}} \tag{8.80}$$

If d_w is the water depth and Z_i is the vertical position of the node i in the global reference system, the seabed only introduces a force on the node i when the condition:

$$Z_i < (d_w - \delta S_0) \tag{8.81}$$

is fulfilled. This force, provided by the spring at the node i and denoted as $\vec{F}_{sc}^{\,i}$ is calculated as:

$$\vec{F}_{sc}^{\,i} = \begin{bmatrix} 0 \\ 0 \\ -K_{sc}(Z_i - d_w - \delta S_0) - D_{sc}\dot{Z}_i \end{bmatrix} \tag{8.82}$$

Where $\dot{Z}_i$ is the vertical velocity of the node i.

Thus, the elements resting at the seabed will be located at D_w. If the elastic forces compensate only part of the weight of the element, the node will be located between D_w and $D_w - \delta S_0$.
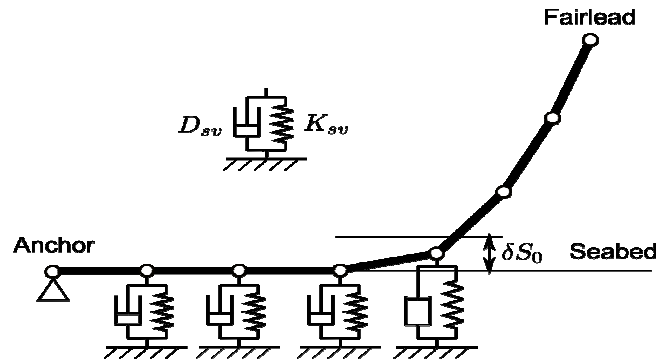
Figure 8.7: Cable-seabed contact model

8.4.4   Time integration

The system of equations that we have obtained through the Finite Element method, (8.64), can be rewritten as:

$$\ddot{\vec{X}} = M^{-1}\left(\vec{F} - C\dot{\vec{X}} - K\vec{X}\right) \tag{8.83}$$

Three different integration schemes for the equation of motions have been implemented in OPASS.

The first one is a simple explicit scheme described in [8.12], based in the central difference formula.
A the second integrator is the Runge-Kutta-Nyström scheme as described in [8.7]. This method requires four evaluations of the equations of the lines (8.83) per time step, increasing the computational effort, but, on the other hand, it allows to increase the size of the time step.

INNWIND.EU, D4.21, State-of-the-art and implementation of design tools for floating structures

Finally, the third integrator is the Adams-Moulton-Bashforth predictor-corrector scheme [8.4], where the solution at each time step is achieved by evaluating twice the equations of motion (8.83). In the first evaluation, called predictor stage, the accelerations are obtained from the equations of motion of the system and they are used to calculate the positions and velocities of the line's degrees of freedom at the next time step. In a second stage, called corrector, this solution is refined using the next time step positions and velocities to obtain more accurate accelerations for the next step. A final estimation of positions and velocities from these accelerations is performed and one time step is advanced. To start this integration scheme, a Rünge-Kutta methos is applied at the first time steps.

8.4.5 Coupling with FAST

The mooring lines model originally implemented in FAST uses a quasi-static formulation that implies several limitations: inertia, damping or hydrodynamic drag forces are not considered and friction is only modelled in the tangential direction. In order to introduce new dynamic capabilities into the FAST code for the simulation of moored floating platforms, CENER's code has been coupled with FAST using a loose scheme: each of the code uses its own time integrator and every time step FAST transfers to OPASS the positions and velocities of the platform and OPASS provides FAST the tension of the lines. FAST uses an Adams-Moulton-Bashforth predictor-corrector integrator, where the solution at each time step is achieved in two steps. The first one (predictor) provides a rough approximation of the solution that is refined in the second step (corrector). The method needs to be initialized solving the first time steps with the Runge-Kutta method.

The coupling of the OPASS code with FAST required the increase of FAST's wave generator capabilities. The original wave generator was only able to generate wave kinematics at different depths located at the tower centreline. The reason is that the wave velocities at the tower centreline are used to calculate viscosity forces over the platform, considered as a cylinder. The original quasi static model in FAST for the mooring lines did not consider wave loading over the lines. For this reason, wave kinematics calculation at the lines nodes was not necessary. As the new dynamic code considers hydrodynamic drag over the lines, FAST wave generator has been improved to calculate wave velocities at the nodal positions. The whole wave time history is calculated at the position of the nodes in the lines static solution before the dynamic simulation starts.

Wave kinematics time step can be higher than simulation time step (in fact, it is usually higher). The FAST function *InterpStp* is used to calculate the wave velocities at the simulation time step by interpolation. If the size of the vectors in the call of this function is high, the computational cost of this function is very expensive. This is much worse in this case where the OPASS dynamic code has been coupled with FAST, because the wave kinematics history is calculated in many more points of the space (all the nodes of the lines). For this reason, the call of the function in FAST has been optimised improving CPU time.

8.5 Verification of the OPASS code

8.5.1 Natural Frequencies

A first verification of the stand alone code was performed comparing the results of simulating the out of plane free oscillation of a submerged line with the corresponding natural frequency calculated according to semi-empirical expressions provided by [8.20]. The properties of the line are summarized in Table 8.2. The horizontal distance between the anchor and the fairlead is 100m and the vertical distance is 45m.

INNWIND.EU, D4.21, State-of-the-art and implementation of design tools for floating structures

Line length	113	m
Mass/Unit Length	135.35	kg/m
Line density	7800	kg/m^3
Line diameter	0.076	m
EA	5e8	N
Number of Elements	15	-
Water density	1025	kg/m^3
C_{mn}	3.8	-
C_{dt}	0.5	-
C_{dn}	2.5	-

Table 8.2: Line Properties for the Natural Frequencies Calculation

The differences between predicted (0.1336 Hz) and simulated (0.1333 Hz) frequencies were below 0.2%.

8.5.2 Comparison with 3Dfloat

The results provided by OPASS were verified through comparison with 3Dfloat simulations. 3Dfloat is a code based on FEM theory and developed by IFE [8.17].

The mooring line model used in these verification exercise was based in the OC4 phase semisubmersible platform model [8.21]. The parameters of the line are summarized in Table 8.3.

Line length	902.2	m
Mass/Unit Length	113.35	kg/m
Line density	7800	kg/m^3
Line diameter	0.076	m
EA	7.536E8	N
Number of Elements	64	-
C_{mn}	0.97	-
C_{dt}	0.0	-
C_{dn}	0.6	-
Water density	1025	kg/m^3
Fairlead draft	70	m
Hor. Dis.t anchor & fairlead	848.67	m

INNWIND.EU, D4.21, State-of-the-art and implementation of design tools for floating structures

Water depth	320	m

Table 8.3: Line Properties for the Verification with 3DFloat

Contact with the seabed was considered, but no friction. The line was divided into 64 elements. Resolution checks doubling the number of elements were run for both models. The results were essentially the same. Resolution checks were also carried out for the time step length.

A horizontal harmonic displacement of amplitude 5m in the in-plane direction was applied in the fairlead with two different periods: 10s and 30s. A sketch of the displacements applied to the fairlead around its nominal position (0 displacement) is shown in Figure 8.8. When the fairlead is displaced horizontally far from the anchor, the displacement is considered positive, and when the fairlead is approached to the anchor, the displacement is negative.
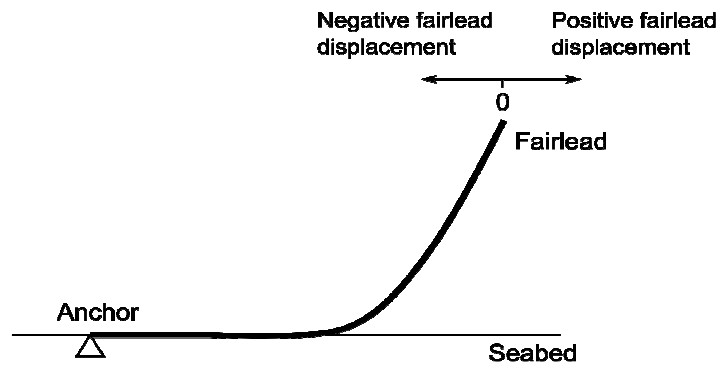
Figure 8.8: Displacements applied to the fairlead around its nominal position

The curves for Tension-Displacement obtained by both codes are shown in the Figures 8.9 and 8.10. The first seconds of the simulation have been discarded to avoid transients. In Figure 8.9, the initial position of the fairlead is 0m. In Figure 8.10, the fairlead is initially displaced 20m in the horizontal in-plane direction and thus, the line tension is higher. Results show a good agreement between both codes.
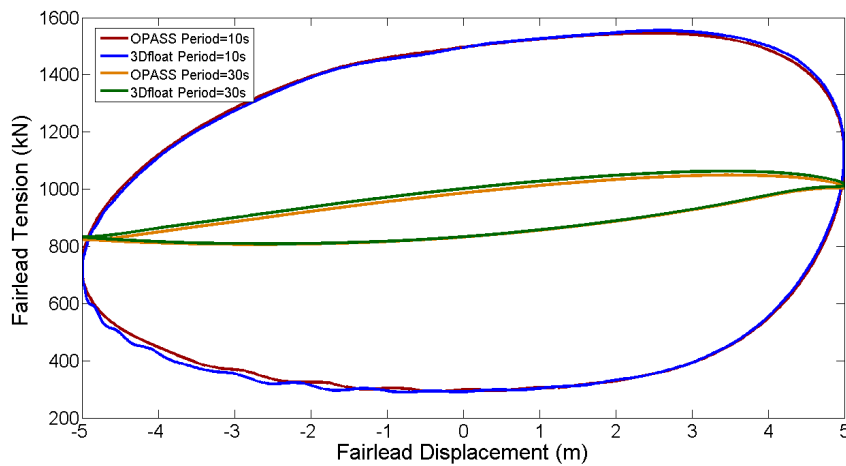
Figure 8.9: Initial Position of the Fairlead: 0m

INNWIND.EU, D4.21, State-of-the-art and implementation of design tools for floating structures
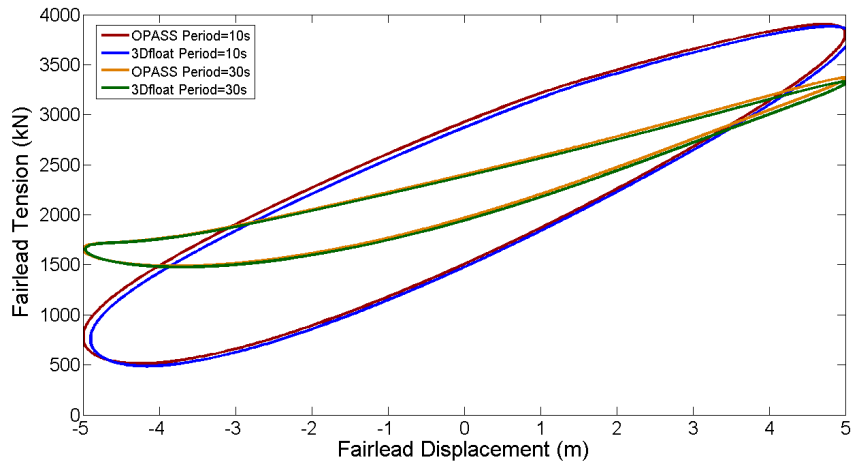
Figure 8.10: Initial Position of the Fairlead: 20m

8.5.3 Influence of Dynamic Effects

The simulations performed in the previous paragraph for verification (oscillation of 5m prescribed at the fairlead) were extended for an additional period of 20s and also for fairlead initial positions of -30m and +30m. The properties of the mooring line model were the same.

Figure 8.11 shows the Tension-Displacement dynamic loops generated in these calculations in comparison with the static Tension-Displacement curve (in gray). Tension is increased by dynamics up to 60% (relative to the static) for the simulation with fairlead initial position of 0m and period of 10s. Dynamic effects are smaller when the fairlead initial position is 30m (and thus the tension at the line is higher), even for the 10s period simulation. This suggests that for taut lines a quasi-static model may be an acceptable approximation. Dynamic effects are also smaller at position -30m, where tension is low.

INNWIND.EU, D4.21, State-of-the-art and implementation of design tools for floating structures
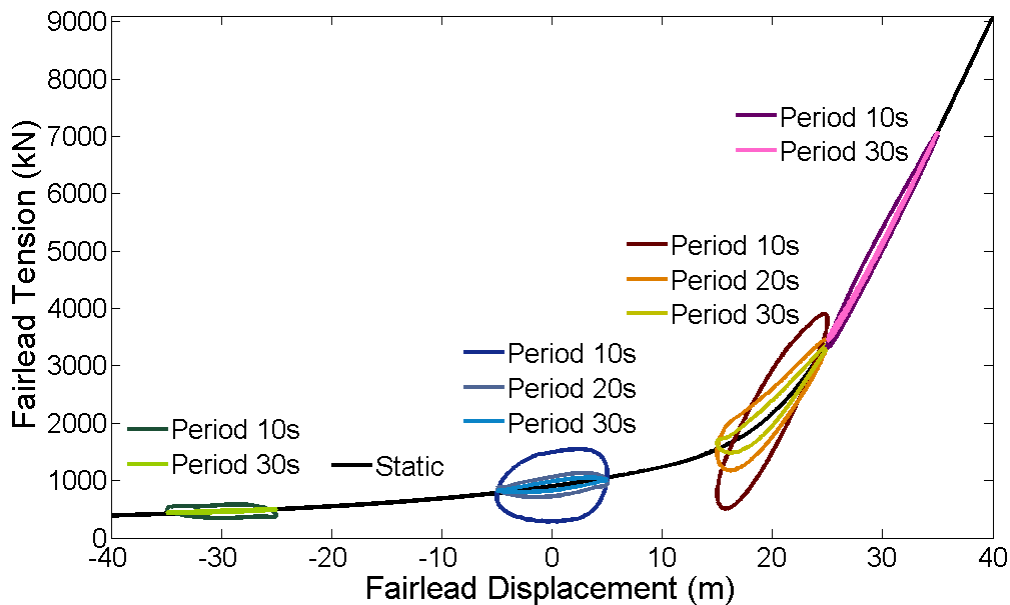
Figure 8.11: Dynamic Effects in a Mooring Line

8.6 CONCLUSIONS

A new code called OPASS (Offshore Platforms Anchoring System Simulator) for the dynamic simulation of mooring lines have been developed. OPASS formulation is based on finite elements, with three translational degrees of freedom defined at each node. The code considers the structural damping and the axial stiffness of the line inertia, added mass, water tangential and normal drag and seabed interaction (contact and friction). The code neglects the bending stiffness and thus, it is suitable for the simulation of mooring systems, that are usualyy built with chains or wires with low bending stiffness.

The code has been verified with semi empirical expressions for the natural frequencies and by comparison with the SIMO-RIFLEX and 3Dfloat codes with positive results.

Simulations performed prescribing a harmonic horizontal displacement at the fairlead have been performed resulting in an increase in the tension at the fairlead up to 60% with respect to the static value. In very taut lines dynamic effects are smaller and the quasi-static model or linear spring model could be an acceptable approximation.

Most of the programs with capabilities for the modeling of mooring lines dynamics do not allow to represent with accuracy the integrated dynamic simulation of the whole floating wind turbine system. On the other hand, many of the codes developed within the wind energy sector for the simulation of floating wind turbines use simplified models for the representation of the mooring lines. The OPASS code has been integrated in FAST, improving its capabilities for simulating floating platform wind turbines. The resulting tools is able to simulate floating wind turbines considering the aerodynamics, hydrodynamics, structural dynamics, mooring system dynamics and control in a coupled computation. The validation of this tool is concluding successfully within the IEA Annex30 (OC4).

The bending stiffness feature is currently under implementation and will allow to simulate slender structures with high bending stiffness as dynamic cables, providing the loads on the cable and evaluating its influence over the floating wind turbine dynamics.

INNWIND.EU, D4.21, State-of-the-art and implementation of design tools for floating structures

It is also planned to implement in the future a new "stiff" integration scheme for the equations of motion as the Generalized -α method. This method will provide a higher calculation time step improving the computational simulation time.

Though a preliminar verification against other codes as Simo-Riflex of the cable-seabed friction model has been already successfully performed, more extensive work of the cable-seabed friction model will be carried out in the future.

8.7   References

[8.1] *ARIANE7 Theoretical Manual.* Bureau Veritas. July 2011.

[8.2] *Bladed Theory Manual Version 4.0*. GL Garrad Hassan. Oct. 2010.

[8.3] Dewey, R.K. "Mooring Design and Dynamics-a Matlab package for designing and analyzing oceanographic moorings". In: *Marine Models Online* 1 (1999), pp. 103-157.

[8.4] Faires, J.D. and Burden, R. *Numerical Methods.* Third Edition. Pacific Grove, CA: Thomson-Brooks/Cole, 2003.

[8.5] Fylling, I. J. and Mo, K. and Merz, K. and Luxcey, N. E. "Floating wind turbine -
Response analysis with rigid-body model". In: *European Offshore Wind.* Stockholm, Sweden, 2009.

[8.6] Gobat, J.I. and Grosenbaugh, M.A. WHOI *Cable v2.0: Time Domain Numerical Simulation of Moored and Towed Oceanographic Systems.* Technical Report WHOI-2000-08. Woods Hole Oceanographic Institution, 2000.

[8.7] Hansen, Martin O. L. *Aerodynamics of Wind Turbines.* Second Edition. London: Earthscan, 2008.

[8.8] HYBER *User Manual.* USFOS. Mar. 2006.

[8.9] Jonkman, J.M. "Dynamics Modeling and Loads Analysis of an Offshore Floating Wind Turbine". PhD Thesis. University of Colorado, 2007.

[8.10] Larsen, T.J. and Hansen, A.M. *How 2 HAWC2, The User's Manual.* Risoe National Laboratory. Dec. 2007.

[8.11] Larsen, T.J. and Hanson, T.D. "A method to avoid negative damped low frequent tower vibrations for a floating, pitch controlled wind turbine". In: *Journal of Physics: Conference Series 75* (2007).

[8.12] Lindahl, J. and Sjöberg, A. "Dynamic Analysis of Mooring Cables". MSc Thesis. Chalmers University of Technology, 1983.

[8.13] Masciola, M. and Robertson, A. and Jason, J.M. and Driscoll, F. "Investigation of a FAST-OrcaFlex Coupling Module for Integrating Turbine and Mooring Dynamics of Offshore Floating Wind Turbines". In: *International Conference on Offshore Wind Energy and Ocean Energy.* Beijing, China, 2011.

[8.14] Matha, D. and Hauptmann, S. and Hecquet, T. "Methodology and Results of Loads Analysis of Wind Turbines with Advanced Aeroelastic Multi-Body Simulation". In: *DEWEK.* Bremen, Germany, 2010.

INNWIND.EU, D4.21, State-of-the-art and implementation of design tools for floating structures

[8.15] Matha, D. and Schlipf, M. and Cordle, A. and Pereira, R. and Jonkman, J. "Challenges in Simulation of Aerodynamics, Hydrodynamics, and Mooring-Line Dynamics of Floating Offshore Wind Turbines". In: *21st International Offshore and Polar Engineering Conference.* Maui, Hawaii, United States, 2011.

[8.16] Morison, J.R. and O'Brien, M.P. and Johnson, J.W. and Schaaf, S.A. "The force exerted by surface waves on piles". In: *Journal of Petroleum Technology 2.5* (1950), pp. 149-154.

[8.17] Nygaard, T.A. and Myhr, A. and Maus, K.J. "A comparison of two conceptual designs for floating wind turbines". In: *Proceedings of the European Offshore Wind. Stockholm,* Sweden, 2009.

[8.18] *OrcaFlex Manual*. Version 9.6a. Orcina Ltd. 2012.

[8.19] Ormberg, H. and Bachynski, E. E. "Global Analysis of Floating Wind Turbines: Code Development, Model Sensitivity and Benchmark Study". In: *ISOPE*. Rhodes, Greece, 2012.

[8.20] Pugsley, A.G. "On the Natural Frequencies of Suspension Chains". In: *Quaterly Journal of Mechanics and Applied Mathematics 2.*4 (1949), pp. 412-418.

[8.21] Robertson, A. and Jonkman, J. and Masciola, M. and Song, H. and Goupee, A. and Coulling, A. and Luan, C. "Definition of the Semisubmersible Floating System forPhase II of OC4". In: [To be published] .

[8.22] Shim, S. and Kim, M.H. "Rotor-Floater-Tether Coupled Dynamic Analysis of Offshore Floating Wind Turbines". In: *ISOPE*. Vancouver, Canada, 2008.

[8.23] Skaare, B. and Hanson, T. D. and Nielsen F. G. and Yttervik, R. and Hansen, A. M. and Thomsen, K. and Larsen, T. J. "Integrated Dynamic Analysis of Floating Offshore Wind Turbines". In: *European Wind Energy Conference and Exhibition*. Milan, Italy, 2007.

[8.24] Webster,R. L. and Palo, P. A. *SEADYN User's Manual*. US Navy. Apr. 1982.

8.8   Nomenclature

β	Rayleigh damping coefficient proportional to stiffness
γ	Line mass per unit of cable unstretched length
γ_r	Equivalent mass per unit length of the cable submerged in water
ε	Axial deformation
$\dot{\varepsilon}$	Axial deformation velocity
ξ_i	Element local coordinate
ρ_c	Density of the cable material
ρ_w	Density of the water
ψ_1	Staircase function number 1
ψ_2	Staircase function number 2
A	Cable section area
A_i	Adjacency matrix for the element i

INNWIND.EU, D4.21, State-of-the-art and implementation of design tools for floating structures

B	Derivative of matrix N
B_{gi}	Derivative of matrix N_{gi}
C	Structural damping matrix of the complete FEM system
C_2	Constant for the calculation of tangential drag force
C_3	Constant for the calculation of normal drag force
C_4	Constant for the calculation of added mass force
C_{dt}	Tangential drag coefficient
C_{dn}	Normal drag coefficient
C_{mn}	Normal added mass coefficient
C_i	Element structural damping matrix in the global reference system
c_i	Element structural damping matrix in the local reference system
D	Diameter of the cable for hydrodynamic calculations
D_{sc}	Damping of the seabed per unit length used in the cable-seabed contact model
d_w	Water depth
E	Cable material Young's modulus
$\vec{e}_{1i}$	Unit vector in the x local axis for element i
$\vec{e}_{2i}$	Unit vector in the y local axis for element i
$\vec{e}_{3i}$	Unit vector in the z local axis for element i
F_D	Module of the structural damping force dl Infinitesimal length of cable
$\vec{F}$	Total external forces of the complete FEM system
$\vec{F}_1$	Resultant gravity and buoyancy force per unit of unstretched length in the global reference system
$\vec{F}_i$	Element total external force vector in the global reference system
$\vec{F}_{1i}$	Element i resultant gravity and buoyancy force per unit of unstretched length in the global reference system
$\vec{F}_{2i}$	Element i tangential drag force per unit of unstretched length in the global reference system
$\vec{F}_{3i}$	Element i normal drag force per unit of unstretched length in the global reference system
$\vec{F}_2$	Hydrodynamic tangential drag force per unit of unstretched length in the global reference system
$\vec{F}_3$	Hydrodynamic normal drag force per unit of unstretched length in the global reference system
$\vec{F}_4$	Hydrodynamic inertial force per unit of unstretched length in the global reference system
$\vec{f}_{1i}$	Element i resultant gravity and buoyancy force per unit of unstretched length in the local reference system
$\vec{f}_{2i}$	Element i tangential drag force per unit of unstretched length in the local reference system
$\vec{f}_{3i}$	Element i normal drag force per unit of unstretched length in the local reference system

$\vec{f}_i$	Element total external force vector in the local reference system
g	Gravity constant
i	Element number
j	Index
K	Stiffness matrix of the complete FEM system
K_{sc}	Stiffness of the seabed per unit length used in the cable-seabed contact model
K_i	Element stiffness matrix in the global reference system
k_i	Element stiffness matrix in the local reference system
L	Cable length
L_i	Length of the element i
l	Distance along the stretched length of the cable
l_0	Distance along the unstretched length of the cable
l_{0i}	Length along the unstretched cable to the initial node of the element i
M	Mass matrix of the complete FEM system
M_i	Element mass matrix in the global reference system
m_i	Element mass matrix in the local reference system
N_1	Linear shape function number 1
N_2	Linear shape function number 2
N	Shape functions matrix
N'	Shape functions matrix with staircase interpolation functions
P	Point at the cable
$\vec{n}_1$	Vector in the x local axis before normalization
$\vec{n}_2$	Vector in the y local axis before normalization
$\vec{n}_3$	Vector in the z local axis before normalization
$\vec{N}_2$	Vector used in the calculation of the element local reference unit vectors
N_{gi}	Shape functions matrix in the global coordinate system
N'_{gi}	Shape functions matrix with staircase interpolation functions in the global coordinate system
$\vec{P}_i$	Element i nodal displacement vector in the global reference system
$\vec{p}_i$	Element i nodal displacement vector in the element reference system
$\delta\vec{P}_i$	Element i nodal virtual displacement vector in the global reference system
$\delta\vec{P}$	Vector with the virtual displacements of the system nodes in the global reference frame
$\delta\vec{p}_i$	Element i nodal virtual displacement vector in the element reference system
R	Initial reference configuration of the mooring line
$\vec{R}$	Position vector in the global reference system
$\vec{R}_0$	Initial position vector of the point P in the global reference system
$\dot{\vec{R}}$	Velocity vector in the global reference system
$\ddot{\vec{R}}$	Acceleration vector in the global reference system
$\vec{r}$	Position vector in the element reference system

INNWIND.EU, D4.21, State-of-the-art and implementation of design tools for floating structures

$\vec{r}$	Velocity vector in the element reference system
$\ddot{\vec{r}}$	Acceleration vector in the element reference system
δS_0	Indentation of the line into the seabed due to self-weight
T	Line tension
T_i	Local to global transformation matrix
T_I	Element local to global transformation matrix
t	Time
$\vec{t}$	Vector tangential to the cable at point P
$\vec{U}$	Displacement vector in the global reference system
$\vec{u}$	Displacement vector in the element reference system
$\delta\vec{U}$	Virtual displacement vector in the global reference system
$\delta\vec{u}$	Virtual displacement vector in the element reference system
$\vec{V}_i$	Element i nodal vector for the relative water velocity in the global reference system
$\vec{V}$	Relative velocity of the water with respect to the cable in the global reference system
$\vec{V}_t$	Tangential component of the relative velocity between the water and the cable in the global reference system
$\vec{V}_n$	Normal component of the relative velocity between the water and the cable in the global reference system
$\vec{v}$	Relative velocity of the water with respect to the cable in the local reference system
$\vec{v}_i$	Element i nodal vector for the relative water velocity in the local reference system
$W_{elastic}$	Work produced by the elastic forces
W_{damp}	Work produced by the structural damping forces
$W_{external}$	Work produced by the external forces
W_V	Virtual work
$W_{inertia}$	Work of the inertial forces
$\vec{X}$	Position vector of the complete FEM system in the global reference system
$\vec{X}_i$	Element i nodal position vector in the global reference system
$\dot{\vec{X}}$	Velocity vector of the complete FEM system in the global reference system
$\dot{\vec{X}}_i$	Element i nodal velocity vector in the global reference system
$\ddot{\vec{X}}$	Acceleration vector of the complete FEM system in the global reference system
$\ddot{\vec{X}}_i$	Element i nodal acceleration vector in the global reference system
$\vec{x}_i$	Element i nodal position vector in the element reference system
x_1	Coordinate x in the global reference system of the i element initial node
x_2	Coordinate x in the global reference system of the i element final node
$\dot{\vec{x}}_i$	Element i nodal velocity vector in the element reference system
$\ddot{\vec{x}}_i$	Element i nodal acceleration vector in the element reference system
y_1	Coordinate y in the global reference system of the i element initial node

INNWIND.EU, D4.21, State-of-the-art and implementation of design tools for floating structures

y_2 Coordinate y in the global reference system of the i element final node

Z_i Vertical position of the node i

$\dot{Z}_i$ Vertical velocity of the node i

z_1 Coordinate z in the global reference system of the i element initial node

z_2 Coordinate z in the global reference system of the i element final node

INNWIND.EU, D4.21, State-of-the-art and implementation of design tools for floating structures

9 FULLY NONLINEAR WAVE FORCING OF A TLP WIND TURBINE

9.1 Introduction

The present chapter presents a coupled aero-hydro-servo-elastic model for a floating TLP wind turbine configuration developed as an extension to the Flex5 aero-servo-elastic model. The model is based on [9.19] which is here extended to include forcing from fully nonlinear incident waves.

The background for the extension is the observation of ringing effects on floating wind turbine models, where steep waves can excite structural frequencies. Such events have been observed by Wehmeyer (2013, private communication) and also in [9.5]. Further, for monopile wind turbines, the effect has been investigated numerically in [9.20] and experimentally in [9.3]. For the bottom-fixed structures at intermediate depth, the excitation often occurs as impulsive excitation with a sudden forcing to a large displacement and subsequent damped vibration. At deep water, the classical ringing phenomenon is associated with resonant excitation of the structural frequency over the time scale of a wave period. This happens during the passage of a steep wave. The resonant motion next decays subject to damping after the passage of the large wave.

The central cause of the ringing is the presence of higher harmonics in the force signal of large-amplitude waves. These harmonics may be close to a structural eigenfrequency. This leads to the necessity of a nonlinear forcing theory for offshore wind turbines.

In the present chapter, the forcing is based on kinematics from fully nonlinear potential flow computations. The extended description is applied to model the response of a TLP wind turbine to a focused wave group of the New Wave type [9.24]. Comparison is made to forcing from a linear wave description and the effect of simultaneous wind forcing is investigated.

It is found that for the present example the linear wave forcing leads to a larger platform response than the nonlinear wave forcing. This is explained through dynamic build-up of the response during the passage of the wave group and the different relative placement of the main wave in the group. Here the main nonlinear wave arrives one period earlier than the linear wave. This effect is subject to ongoing research. For the effect of wind forcing, the two intermediate wind speeds are found to be associated with the largest pitch amplitude response for the floater. This is against expectation, as the strongest aerodynamic damping is expected for these wind speeds. However, a dependency of the natural pitch frequency to the mean surge is observed. As the natural frequency is nearly coincident with the second harmonic wave frequency, the strong amplitudes are likely to be caused by resonance.

9.1.1 Role in InnWind project

The extension of Flex5 to nonlinear waves is part of the model development in the InnWind project. It is intended that the model is validated against experimental data obtained in the InnWind project. Here the focus on combined large-amplitude waves and wind is central.

9.2 The Flex5 aero-elastic model

The Flex5 aero-elastic code [9.16] has been developed through the 80'ties and 90'ties and is widely used in the wind turbine industry. The structural formulation is based on beam elements and the deflections are described in terms of pre-selected shape functions similarly to classical modal analysis. For example each blade is described through two flap-wise and one edge-wise modes, while the tower deflection is described by the two first natural modes in each of the inline and transverse directions. The total number of Degrees Of Freedom (DOFs) is 28, including 6 DOFs for the deflection of the tower bottom. This allows inclusion of a substructure. For example a monopile formulation has been implemented and was tested in the OC3 project [9.8]. Other substructures studied are the Principle Power tri-floater and a TLP platform which are both detailed

INNWIND.EU, D4.21, State-of-the-art and implementation of design tools for floating structures

below. The coupled dynamics of 28 DOFs is next described through the coupled equations of motion subject to the loads from aerodynamics, gravity and hydrodynamics.

The aero-dynamic loads are described by a state of the art unsteady BEM code that includes dynamic stall, dynamic inflow, and Prandl's tip-loss correction due to a finite number of blades. Flex5 can read output of the Mann turbulence model [9.13] for inflow data.

9.2.1 The monopile implementation in Flex5

The monopile formulation is also based on shape function approach, where two static deflection shapes are included in the inline and transverse directions. These each correspond to a unit deflection and a unit rotation of the monopile top respectively. The reason for use of a static shape here is that the monopile is very stiff relatively to the tower. Hence it will respond almost statically to the forcing from the tower bottom.

The wave loads on the monopile are described in terms of linear irregular waves with Wheeler stretching [9.25]. The local forces are next obtained in terms of the Morison equation. Recently, Schløer [9.21] has incorporated the ability to apply fully nonlinear irregular wave kinematics from the OceanWave3D model [9.4] and extended the force model to that of Rainey [9.17], [9.18].

9.2.2 Floating wind turbine implementations in Flex5

The 6DOF foundation description of Flex5 at the bottom of the tower allows for other substructures than the monopile. Sist [9.23] and Krieger [9.10] implemented the PrinciplePower semisub foundation with a hydrodynamic description based on temporal convolution with Wamit output data using the method of Cummings. Ramachandran [9.19] incorporated a foundation for a TLP floating platform into Flex5. The combined model was applied to study the dynamics of a floating TLP configuration subject to wind forcing and linear wave forcing. The linear forcing was based on the Morison equation. This force formulation is extended in the present work to allow for fully nonlinear irregular waves.

9.2.3 The HAWC2 model and its application to floating wind turbines

Additionally to Flex5, the HAWC2 aero-elastic model is extensively applied in the research at DTU Wind Energy. HAWC2 was initially developed at DTU Wind Energy in 2003–2007 and is still under active extension in the ongoing research, see e.g. [9.9]. For example the dynamic meandering wake model has recently been added [9.12]. HAWC2 has been applied to a number of floating wind turbine designs including the Hywind spar, the OC4 semisub and a TLP concept. The hydrodynamic forcing in HAWC2 can be modelled by the Morison equation as well as through temporal convolution with Wamit output. While the present work is implemented into Flex5, there is no principal difficulty in applying the same implementation into HAWC2.

9.3 The OceanWave3D fully nonlinear potential flow wave model

The OceanWave3D model has been developed at DTU Mechanical Engineering [9.4] and is further maintained and developed together with DTU Compute.

INNWIND.EU, D4.21, State-of-the-art and implementation of design tools for floating structures
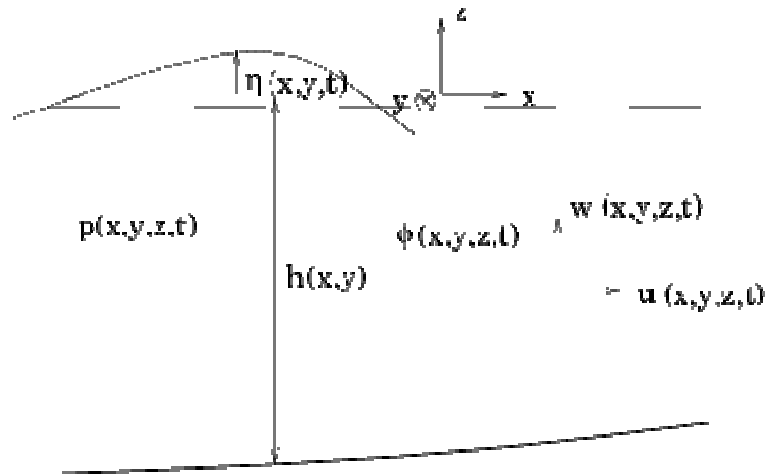
Figure 9.1: Definition sketch for solution of fully nonlinear potential flow water wave problem.

It solves the Laplace equation for the velocity potential of an inviscid, incompressible fluid

$$\nabla^2 \phi = 0 \quad , \quad -h < z < \eta \tag{9.1}$$

subject to the kinematic and dynamic free surface conditions

$$\eta_t + \nabla_H \phi \cdot \nabla_H \eta - \phi_z = 0 \quad , \quad z = \eta \tag{9.2}$$

$$\phi_t + g\eta + \frac{1}{2}\nabla\phi \cdot \nabla\phi = 0 \quad , \quad z = \eta \tag{9.3}$$

and the impermeability condition at the sea bed

$$\nabla_H \phi \cdot \nabla h + \phi_z = 0 \quad , \quad z = -h. \tag{9.4}$$

Here $\nabla_H = (\partial_x, \partial_y)$ denotes the horizontal gradient operator. A definition sketch is shown in Figure 9.1 where a Cartesian coordinate system (x, y, z) is defined with the z-axis pointing vertically upwards from the still water level. The corresponding velocities are denoted (u, v, w) and the velocity potential ϕ satisfies $\nabla\phi = (u, v, w)$. Further, the free surface elevation is denoted η, the pressure field p, the depth h and g is the acceleration of gravity.

Given initial data for the free surface elevation and the velocity potential at the free surface, OceanWave3D solves for the temporal evolution of the wave field by stepping (9.2)–(9.3) forward in time. This is done in terms of a standard fourth-order Runge-Kutta scheme. Boundary conditions at the inlet and outlet are imposed through relaxation zones, where the solution variables for η and ϕ are gradually forced to follow a pre-described variation.

Schløer [9.20], see also [9.21], applied the OceanWave3D to model fully nonlinear wave loads on the NREL 5MW monopile wind turbine. The model was also applied by Bredmose et al [9.3] to numerically reproduce the response of a flexible monopile subject to steep and breaking waves. The ability of computing a fully nonlinear wave field up to the point of breaking is a great advantage

INNWIND.EU, D4.21, State-of-the-art and implementation of design tools for floating structures

9.4 The TLP configuration and its modelling in Flex5

In this study, we consider the TLP configuration also used by [9.19] which originates from the work of Joensen et al [9.7]. This is sketched in Figure 9.2. The floater consists of a truncated circular cylinder, 10 m high, with the bottom face placed at a depth of 25 m. The diameter is $D_{floater} = 16$ m. The transition piece is mounted directly at the floater and has a diameter of $D_{trans} = 6$ m. It reaches up to a height of 10 m above the still water level, where the NREL 5MW reference tower begins. The wind turbine is the NREL 5MW reference wind turbine. The hub height is 100 m above the still water level. The depth is h =200 m.

The mooring system consists of four spokes that spreads out from the bottom of the floater with an internal angle of 90°. In the computations of the present study, the wind and wave direction are assumed co-linear and the spoke configuration is angled 45° to this direction as illustrated in Figure 9.3.
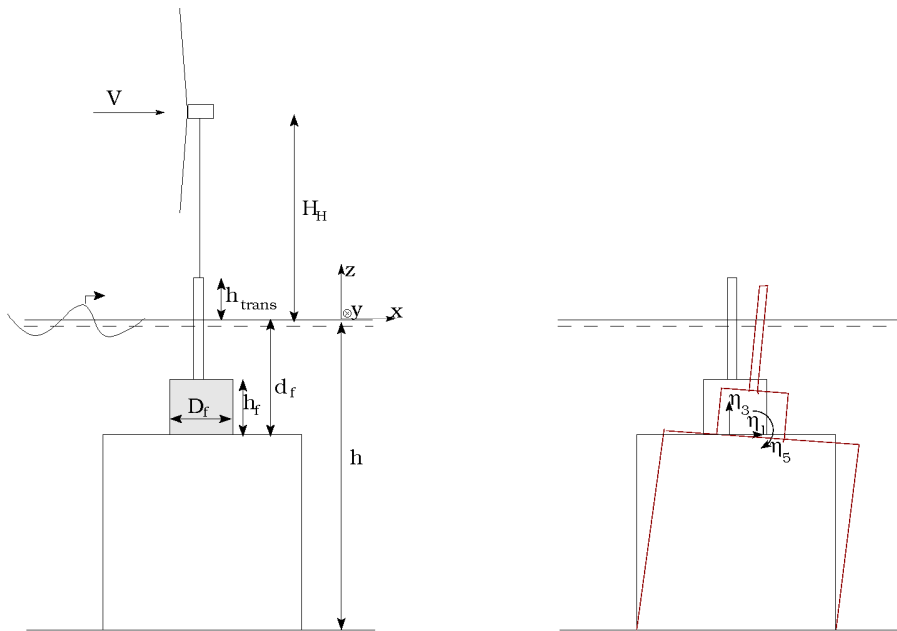

Figure 9.2: Definition sketch of the TLP configuration and the planar degrees of freedom for the floater.
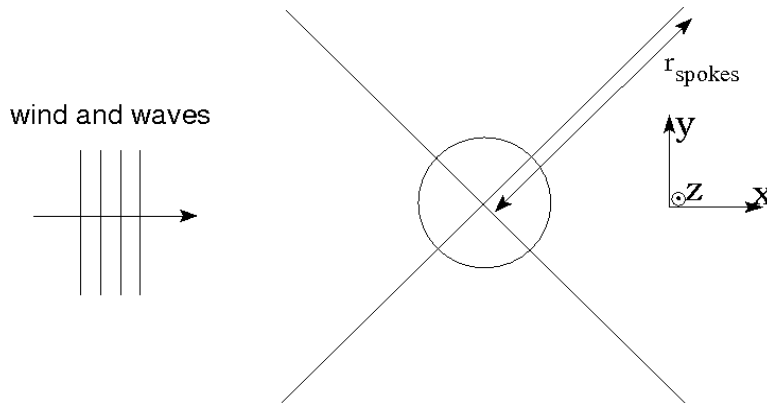
Figure 9.3: Definition sketch of the TLP mooring configuration.

INNWIND.EU, D4.21, State-of-the-art and implementation of design tools for floating structures

Quantity	Definition	Value
D_f	floater diameter	16m
h_f	floater height	10m
d_f	draught of floater	25m
h_{trans}	height of transition piece above SWL	10m
H_H	hub height above SWL	100m
r_{spokes}	distance from tendon attachment to center of floater	30m
h	Water depth	200m

Table 9.1: Floater dimensions

### 9.4.1 Incorporation of the floater motion into Flex5
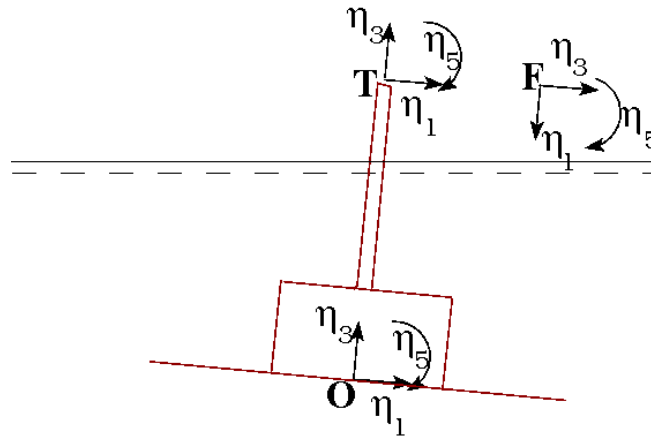
Figure 9.4: Coordinate systems for floater motion described with respect to the centre of the floater bottom (O), the bottom of the tower (T) and the bottom of the tower (F; Flex5 coordinate system).

The incorporation of the floater dynamics and forcing into Flex5 is done through a rigid transfer of the transformed mass matrix, stiffness matrix and force vector into Flex5. This is detailed in the following. Reference is made to Figure 9.4 which shows the three coordinate systems involved.

In Flex5, the motion of the substructure is described with reference to the bottom of the tower, in a coordinate system that has its first axis pointing down in the axial direction of the tower and its third axis pointing in the inline direction. This system is shown in Figure 9.4 and is denoted (F). The equation of motion for the tower bottom point in Flex5 can be expressed as

INNWIND.EU, D4.21, State-of-the-art and implementation of design tools for floating structures

$$\mathbf{M}_F^A \ddot{\eta}_F + \mathbf{K}_F^A \eta_F = \mathbf{F}_F^A \qquad (9.5)$$

where superscript (A) indicates 'Aerodynamic' and thus refers to all aspects of dynamics from the wind turbine from the tower interface and upwards, while subscript (F) refers to the F coordinate system. Further η_F is the 6 degree of freedom displacement of the tower bottom point, measured in the F coordinate system from the initial position. Finally $\mathbf{F}_F^A$ is the forcing of the bottom point exerted by aerodynamic forcing and structural motion above the tower interface point.

The floater is considered as a rigid body. The dynamic description uses the centre of the floater bottom as reference point. Here the coordinate system (O) is defined, with its first axis pointing in the inline direction and its third axis pointing vertically up. Similarly to (9.5), the floater motion in this coordinate system may be written as

$$\mathbf{M}_O^H \ddot{\eta}_O + \mathbf{K}_O^H \eta_O = \mathbf{F}_O^H \qquad (9.6)$$

where superscript (H) indicates 'Hydrodynamic' and thus refers to all dynamics and forcing induced by the water, floater, waves and mooring system. Further subscript (O) designates the (O) coordinate system and η_O is the 6 degree of freedom displacement of the floater bottom in the (O) coordinate system. Finally $\mathbf{F}_O^H$ is the forcing of the floater due to water, waves and mooring with respect to the (O) coordinate system.

A rigid coupling of the wind turbine and floater motion can be achieved by transformation of (9.6) to the (F) coordinate system. This is obtained through the (T) system which is also placed at the tower bottom, but has the same orientation as system (O). As the first step, for small rotations, the displacement in the (T) system can be written as

$$\begin{pmatrix} \eta_1 \\ \eta_2 \\ \eta_3 \end{pmatrix}_T = \begin{pmatrix} \eta_1 \\ \eta_2 \\ \eta_3 \end{pmatrix}_O + \begin{pmatrix} \eta_4 \\ \eta_5 \\ \eta_6 \end{pmatrix}_T \times \mathbf{r}_{OT} \qquad (9.7)$$

where

$$\mathbf{r}_{OT} \begin{pmatrix} 0 \\ 0 \\ d_f + h_{trans} \end{pmatrix} \qquad (9.8)$$

is the position of point (T) in the (O) coordinate system. Note here that the rotational displacements in system (O) and (T), $\eta_{4,5,6}$ are identical. Hereby, the displacement of the floater in the (T) system can be expressed from the displacements in the (O) system by the linear transformation

$$\eta_T = \mathbf{T}_{OT} \eta_O \qquad (9.9)$$

where $\mathbf{T}_{OT}$ is defined through (9.7) and the rotational identity between system (T) and (O). The displacements in the (T) system can further be transformed to displacements in the (F) system by the linear transformation

$$\eta_F = \mathbf{T}_{TF} \eta_T \qquad (9.10)$$

such that the full transformation from the (O) system to the (F) system of the displacements is

$$\eta_F = \mathbf{T}_{TF} \mathbf{T}_{OT} \eta_O \equiv \mathbf{T}_{OF} \eta_O \qquad (9.11)$$

The inverse of this transformation is also linear and is written as

INNWIND.EU, D4.21, State-of-the-art and implementation of design tools for floating structures

$$\eta_O = \mathbf{T}_{FO}\eta_F \qquad (9.12)$$

As the second step, we observe that the translational forces in the (T) and (O) systems are identical. The moments in the two systems are related through

$$\begin{pmatrix} F_4 \\ F_5 \\ F_6 \end{pmatrix}_T = \begin{pmatrix} F_4 \\ F_5 \\ F_6 \end{pmatrix}_O + \begin{pmatrix} F_1 \\ F_2 \\ F_3 \end{pmatrix}_O \times \mathbf{r}_{OT} \qquad (9.13)$$

whereby a the linear transformation

$$\mathbf{F}_T = \mathbf{TF}_{OT}\mathbf{F}_O \qquad (9.14)$$

can be defined. Further, as the forces in the (T) and (F) systems are related through

$$\mathbf{F}_F = \mathbf{T}_{TF}\mathbf{F}_T \qquad (9.15)$$

the full transformation of the force vector from system (O) to (F) can be defined as

$$\mathbf{F}_F = \mathbf{T}_{TF}\mathbf{F}_T = \mathbf{T}_{TF}\mathbf{TF}_{OT}\mathbf{F}_O \equiv \mathbf{TF}_{OF}\mathbf{F}_O. \qquad (9.16)$$

These two steps allows transformation of the hydrodynamic floater equation (9.6) to the (F) coordinate system. First η_O is relaced by η_F through substitution of (9.12). Next, by virtue of (9.16), the full equation is multiplied from the left side of each term by $\mathbf{TF}_{OF}$. Hereby one obtains

$$\mathbf{TF}_{OF}\mathbf{M}_O^H\mathbf{T}_{FO}\ddot{\eta}_F + \mathbf{TF}_{OF}\mathbf{K}_O^H\mathbf{T}_{FO}\eta_F = \mathbf{TF}_{OF}\mathbf{F}_O^H = \mathbf{F}_F^H. \qquad (9.17)$$

The two equations (9.5) and (9.17) now both describes the motion of the tower bottom point, for the wind turbine and floater, respectively. Imagine, the floater and tower where connected by a connection force. This would appear at the right hand sides of each equation and with opposite signs. Addition of the two equations will thus establish a dynamic equation for the tower bottom point that includes the mass, stiffness and forcing from both the aerodynamic and hydrodynamic forces and with no appearance of a connection force. The coupling is thus achieved by addition of the mass matrix of (9.17) into the existing mass matrix in Flex5 for the tower bottom point and by addition of the hydrodynamic forcing and mooring forcing, referenced to point (F) into Flex5. The stiffness matrix is treated similarly. Hereby, a rigid coupling is obtained with no need for iteration for equilibrium in each time step and with only one set of resulting dynamic equations.

It should be noted that this method of coupling assumes that the angles for pitch, roll and yaw are small as these are linearized in the transformation matrices. This limitation, however, is consistent with the common method of hydrodynamic modelling with e.g. Wamit, which also builds on linearized motion.

9.5 Force models for fully nonlinear wave loads

Two standard methods for the description of floating bodies are widely used in the content of floating wind turbines. One is based on Wamit [9.15] where the linearized equations of motion for the flow around a floating body are solved for the radiation and added mass forces associated with oscillatory motion around its equilibrium point along with the excitation force from linear waves. The associated frequency-dependent results can be applied in time-domain description by the method of Cummings.

As an alternative, the Morison equation [9.14] may be applied under the assumption of a slender body. This is justified when the diameter D does not cover more than 20% of the incident wave length. In this siuation the hydrodynamic forcing can be described by a strip-theory approach, where the body is divided into a number of slices confined between horizontal planes. For each slize, the force per unit length is then a sum of a drag term and two inertia terms

$$f = \frac{1}{2}\rho C_D D(u - \dot{x})|u - \dot{x}| + \rho A C_m(\dot{u} - \ddot{x}) + \rho A \dot{u}.$$ (9.18)

For small waves, linear theory is adequate, and the fluid acceleration $\dot{u}$ can be consistently substituted by the Eulerian derivative $\frac{\partial u}{\partial t}$. This formed the basis for the force description in [9.19] and has been used in many studies of floating wind turbines. More-over, within the linear accuracy for small waves, the vertical integration of (9.18) may be carried out only up to the still water level and not all the way to the wave crest. In practice this is not a severe limitation, as the loads are often inertia dominated, such that the largest forces occur when the free surface elevation is close to zero.

For large-amplitude waves, the wave nonlinearity becomes appreciable and the time derivative of u needs to expressed as the total Lagrangian acceleration

$$\dot{u} = \frac{du}{dt} = u_t + u u_x + v u_y + w u_z$$ (9.19)

This has been formally derived in [9.17], [9.18] where it is also found that an extra term $\rho A C_m w_z(u - \dot{x})$ must be included in (9.18) along with a surface intersection force

$$F_{\text{surface}} = -\frac{1}{2}\rho A C_m \eta_x(u - \dot{x})^2.$$ (9.20)

The first of these, $\rho A C_m w_z(u - \dot{x})$ is denoted the axial divergence force and is due to the non-slenderness of the body in the vertical direction. The surface intersection force is due to the change of kinetic energy in the flow around the structure when the wetted extent of it is changed. This force model is suited for fully nonlinear incident waves and was used in [9.2] and [9.3] for higher-harmonic forcing of monopiles. More-over it has been used by [9.20] within the Flex5 model, also in relation to fully nonlinear wave forcing.

While the Rainey force model is a natural choice of force model and will be applied within the TLP framework, the results of the present study have been obtained with the standard Morison equation (9.18).

Recently [9.22] has presented a forcing formulation for floating bodies subjected to fully nonlinear waves. In contrast to classical force theories that are based on integration of the instantaneous pressure on the surface of the body and therefore involves evaluation of $(\nabla\phi)^2$ at the body surface, the Sclavounos force formulation is based on the fluid impulse and therefore simply needs integration of the potential at the body face. The influence of the radiated and diffracted waves are taken fully into account at the body surface, while their interaction with the incident wave field is treated approximately through linearization of the free surface conditions around the incident wave field. This is justified for slender bodies, where the diffracted and radiated wave fields are small in magnitude.

The method of Sclavounos seems to be an attractive way forward for fully nonlinear forcing of floating wind turbines. It is based on the idea that the incident wave field has been pre-computed

INNWIND.EU, D4.21, State-of-the-art and implementation of design tools for floating structures

such that the forcing is determined afterwards. In contrast to the method of Rainey, however, a boundary value problem for the diffracted and radiated wave field must be solved in each time step around the body and the free surface. While further work with this method is intended at DTU, the present study is based on the Morison equation. As a first simple improvement this will be extended to the Rainey force formulation and then as a further step, the method of Sclavounos will be considered.

9.6 Focused wave groups and their application as design waves

Focused wave groups can be conveniently used as design waves due to their transient nature. In physical experiments, a focused wave group is attractive as its short duration eliminates the problem of reflections from the down-wave boundary of a wave tank. The NewWave theory was first presented in [9.24] where it was shown that the NewWave is the average shape of a large-amplitude wave realization and further takes the form of the auto-correlation of the spectrum function. Thus for a wave spectrum S , the New Wave takes the form

$$\eta(x,t) = \frac{\alpha}{\sigma^2} \sum_{j=1}^{N} S_j \Delta f \cos\left(\omega_j(t - t_0) - k_j(x - x_0)\right)$$

$$(9.21)$$

where $\sigma^2 = \int_0^\infty S df$ is the variance of the free surface elevation, Δf is the frequency spacing, (ω_j, k_j) are the radian frequency and wave number for each wave component and (x_0, t_0) is the focus location and focus time. An example of a focused wave group is given in Figures 9.6 and 9.9.

The focused wave group theory has got increasing attention since the record of the Draupner wave on January 1st 1995 at the Draupner platform in the North Sea. This giant wave resembled remarkably well the shape of a New Wave and has since been analysed by many researchers, see e.g. [9.1]. The New Wave theory is sometimes applied in wind turbine design through embedment of a New Wave signal into an irregular wave record.

In the present study, a New Wave realization of a JONSWAP spectrum will be applied to study the influence of wave nonlinearity to forcing from steep and near-breaking water waves.

9.7 Results

The response of the TLP configuration subjected to nonlinear wave forcing is now investigated. A generic wave event produced by a focused nonlinear wave group is applied along with four different wind climates.

9.7.1 The incident waves and wind fields

The incident wave group is produced from a JONSWAP spectrum [9.6] and has a linear crest height of 14.5 m. The peak period of the spectrum is T_p = 13.8 s. The wave is propagated at a depth of h = 200m in the domain shown in Figure 9.5 where the peak wave length is indicated by the spacing between the vertical lines. The waves are generated in a zone that stretches two peak wave lengths from the western boundary. The linear focus point is at x = 1486m which is two peak wave lengths from the inward boundary of the generation zone. This is marked by the red vertical line.
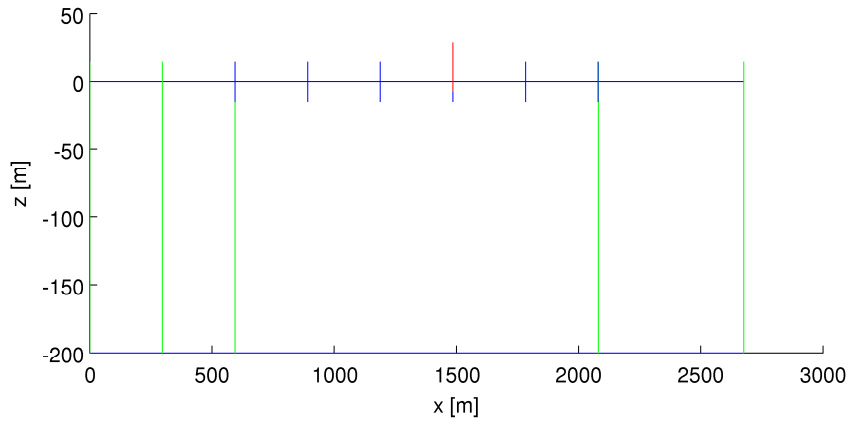
Figure 9.5: Computational domain for incident wave group.

The resulting time series of wave elevation is shown in Figure 9.6 in the bottom panel. The wave reaches a maximum crest elevation of 18.0 m and the wave height, when measured to the following trough is 27.6 m. A later comparison to a linear computation with the same incident wave signal shows that the largest crest of the nonlinear group occur one wave period earlier than for the linear realization. This is discussed further in a subsequent section.

The four wind fields are illustrated in terms of incident wind speed at the hub height in the upper panel. The turbulent wind fields were generated by the Mann turbulence model [9.13] and are identical to the ones applied in [9.20]. The mean wind speeds and turbulence intensities are listed below:

V_{mean}	Turbulence intensity	Turbine state
[m/s]	[-]	[-]
9	0.19	Gen
15	0.16	Gen
20	0.14	Gen
28	0.13	Idled

Table 9.2: Wind climates

INNWIND.EU, D4.21, State-of-the-art and implementation of design tools for floating structures
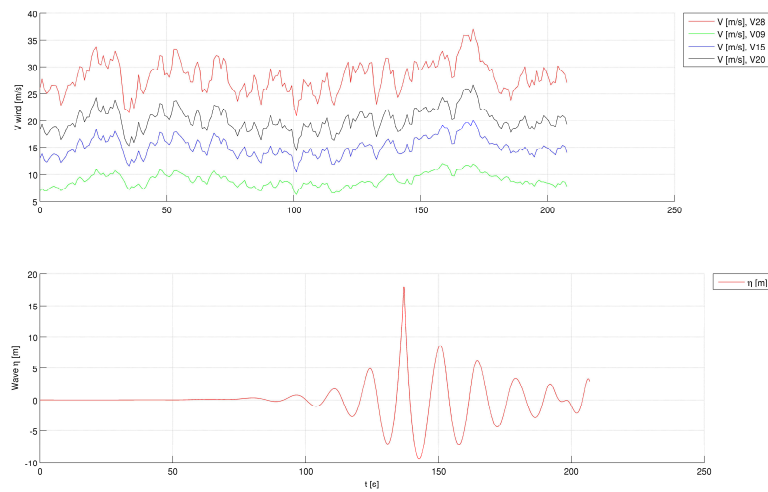
Figure 9.6: Upper panel: Time series of wind speeds at hub height. Lower panel: Time series of free surface elevation for the nonlinear focused wave group.

9.7.2   Response of the TLP wind turbine in storm condition

We first consider the response of the TLP wind turbine to the focused nonlinear wave group at the strong wind speed of 28 m/s. In this wind condition, the wind turbine is idled with blades pitched to feather position of an 87 deg angle. Hence in this situation the main wind forcing is from turbulent components perpendicular to the inline wind direction and the response is wave-dominated.

The platform response is shown in Figure 9.7 as time series for time series of platform surge, platform pitch and platform heave. The platform motions are described in the (T) coordinate system with origin at the bottom of the tower. Also included in the figure are the time series of wind speed and free surface wave elevation for reference. The corresponding raw power spectra are shown in Figure 9.8 which is utilized in the analysis.

The surge signal has an almost zero mean due to the idled state of the wind turbine. A clear forcing from the wave is seen, leading to a maximum surge amplitude of 11 m. The largest response, however, occur for the second large wave in the group which is less steep than the first wave. Although the natural surge frequency of 0.026 Hz is way below the wave forcing frequency of 0.073 Hz, it is speculated if this effect may be due to dynamic motion of the TLP which is initiated by the first wave and enhanced by the second wave.

Also the platform pitch signal shows clear forcing from the waves and also excitation of the natural pitch frequency of 0.15 Hz. This is a very likely effect as this natural frequency is close to twice the primary wave frequency.

The heave motion is seen to follow the surge motion through the set-down effect, where large surge displacements lead to negative heave due to the geometric constraint of the mooring tendons. Also some heave-pitch coupling is evident from inspection of the power spectra.

INNWIND.EU, D4.21, State-of-the-art and implementation of design tools for floating structures
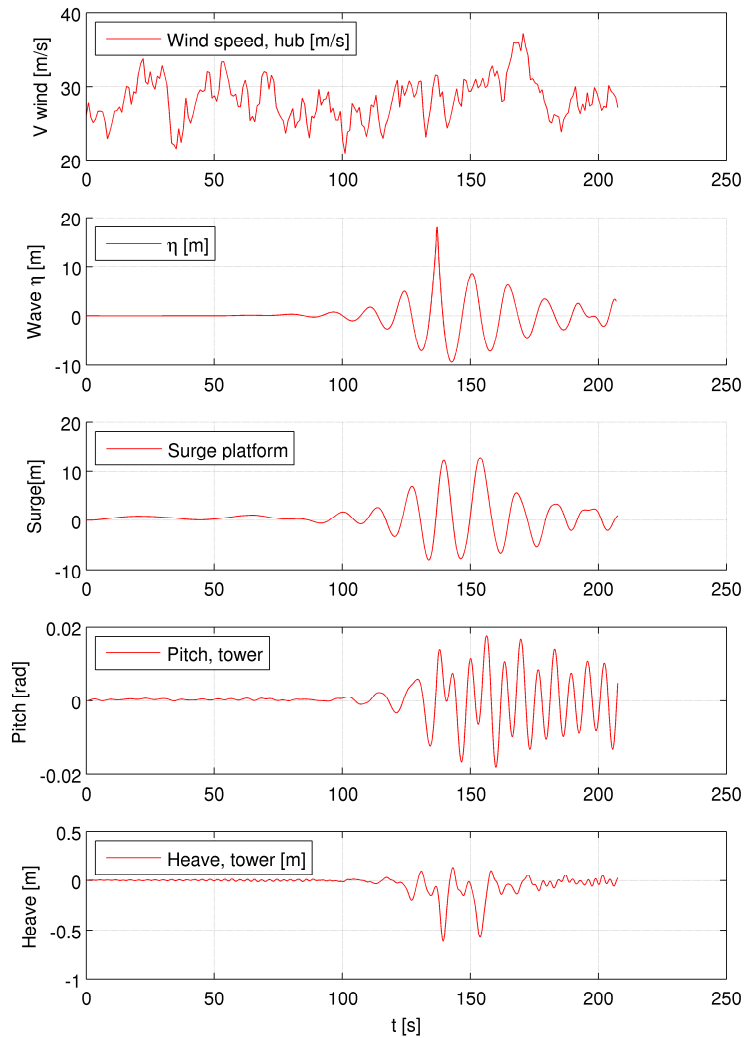
Figure 9.7: TLP response to focused wave group. From top panel to bottom panel, time series of wind speed, free surface elevation, platform surge, platform pitch and platform heave. Platform motions are measured at the interface point with the bottom of the tower.

INNWIND.EU, D4.21, State-of-the-art and implementation of design tools for floating structures
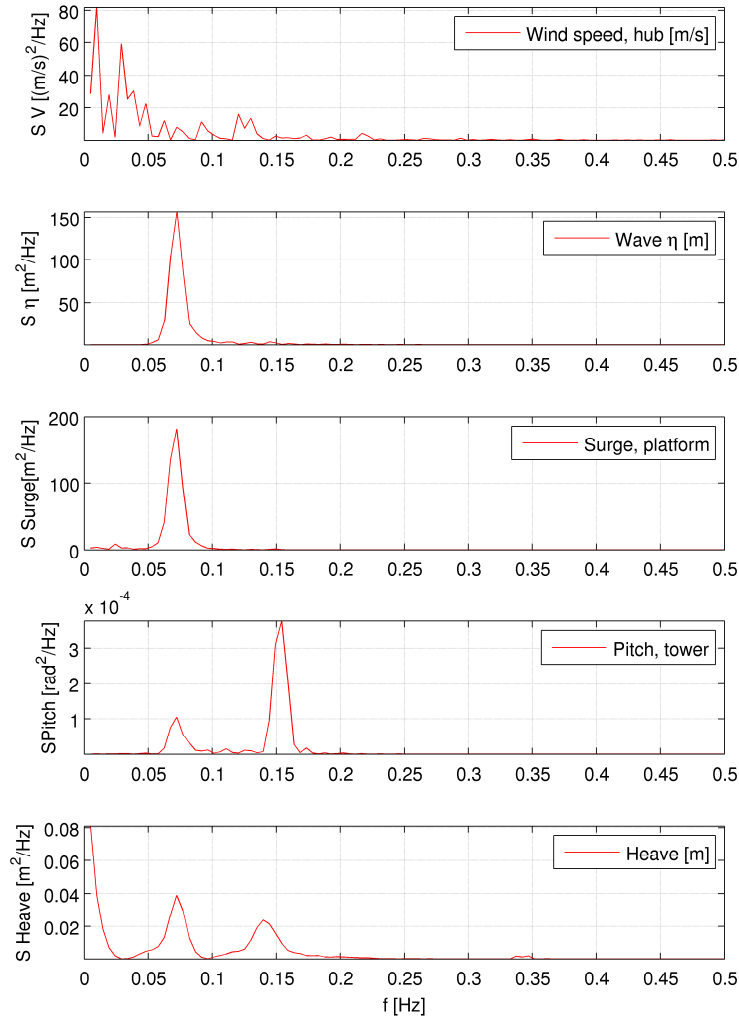
Figure 9.8: Raw power spectra of the time series of Figure 9.7 of TLP response to focused wave group. From top panel to bottom panel, power spectra of wind speed, free surface elevation, platform surge, platform pitch and platform heave. Platform motions are measured at the interface point with the bottom of the tower.

9.7.3   Comparison to linear wave forcing

A comparison between the response to linear and nonlinear wave forcing is shown in Figure 9.9. The wind climate still has a mean hub wind speed of 28 m/s. We first note that the free surface elevation η is quite different between the two signals. While the linear signal has a symmetric shape around the focus point with the largest crest centered in the group, the nonlinear wave signal shows a strong focusing of the first wave in the group and smaller amplitude for the following crest. These differences lead to differences in the response. Although for the initial large wave, the platform surge is largest for the nonlinear wave, the largest surge amplitude for the full event occur due to linear forcing. For the nonlinear signal, a clear dynamic build up of motion is seen through the larger response to the second wave, which however, is smaller in amplitude than

INNWIND.EU, D4.21, State-of-the-art and implementation of design tools for floating structures

the first wave. It is thus likely that a nonlinear signal with its largest wave centered at the mid point of the group would have lead to an even stronger surge amplitude.

Similar findings apply for the pitch motion where both wave groups are able to excite the natural pitch frequency. The largest pitch response occur due to the linear wave. The heave signal shows the same tendency. These results are in disagreement with the expectation that nonlinear waves through their higher-harmonic frequency content should be most able to excite the natural motion of at least the platform pitch frequency. Such observations has been described in [9.20] for monopile wind turbines in nonlinear waves. It must be noted, though, that for the investigated monopile structure, the lowest natural frequency was 0.28 Hz and thus about twice as large as the pitch frequency of the present configuration.

Additionally to the likely explanation through resonant dynamics and the placement of the largest wave within the group envelope, another effect that reduces the significance of nonlinearity is the placement of the main floater volume below the free surface. Hereby most of the forcing is inertia dominated and thus mainly linear. More-over, the higher-harmonic wave components decay rapidly over depth and are therefore less severe for a submerged floater than for a surface piercing structure with no significant submerged volume.
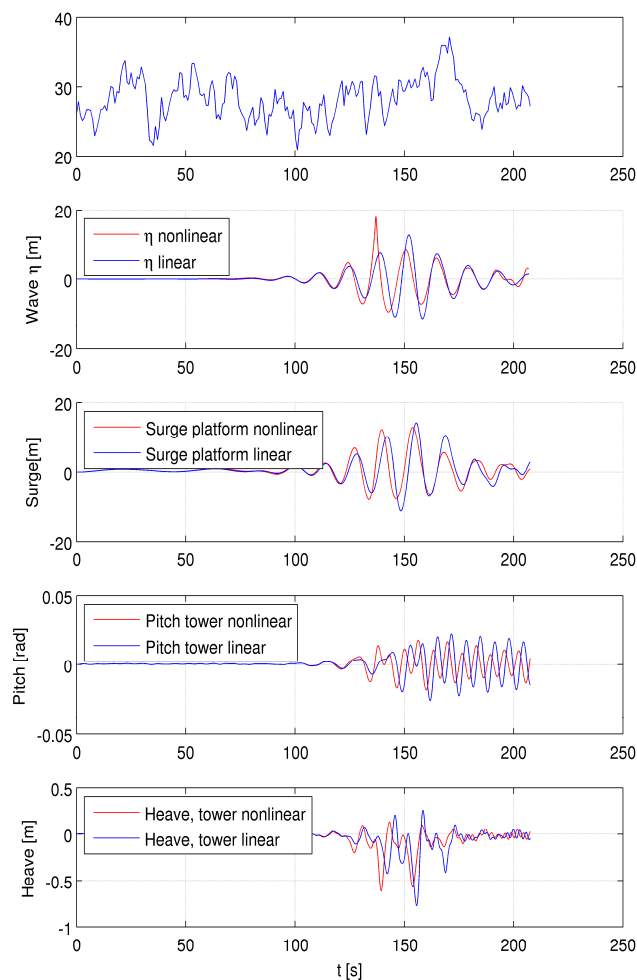

Figure 9.9: Comparison of TLP response to focused wave group from linear and nonlinear computation of wave transformation.

INNWIND.EU, D4.21, State-of-the-art and implementation of design tools for floating structures

9.7.4   Comparison of response at varying wind speed

We now study the TLP response to the nonlinear wave group subject to the four different wind climates. This will show to which extent the aerodynamic damping affects the floater response. Comparisons of platform surge, platform pitch and overturning moment at the bottom of the tower are shown in Figure 9.10.

The mean surge displacement is largest for the wind speed of 9 m/s. This wind speed is relatively close to the rated wind speed of 11.4 m/s where the mean thrust is largest. For the wind speeds of 15 m/s, 20 m/s and 28 m/s the mean surge becomes smaller due to the corresponding decrease in mean thrust above rated wind speed. The largest surge response to the wave forcing is seen for V = 28 m/s, where the damping is also smallest. For the other wind speeds, there is no clear trend in the surge amplitude as function of wind speed.

The response pitch response is wave dominated, as almost no motion is seen prior to the arrival of the wave group. The largest excitation occur for the wind speeds of 15 m/s and 20 m/s. This is against the expectation of strong aerodynamic damping at these wind speeds. Several researchers have reported on the issue of negative damping of pitch motion through the blade pitch system for floating wind turbines, see e.g. [9.11]. This, however, has been in the context of spar buoy floating wind turbines which has a much lower natural pitch frequency (~ 0.03 Hz) than the present TLP configuration. Also Ramachandran [9.19] investigated the possible pitch instability to the controller action for the present configuration and found that this instability did not occur.

A closer inspection, however, shows that the natural pitch frequency varies slightly as function of the mean surge. For the two wind speeds of 15 m/s and 20 m/s it is identical and equal to 0.149 Hz. For the two other wind speeds, the natural pitch frequency falls at each side of this value. With a primary wave frequency of 0.0725 Hz, the exact placement of the pitch frequency may be the determining factor for the amplitude of the response through dynamic amplification. This seems a likely explanation for the largest response at these two wind speeds.

The tower bottom moment is seen in the lower panel of the figure. This signal shows the same trends as the platform pitch signal with respect to the wind speed. The largest response occur for wind speeds of 15 m/s and 20 m/s and the smalles response is for $V = 28$ m/s.
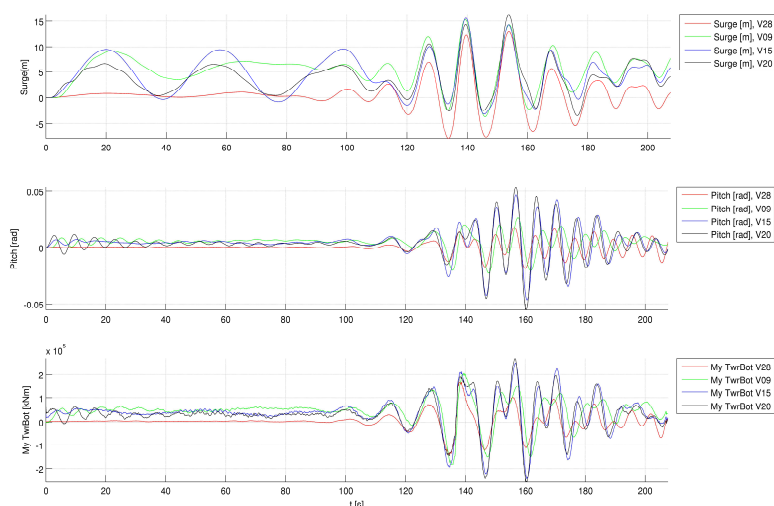

Figure 9.10: Comparison of TLP response to nonlinear focused wave group in various wind climates. From top panel to bottom panel, time series of platform surge, platform pitch and overturning moment at tower bottom.

INNWIND.EU, D4.21, State-of-the-art and implementation of design tools for floating structures

9.8 Conclusions, discussion and future work

The basic theory behind the Flex5 aero-elastic model has been summarized. Flex5 has been applied to TLP floating wind turbines and the Principle Power semisub configuration. In the present study, the TLP configuration has been extended with fully nonlinear wave forcing from waves of the potential flow model 'OceanWave3D' [9.4] in combination with the Morison equation. A straigh-forward extension to the force formulation of Rainey [9.17], [9.18] is planned. Further, the recent force formulation presented in [9.22] has been mentioned as a noteworthy alternative, although it requires the solution of a boundary value problem at each time step to evaluate the radiation and diffraction potential around the floating body.

Generic simulations of response to fully nonlinear focused wave groups at a depth of 200 m have been presented. Contrary to the expectation, the response to the nonlinear waves was not larger than that caused by linear waves. It is suggested that this is due to the different placement of the largest individual wave within the nonlinear and linear wave groups respectively, which allowed for a stronger dynamic build-up of motion for the linear realization. This hypothesis is subject to ongoing investigation. Another factor that influences the importance of nonlinearity is the placement of the main floater volume at a depth of 25–15 m below the still water level. At this depth, the higher-harmonic wave components are decayed relatively to their pressence in the free surface region and the forcing is inertia dominated, leading to a predominantly linear forcing.

The effect of aerodynamic damping of the dynamic response has been investigated by application of four wind climates of increasing wind speed. For the three wind speeds of wind turbine operation, the mean surge follows the mean thrust. Also, the surge motion is largest for the largest wind. For the other wind speeds, however, the expected increasing damping from increasing wind, could not be clearly detected. Further, the platform pitch and tower bottom moment showed the strongest response for the wind speeds of 15 m/s and 20 m/s. It is suggested that for the present example, this is due to resonance of the second harmonic force harmonic with the natural pitch frequency which was found to vary with the mean surge and thus to be a function of the wind speed.

The forcing from nonlinear wave groups and the dynamics of the TLP structure is subject to ongoing research at DTU. The wave coupled aero-servo-hydro-elastic model will further be validated against experimental data.

9.9 References

[9.1] Adcock, T. A. A., Taylor, P. H., Yan, S., Ma, Q. W. and Janssen, P. A. E. M., *"Did the Draupner wave occur in a crossing sea?"*, Proc. Roy. Soc. 467, 3004–3021, 2011.

[9.2] Bredmose, H., Schløer, S. and Paulsen, B., *"Higher-harmonic response of a cantilever beam to fully nonlinear regular wave forcing"* In: 'Proc. of the ASME 31th 2012 Int. Conf. on Ocean, Offshore and Arctic Engng'.

[9.3] Bredmose, H., Slabiak, P., Sahlberg-Nielsen, L. and Schlütter, F., *"Dynamic excitation of monopiles by steep and breaking waves. Experimental and numerical study"* In: 'Proc. of the ASME 32nd 2013 Int. Conf. on Ocean, Offshore and Arctic Engng'.

[9.4] Engsig-Karup, A., Bingham, H. B. and Lindberg, O., *"An efficient flexible-order model for 3D nonlinear water waves"*, J. Comp. Phys. 228, 2100–2118, 2009.

[9.5] Hansen, A. M., Laugesen, R., Bredmose, H., Mikkelsen, R. F. and Psichogios, N., *"Small scale experimental study of the dynamic response of a tlp wind turbine"*, Submitted for publication, 2013.

INNWIND.EU, D4.21, State-of-the-art and implementation of design tools for floating structures

[9.6] Hasselmann, K., Barnett, T. P., Bouws, E., Carlson, H., Cartwright, D. E., Enke, K., Ewing, J. A., Gienapp, H., Hasselmann, D. E., Kruseman, P., Meerburg, A., Müller, P., Olbers, D. J., Richter, K., Sell, W. and Walden, H., *"Measurements of wind-wave growth and swell decay during the joint north sea wave project (JONSWAP)"*, Ergänzungsheft zur Deutchen Hydrographischen Zeitschrift. 95 pages, 1973.

[9.7] Joensen, S., Jensen, J. J. and Mansour, A. E., *"Extreme value predictions for wave and wind-induced loads on floating offshore wind turbines using FORM"*, In: 'Proc. 10th Int. PRADS Symp.', Pennsylvania, US, 2007.

[9.8] Jonkman, J., Larsen, T., Hansen, A., Nygaard, T., Maus, K., Karimirad, K., Gao, Z., Moan, T., Fylling, I., Nichols, J., Kohlmeier, M., Vergara, J. P., Merino, D., Shi, W. and Park, H., *"Offshore code comparison collaboration within IEA task 23: Phase IV results regarding floating wind turbine modeling"*, In: '2010 Eur.Wind Energy Conf (EWEC)',Warsaw, Poland, 2010.

[9.9] Kim, T., Hansen, A. M. and Branner, K., *"Development of an anisotropic finite beam element for composite wind turbine blades in multi-body system"*, Renewable Energy 59, 172–183, 2013.

[9.10] Krieger, A., *"Aero and hydrodynamic analysis of a wind turbine on a semi-submersible structure"*, Master's thesis, DTU Mech. Engng, 2011.

[9.11] Larsen, T. J. and Hanson, T. D., *"A method to avoid negative damped low frequency tower vibrations for a floating pitch regulated wind turbine"*, Journal of Physics: Conference Series. The Science of Making Torque from Wind, 2007.

[9.12] Larsen, T. J., Madsen, H. A., Larsen, G. C. and Hansen, K. S., *"Validation of the dynamic wake meander model for loads and power production in the Egmond aan Zee wind farm"*, Wind Energy 16(4), 605–624, 2013.

[9.13] Mann, J., *"Wind field simulation"*, Prob. Engng. Mech. 13, 269–282, 1998.

[9.14] Morison, J. R., O'Brien, M. P., Johnson, J. W. and Schaaf, S. A., *"The forces exerted by surface waves on monopoles"*, J. Petrol. Techn. 189, 149–154, 1950.

[9.15] Newman, J. N., *Marine Hydrodynamics*, MIT Press, 1977.

[9.16] Øye, S., *"Flex4 simulation of wind turbine dynamics"*, In: 'Proc. 28th IEA meeting of experts concerning state of the aet of aero-elastic codes for wind turbine calculation', IEA, 1996.

[9.17] Rainey, R. C. T., *"A new equation for calculating wave loads on offshore structures"*, Journal of Fluid Mechanics 204, 295–324, 1989.

[9.18] Rainey, R. C. T., *"Slender-body expressions for the wave load on offshore structures"*, Proc. Roy. Soc. London Series A. Math. and Phys. Sci. 450(1939), 391–416, 1995.

[9.19] Ramachandran, G. K. V. R., *"A numerical model for a floating TLP wind turbine"*, PhD thesis, DTU Wind Energy, 2013.

[9.20] Schløer, S., *"Fatigue and extreme wave loads on bottom fixed wind turbines. Effects from fully nonlinear wave forcing on the structural dynamics".*, PhD thesis, DTU Wind Energy. Submitted for defense, 2013.

[9.21] Schløer, S., Bredmose, H., Bingham, H. B. and Larsen, T. J., *"Effects from fully nonlinear irregular wave forcing on the fatigue life of an offshore wind turbine and its monopile foundation"*,

In: 'Proc. of the ASME 31th 2012 Int. Conf. on Ocean, Offshore and Arctic Engng', ASME. Rio de Janeiro, Brazil, 2012.

[9.22] Sclavounos, P. D., *"Nonlinear impulse of ocean waves on floating bodies"*, J. Fluid Mech. 697, 316–335, 2012.

[9.23] Sist, N., *"Hydrodynamic model for a semi-submersible floating wind turbine"*, Master's thesis, DTU Mech. Engng, 2011.

[9.24] Tromans, P. S., Anaturk, A. and Hagemeijer, P., *"A new model for the kinematics of large ocean waves—application as a design wave"*, In: 'Proc. 1st Int. Conf. Offsh. Mech. and Polar Engng. (ISOPE)', Vol. 3, pp. 64–71, 1991.

[9.25] Wheeler, J. D., *"Method for calculating forces produced by irregular waves"*, J. Petrol Techn. pp. 119–137, 1970.

INNWIND.EU, D4.21, State-of-the-art and implementation of design tools for floating structures

10 DNV GL GROUP TOOLS

10.1 DNV GL Approach of coupling ANSYS AQWA and BLADED

For the simulation and assessment of loads of a floating wind turbine DNV GL uses two computer codes: BLADED (GL Garrad Hassan) and AQWA (ANSYS). DNV GL performed an in-house comparison analyses in the frequency and time domain with both codes. While Eigen frequencies of the systems can be found with analysis in the frequency domain, calculation in the time domain are necessary for non-linear, dynamic and transient processes, which are important for load analysis. The hydrodynamic calculations must consider non-linear mooring systems and the effects of radiation and diffraction forces.

GL GH BLADED is the in-house developed dynamic load calculation program for multibody structures with coupled aerodynamic and hydrodynamic loads. BLADED calculates the structure dynamic with a multibody-dynamic-approach. The components such as blades and tower are modelled from single, linear and flexible elements whose deformation is determined by modal analyses. This is done by a linear combination of the calculated Eigenmodes resulting from a finite elements method calculation. The aerodynamic forces are calculated with the blade element momentum theory. In addition BLADED is able to simulate a wake behind the rotor and dynamic stall.

BLADED can simulate regular and irregular waves as well as sea currents. Regular waves are used mainly for determination of extreme loads and will be described as Airy-waves or with the stream function. For fatigue loads a series of irregular waves is created whose amplitude and frequency is defined with a spectral density function as the JONSWAP- or Pierson-Moskowitz spectrum. The hydrodynamic forces are calculated with the Morison equation. The mooring system is represented by a force-displacement ratio, linear or non-linear, and are calculated separately by the user and implemented via a stiffness matrix at the fairlead position [10.1].

ANSYS AQWA is software for hydrodynamic calculations of offshore structures. It consists of several partly stand-alone programs and provides solutions in the frequency and time domain. The calculations are based on the Green function. Structure dynamic solutions are not provided by AQWA. The used programs in the AQWA suite are AQWA-LINE for calculations in the frequency domain based on the potential theory with regular waves and AQWA-NAUT for calculations in the time domain. AQWA-NAUT uses the hydrodynamic coefficients from AQWA-LINE as input and simulates the motions of the floating body in regular and irregular waves. A mooring system can be modelled as either linear or non-linear cables [10.2].

The main purposes of the DNV GL comparison have been a code to code comparison of hydrodynamic forces and motions of two types of moored floating wind turbines, a semi-submersible and a spar buoy between BLADED and AQWA and with measurement data from model tests at University of Ulsan (Korea) respectively. Furthermore load calculations with BLADED of a floating offshore wind turbine, including aerodynamic, hydrodynamic and elastic forces have been performed.
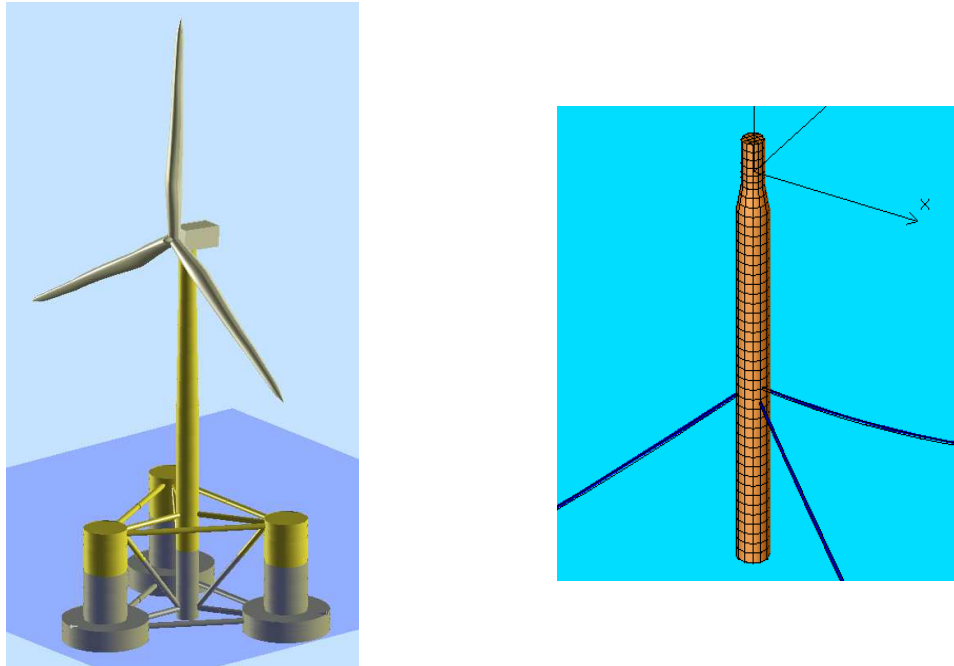
Figure 10.1: Bladed models of semisubmersible and spar buoy floating platforms

Within the scope of the Diploma-Thesis "Numerical Simulation of the Motion Behaviour of Floating Wind Turbine", C. Weber (2012) the two floating structure design types semi-submersible and a spar buoy were analysed in terms of their hydrodynamic behaviour; one of them is defined as hydrodynamic transparent and the other one a hydrodynamic compact. The reference data were taken from the projects Offshore Code Comparison Collaboration and Continuation of the International Energy Agency (IEA).

The turbine used in all phases is the NREL 5 MW turbine (see specifications on section 9 of the paper for the COME 2013 Conference at the University of Hamburg [10.7]).

The analysis focuses on the numerical comparison of the hydrodynamic conclusions from a load-calculation-program for wind turbines that uses the Morison equation for hydrodynamics to a hydrodynamic program based on the Green function method. The expected differences are caused by the fact, that the Morison equation is only valid for calculations of hydrodynamic transparent structures. Since floating structures often comply with the definition of hydrodynamic compact, the question is to what level it is possible to estimate the correct loads from wind and waves using results from the Morison equation or using results on the basis of transfer functions (RAOs).

In a first step the spar buoy type has been analysed in frequency domain with AQWA only. Here the different approaches for AQWA Morison versus AQWA Potential theory have been compared. The spectra for the governing degrees of freedom heave (vertical motion) and pitch (inclination) showed the following results (Figure 10.2):

- Heave   good agreement
- Pitch   overestimated amplitude at resonance frequency

INNWIND.EU, D4.21, State-of-the-art and implementation of design tools for floating structures
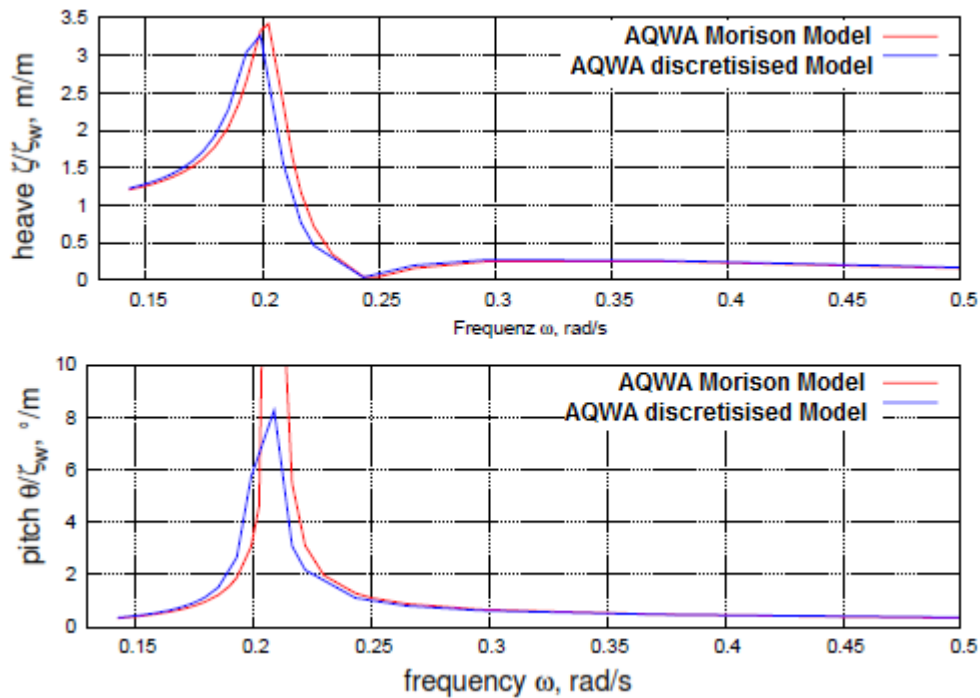
Figure 10.2: Comparison of AQWA Morison vs. AQWA Potential theory for the spar buoy

As an extension AQWA has been compared to BLADED and again the different hydrodynamic approaches have been applied. The results of the spar buoy type transfer functions for heave motion for AQWA Morison/BLADED versus AQWA potential theory/BLADED showed good agreement (Figure 10.3). Thus the spar buoy type can be considered as a hydrodynamic transparent structure and the Morison approach appears as sufficiently accurate.
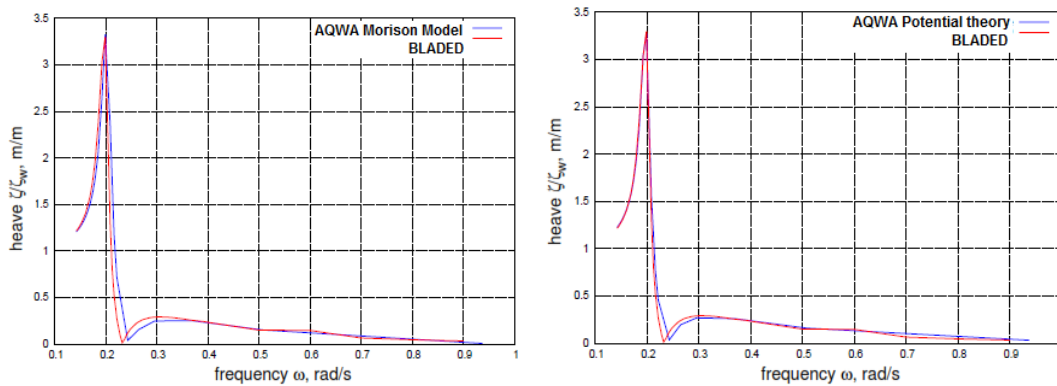
Figure 10.3: Comparison of AQWA Morison vs. Bladed for the spar buoy

The second offshore floating structure type for the code comparison was the semi-submersible. The model has been adopted from the Offshore Code Comparison Collaboration Continuation project (OC4). The transfer functions for heave in AQWA and BLADED (time domain) showed good agreement for resonance frequency and amplitude (see Figure 10.4). However, in BLADED the amplitudes for intermediate frequencies found twice as high as in AQWA. A local check calculation with an analytical approach for heave motion confirmed the AQWA results rather than the BLADED results.

INNWIND.EU, D4.21, State-of-the-art and implementation of design tools for floating structures
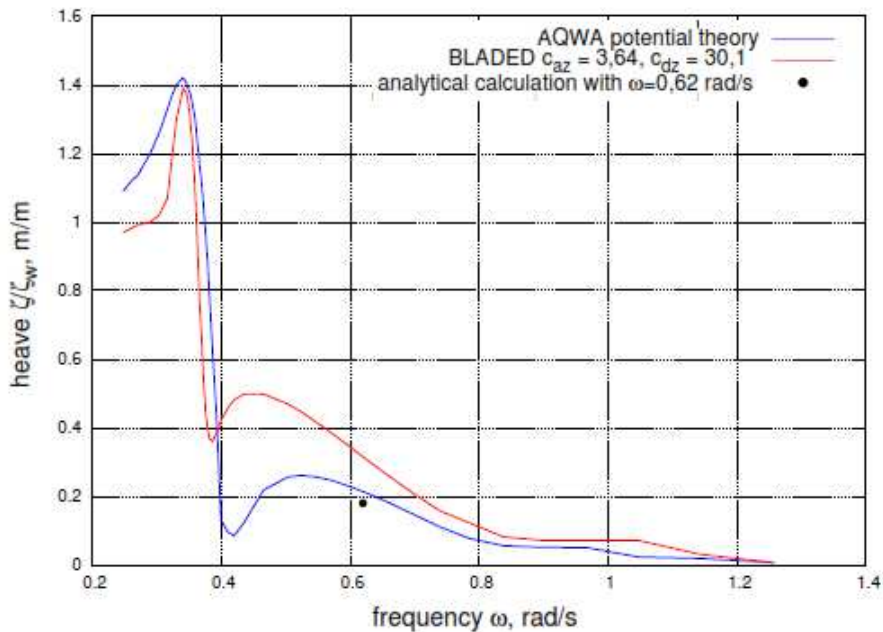
Figure 10.4: Heave RAO calculated by AQWA and Bladed for the semi-sumersible

The results have pointed out that those calculations with BLADED are possible, under the assumption that the hydrodynamic are well equivalently been modelled with help from ANSYS AQWA or similar codes based on the potential theory or with the support from model tests.

Nevertheless this was a very introductory study and many aspects related with the dynamics of the floating bodies should be kept in mind for further studies or code developments [10.3 – 10.7].

Large motions that occur with floating platforms could not be represented correctly by current BLADED versions. Rotational motions were also not adequately represented which are required to account for the pitch motion of floating structures. Therefore, a complete new approach was considered to overcome inherited restrictions. Now, the use of multi-body dynamics within BLADED enables the modeling of separate bodies with individual modal properties which are coupled together using the equations of motion. This allows the modeling of floating structures with all of its six degrees of freedom and large rotations and displacements.

10.2 Sesam Mimosa

Sesam Mimosa (DNV GL) software is the market leader in mooring analysis and calculations for mooring systems. It uses a number of complex variables in its analysis. The Sesam Mimosa mooring software makes it easier to analyse mooring systems.

Its mooring software offers a variety of options such as calculation of the vessel's wave frequency and low-frequency motions and mooring line tensions. Several options are available for analysis of the properties of the mooring system and individual mooring lines. The Sesam Mimosa mooring software is up-to-date with respect to all calculations required by the Norwegian Maritime Directorate (NMD) and the American Petroleum Institute (API) for approval of positioning systems. Sesam Mimosa mooring software covers:

- Static and dynamic environmental forces due to waves, wind and current
- Wave induced motions
- Slow drift motions
- Static and dynamic mooring system analysis
- Composite mooring lines
- Transient motions after line breakage

INNWIND.EU, D4.21, State-of-the-art and implementation of design tools for floating structures

- Non-Gaussian statistics
- Dynamic positioning (DP) with thrusters
- Stability analysis of turret-moored ships
- Long term simulation
- Rayleigh based calculation of extreme response
- API wind gust spectrum

The Sesam Mimosa mooring software is interfaced with the Sesam Wadam software to ease the input of frequency dependent transfer functions and wave drift coefficients.

10.3 Sesam Hydro/Wadam

The Sesam HydroD Wadam software is a general hydrodynamic analysis program for calculating wave-structure interaction for fixed and floating structures of arbitrary shape.
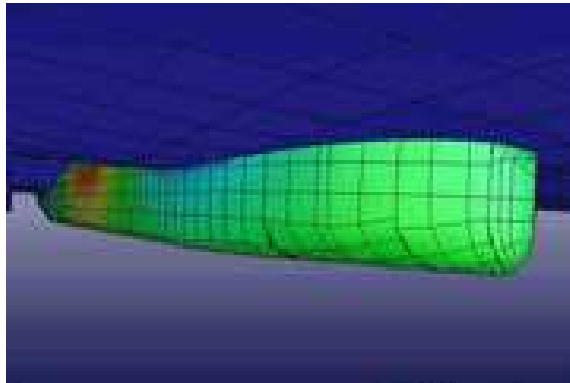

Figure 10.5: Floating Structure in Sesam

It is the ideal tool for semi-submersibles, TLPs, FPSO's, spars, and gravity based structures.
A track record of success in hydrodynamics

The analysis features of the Sesam HydroD Wadam software represent state-of-the-art technology and the program is unsurpassed for practical applications. Airy wave theory is applied and results are presented as complex transfer functions or as deterministic results for specified phases of the wave.

The Sesam HydroD Wadam software is based on widely accepted linear methods for marine hydrodynamics, the 3-D radiation-diffraction theory employing a panel model (created by Sesam GeniE Patran-Pre) and Morison equation in linearised form employing a beam model (created by Sesam GeniE).

The former method is appropriate for voluminous structural parts (having typical dimensions greater than 1/5 of the wavelength). The latter method will predict drag (viscous) forces more accurately and is therefore suitable for more slender structural parts.

For a structure comprised of both slender and voluminous parts the two methods may be used in combination. The user will then establish so-called composite or dual models.

By establishing a dual model in which a structure is modelled by a beam model inside a panel model the advantages of both methods may be utilised. The Sesam GeniE Wadam software will automatically apply the appropriate method based on the ratio of the structural dimension (diameter) to wavelength.

INNWIND.EU, D4.21, State-of-the-art and implementation of design tools for floating structures

The radiation-diffraction part of Wadam is based on software developed by Massachusetts Institute of Technology.

The Sesam HydroD Wadam software is often executed from Sesam HydroD where graphic modelling of the environment is done.

10.4 References

[10.1] Bossanyi, E.A., *GH BLADED Theory Manual*

[10.2] Dinsen and Hansen, H., *ANSYS AQWA-Wave User Manual – Hydrodynamic Load Transfer*, 2009

[10.3] Cordle, C., *"State-of-the-art in design tools for floating offshore wind turbines"* Upwind deliverable D4.3.5

[10.4] Cordle, A., Kaufer, D., Vorpahl, F., Fischer, T., Sørensen, J. D., Schmidt, B., Matha, D., Lucas, J., McCowen, D., Pereira, R. and Argyriadis K, "Enhancement of design methods and standards" Upwind deliverable D4.3.6

[10.5] Cordle, A., Jonkman, J., *"State of the Art in Floating Wind Turbine Design Tools"* ISOPE 2011, Maui, Hawaii, 2011.

[10.6] Matha, D., Schlipf, M., Cordle, A., Pereira, R. and Jonkman, J. *"Challenges in Simulation of Aerodynamics, Hydrodynamics, and Mooring-Line Dynamics of Floating Offshore Wind Turbines"* ISOPE, 2011.

[10.7] Weber, C., Pereira, R. and Abdel-Maksoud, M. *"Motion Behaviour of Wind Turbine Floating Structures"* In: Proceedings on Maritime Energy 2013, COME, Hamburg, Germany, pp. 229-263

INNWIND.EU, D4.21, State-of-the-art and implementation of design tools for floating structures

11 PARTICIPATION IN THE IEA ANNEX 30 (OC4)

The International Energy Agency (IEA) Wind Annex 30 started in 2010 as a collaboration project of different companies, Universities and research institutes to investigate offshore wind turbine coupled simulations. This annex is also known as OC4 (Offshore Code Comparison Collaboration Continuation) since it is a comparison between simulations of the codes developed by the different participants and it is a continuation of the IEA Annex 23 (OC3) that took place between 2006 and 2010.

The second phase of the Annex 30 was focused on a floating platform and several of the participants in the InnWind Task 4.2 have also validated their code developments within this project. For this reason, in this chapter we are presenting a selection of the OC4 phase 2 results obtained by those InnWind partners that have taken part. Our purpose is to provide a more comprehensive view of the tools capabilities and the validation effort that have been performed.

Many of the discussions and conclusions relating the InnWind partner's simulations and codes that are presented in this chapter correspond to the analysis performed during the OC4 project within the group. Further details can be found in the papers that the OC4 group will publish along 2014 with an extensive presentation and discussion of the results provided by all the participants.

Table 11.1 shows a comparison of the capabilities of the codes developed by InnWind Task 4.2 partners that have taken part in the IEA Annex 30. Both GH and NTUA have participated with two different versions of their codes: one with a hydrodynamic model based on the Morison Equation and another one with a hydrodynamic model that combines the Potential Theory with the viscous term of the Morison Equation. CENER has participated with his dynamic mooring lines code, OPASS, coupled with NREL's code FAST. In addition, CENER has improved the FAST hydrodynamic module, including Morison's viscous term in FAST's potential hydrodynamic model. The University of Stuttgart uses the NREL's potential code called HydroDyn, including a quadratic damping in the six degrees of freedom of the platform. All the simulations have been performed with BEM aerodynamic theory, though some of the codes as hydro-GAST have other advanced aerodynamic theories available.

Acronym	Institution	Code	Structural Model	Platform model	Hydrodynamic Model	Mooring Model	Aerodynamic Model	Dynamic Stall
CENER	CENER	OPASS + FAST	Modal + MBS	Rigid	PF + ME	Dynamic	BEM	Yes
DTU	DTU	HAWC2	FEM + MBS	Flexible	ME (IW)	Dynamic	BEM	Yes
GH	GH	Bladed 4.4	Modal + MBS	Flexible	ME (IW)	Quasi-Static	BEM	Yes
GH Adv	GH	Bladed Adv Hydro Beta	Modal + MBS	Flexible	PF + ME (IW)	Quasi-Static	BEM	Yes
NTUA m	NTUA	hydro-GAST	FEM + MBS	Flexible	ME (IP)	Dynamic	BEM	Yes
NTUA p	NTUA	hydro-GAST	FEM + MBS	Rigid	PF + ME (IP)	Dynamic	BEM	Yes
SWE	SWE	SIMPACK + HydroDyn	Modal + MBS	Rigid	PF + QD	Quasi-Static	BEM	Yes

BEM: Blade Element Theory	*MBS: Multi-Body System*	*PF: Potencial Flow*	*IP: Calculation of ME at instantaneous position*
FEM: Finite Elements Method	*ME: Morison Elements*	*QD: Quadratic Drag*	*IW: Integration of ME to wave elevation*

Table 11.1: Summary of the InnWind partners Codes that took part in OC4

INNWIND.EU, D4.21, State-of-the-art and implementation of design tools for floating structures

11.1 Floating Wind Turbine Model

The platform model studied in the OC4 was developed in the DeepCWind project. It consists on a semisubmersible platform with one central column that supports the wind turbine tower and three external cylinders. At the bottom of each cylinder, there is a base cylinder of higher diameter to increase the damping in heave. The central column and the cylinders are connected through pontoons and cross members. The draft of the platform is 20m and the total mass including the ballast is **1.3473E+7 kg.**
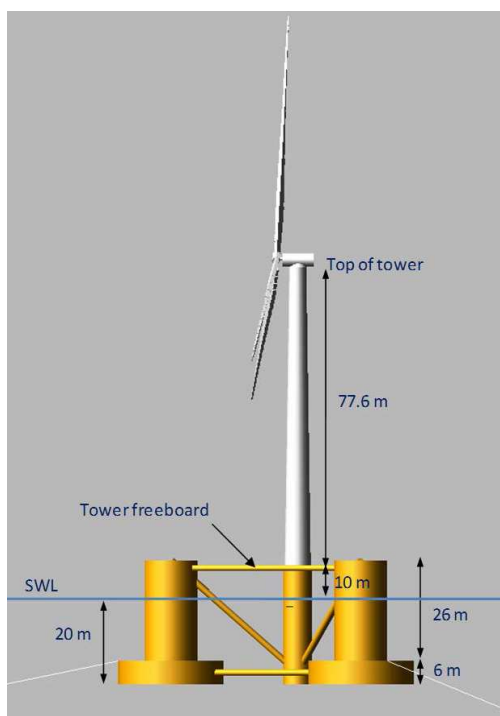

Figure 11.1: OC4-DeepCwind floating wind system design [11.3]

Some general data of the platform are gathered in the Table **11.2**. Further details can be found at [**11.1**] and [**11.3**].

Draft	20 m
Elevation of central column above MSL	10 m
Platform mass including ballast	1.3473E+7 kg
CM position below MSL	13.46 m
Roll inertia abot CM	6.827E+9 kgm2
Pitch inertia abot CM	6.827E+9 kgm2
Yaw inertia abot CM	1.226E+10 kgm2

Table 11.2: General Characteristics of the Platform

The mooring system is composed by three lines attached at the top of the base cylinders (at **14m** of draft below MSL). The location considered for the platform has a depth of 200m and the radius

INNWIND.EU, D4.21, State-of-the-art and implementation of design tools for floating structures

to the anchors from the tower centreline is 837m. The length of the lines is 835.5m. The main properties of the lines are summarized in the following table:

Angle between lines	120º
Depth of the anchors	200 m
Draft of the fairleads	14 m
Radius to Anchors from Platform Centerline	837.6 m
Radius to Fairleads from Platform Centerline	40.868 m
Line Length	835.5 m
Line diameter	0.0766 m
Line Mass Density	113.35 kg/m
Line Extensional Stiffness	7.536E+8 N
Hydrodynamic drag coefficient	1.1

Table 11.3: General Characteristics of the Mooring Lines

The wind turbine supported by the platform is the 5 MW NREL baseline model described in [11.2]. The hub height is 90 m and the diameter of the rotor is 126m.

11.2 Selected Load Cases

A set of the cases simulated in the OC4 project has been selected for the purposes of this chapter. These cases are described in Table 11.4.

Load case	Description	Initial Conditions	Enabled DOFs	Wind Conditions	Wave Conditions	Outputs
1.3a	Surge free decay	Surge = +22m	Platform + mooring	No air	Still water	Time series
1.3b	Heave free decay	Heave = +6m	Platform + mooring	No air	Still water	Time series
2.1	Deterministic waves	-	Platform + mooring	No air	Regular Airy, h=6m, T=10s	Time Series
2.6	White noise waves, no wind	-	Platform + mooring	No air	White noise PSD =1 m2/Hz for 0.05-0.25 Hz	PSD
3.2	Stochastic at rated power	-	All	Turbulent (Mann model) V = 11.4m/s	Irregular Airy (Jonswap) H_s=6m, T_p=10s, ã=2.87	PSD

Table 11.4: Description of Selected Load Cases

INNWIND.EU, D4.21, State-of-the-art and implementation of design tools for floating structures

11.3 Free Decay Cases

The load cases 1.3a and 1.3b are free decay tests in surge and heave respectively. The first one shows a good agreement in the surge natural frequency and damping between the different codes. Bladed seems to show a slight difference in the period that could be due to the differences in the mooring lines modelling.
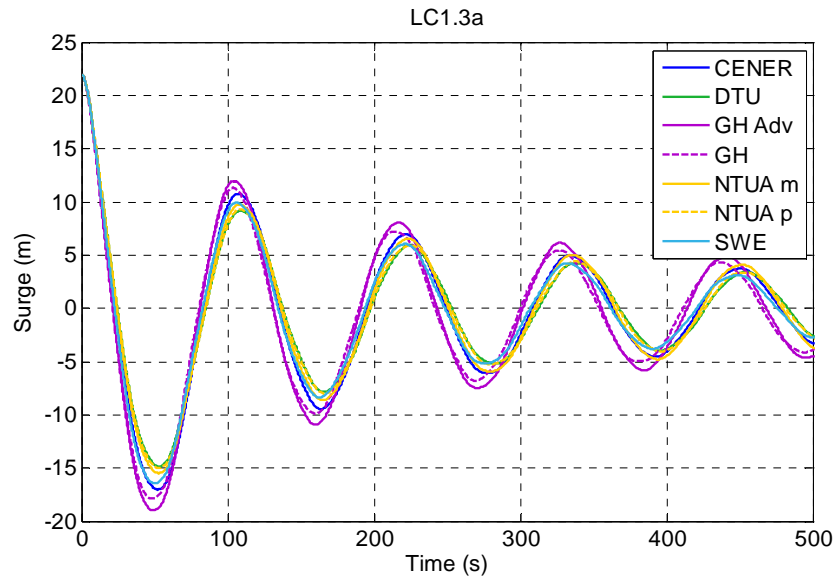

Figure 11.2: Surge displacement in case 1.3a

The 1.3a simulation shows a coupling between the surge and the heave degrees of freedom. Heave is excited during the surge free decay test. The responses in heave of the different codes appear grouped depending on the mooring lines model (dynamic or quasi-static), in particular at the beginning of the simulation.
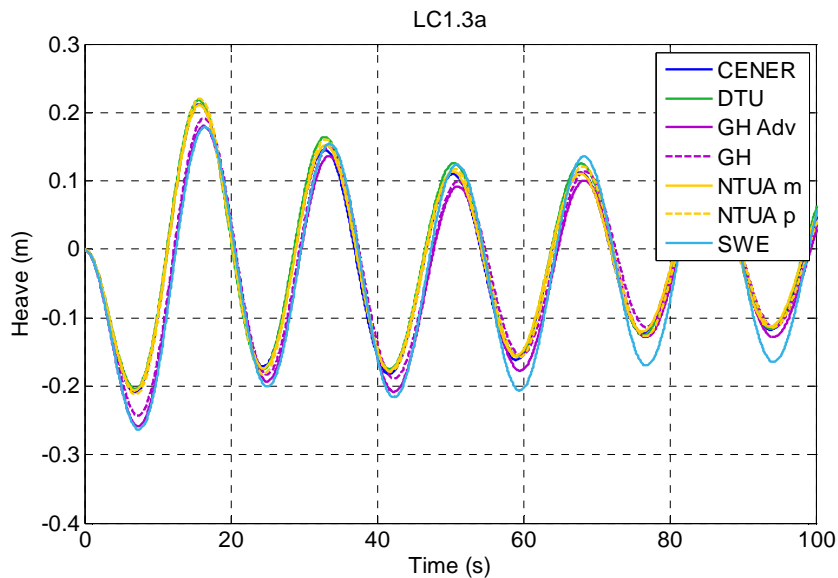
Figure 11.3: Heave displacement in case 1.3a

Relating the heave free decay (load case 1.3b), all the codes show a very similar response, both in the natural period and the damping as it is shown in Figure 11.4:

INNWIND.EU, D4.21, State-of-the-art and implementation of design tools for floating structures
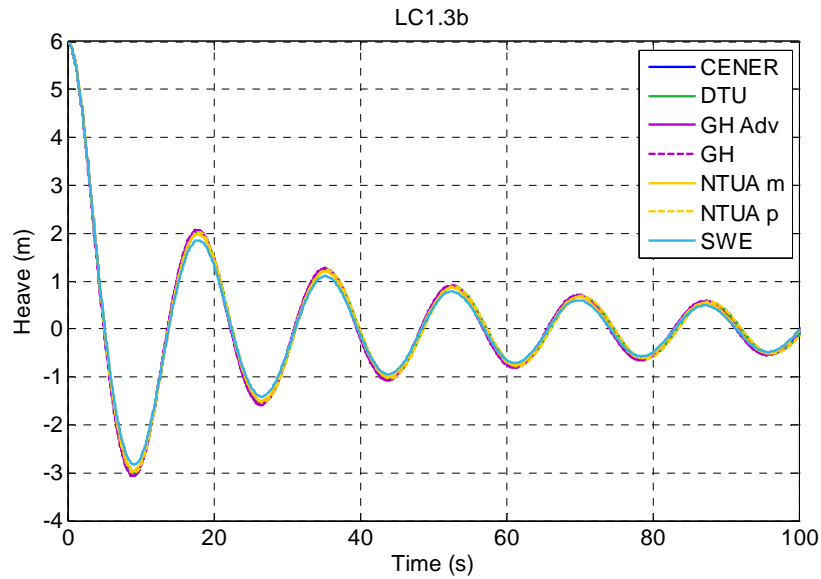
Figure 11.4: Heave displacement in case 1.3b

During the heave free decay, the coupling with the platform pitch is less damped in the SWE simulation that use quadratic damping. This kind of damping has not off-diagonal elements that could couple the heave displacement with the pitch damping. Nevertheless, the effect over the pitch degree of freedom has not a high importance.
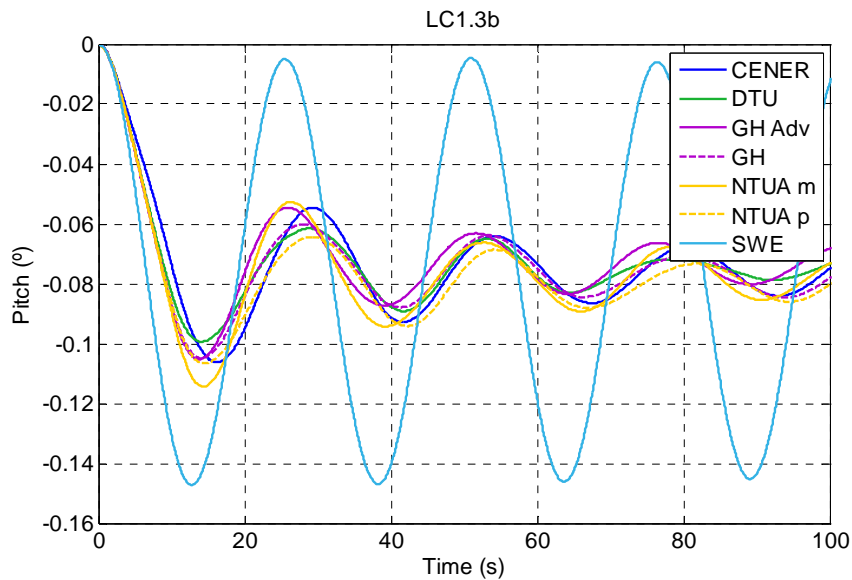
Figure 11.5: Platform pitch displacement in case 1.3b

11.4 Regular waves

Load case 2.1 analyzes the platform behaviour under a regular wave of height 6m and period 10s. No wind is considered. In this case, the codes show differences in the mean surge position due to the method applied to calculate the forces in the Morison elements. Garrad Hassan calculates the hydrodynamic force over the Morison elements considering the instantaneous wave height. This

INNWIND.EU, D4.21, State-of-the-art and implementation of design tools for floating structures

seems to have an important effect over the GH simulation, which is based only in Morison, and less importance in the GH Adv simulation, where the wave loading calculation is based on potential theory and the Morison equation is only applied to estimate the viscous component.
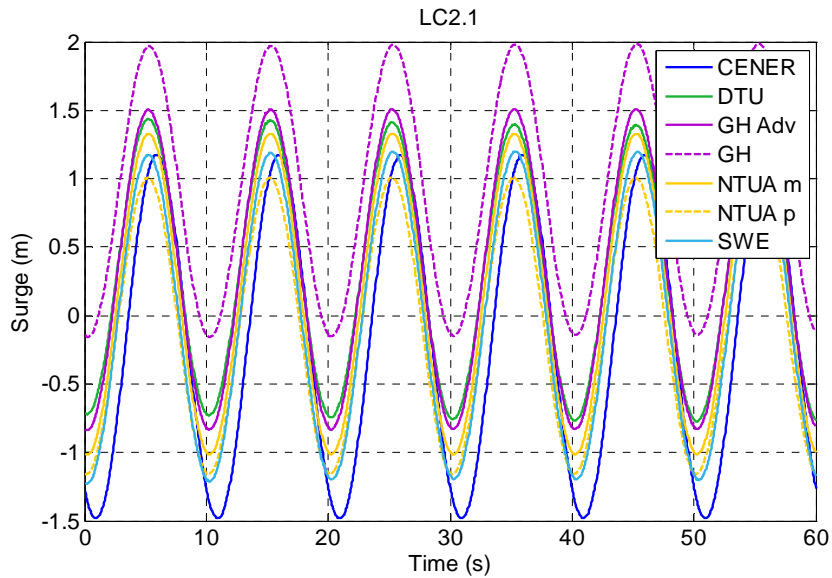
Figure 11.6: Surge displacement in case 2.1

Important differences appear when looking to the fairlead tension of the line aligned with the waves. As can be observed in Figure 11.7, there is a difference in the phase between the models with dynamic and quasi-static mooring models. In addition, dynamic models provide higher tension than quasi-static, though these differences has not a great influence over the global motions of the platform.
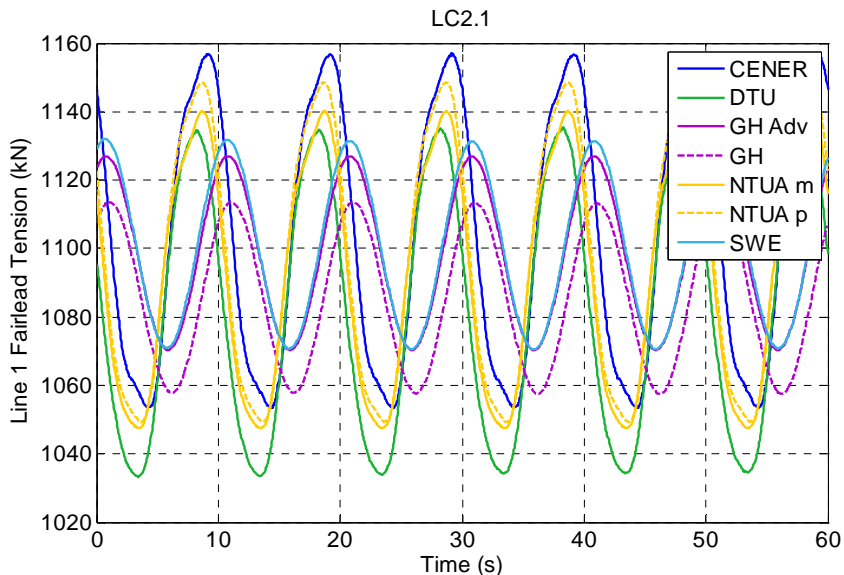

Figure 11.7: Fairlead tension in case 2.1

INNWIND.EU, D4.21, State-of-the-art and implementation of design tools for floating structures

11.5 White noise wave spectrum

In the load case 2.6, the wave spectrum is white noise with a power spectral density (PSD) of 1 m2/Hz between the frequencies 0.05 and 0.25 Hz. No wind is considered.

The codes show a good agreement in the wave excitation range of frequencies. The response at the surge natural frequency is around 0.009 Hz, out of the wave excitation range, and thus it is activated by nonlinearities, showing certain dispersion.
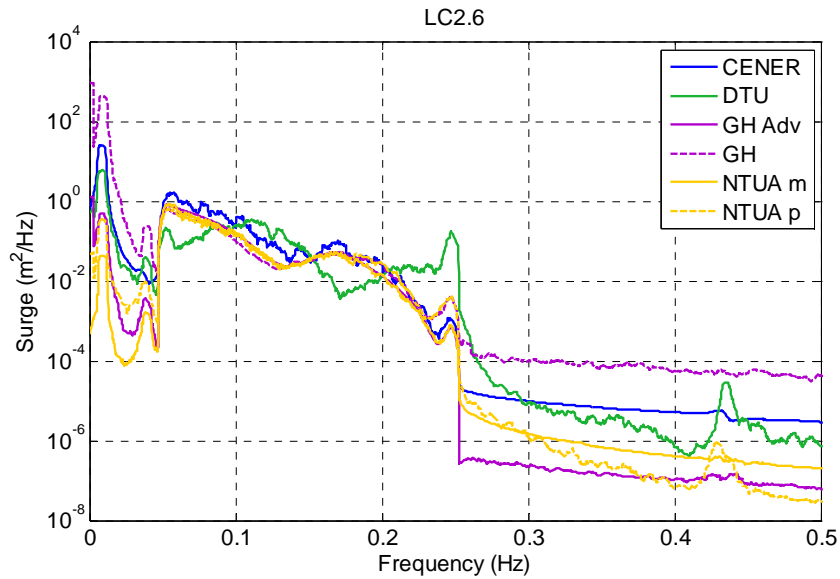
**Figure 11.8: PSD of surge displacement in case 2.6**

The platform's heave natural frequency is 0.058 Hz, and it is located within the white noise frequency range. The response of the different codes at this frequency is very similar (Figure 11.9).
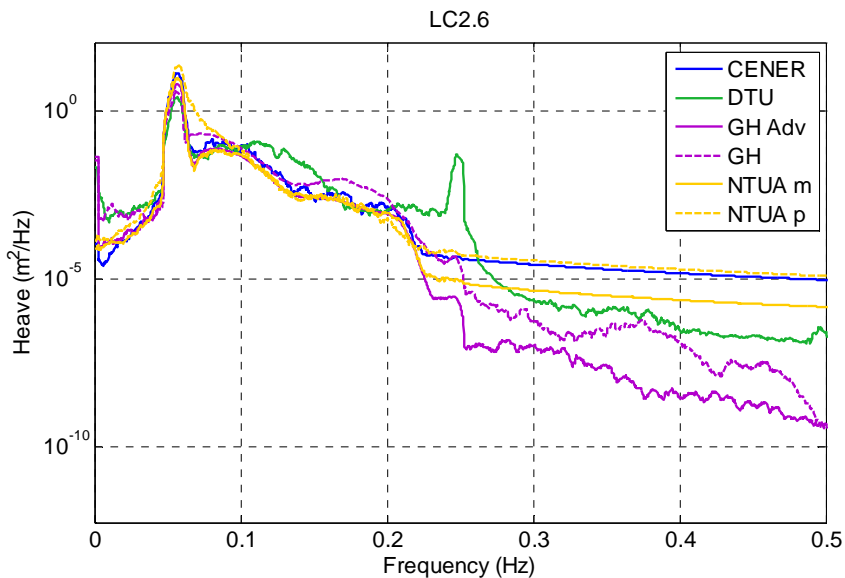
Figure 11.9: PSD of heave displacement in case 2.6

INNWIND.EU, D4.21, State-of-the-art and implementation of design tools for floating structures

If we look to the mooring line tension, a clear difference between the dynamic models and the quasi-static models appear, with the dynamic models (CENER, DTU, NTUA m and NTUA p) showing a much higher response within the wave excitation range.
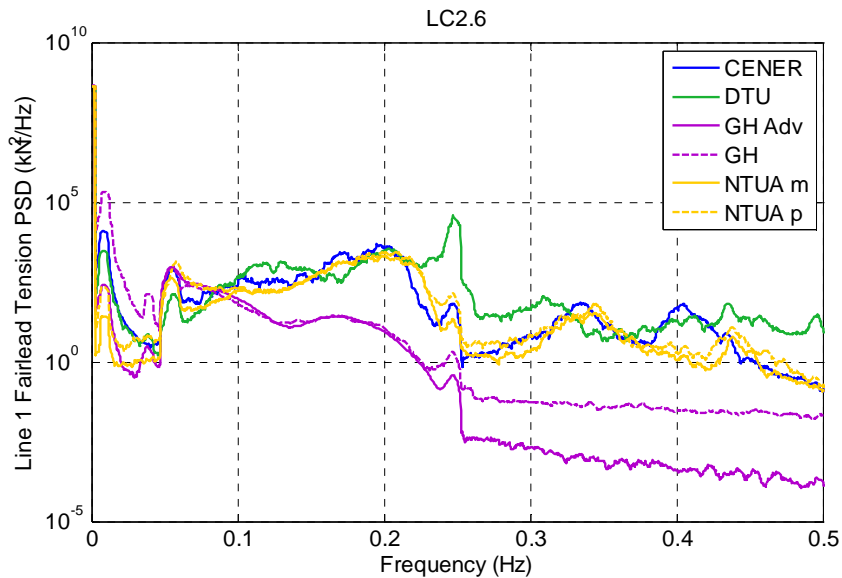
**Figure 11.10: PSD of fairlead tension in case 2.6**

11.6 Stochastic wind and waves

In the load case 3.2 both irregular waves and turbulent wind are acting over the platform. The average wind speed is 11.4m/s, which corresponds to the rated speed and the turbulence follows the Mann model. The irregular waves have been calculated according to the Jonswap spectrum with Hs=6m, Tp=10s and γ=2.87. In this case all the flexibility degrees of freedom of the wind turbine have been activated.

The responses of the blade in the in plane direction predicted by all the codes are very similar (Figure 11.11). The main peak in the blade in plane deflection PSD corresponds to the 1P excitation frequency (around 0.2Hz). Lower peaks can be observed at the tower natural frequency (0.42Hz) and the 3P frequency. A certain excitation at the wave peak frequency (0.1Hz) is present. There is also an important peak that corresponds to the edgewise blade natural frequency, that is located by most of the codes at 1.08Hz and at a bit lower frequency (around 1Hz) by DTU.

INNWIND.EU, D4.21, State-of-the-art and implementation of design tools for floating structures
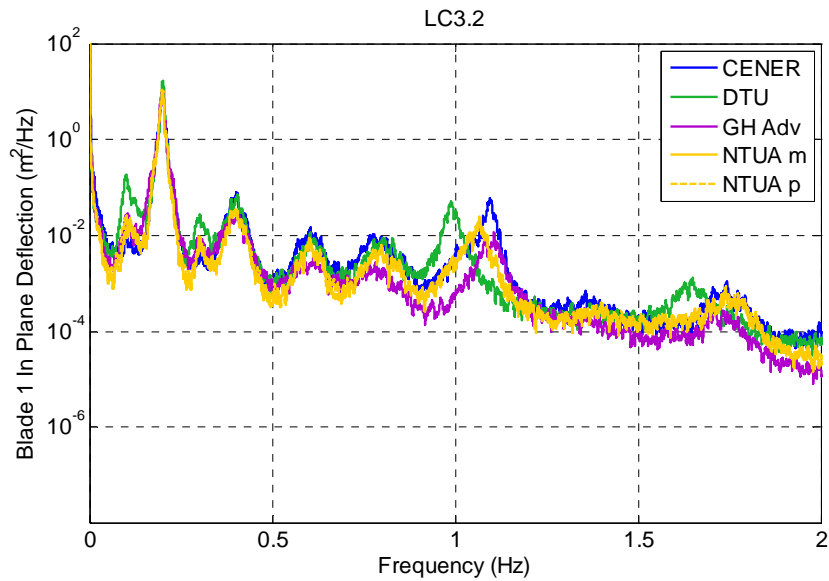
Figure 11.11: PSD of blade in plane deflection in case 3.2

Relating the response of the blade in the out of plane direction, the agreement is also good (see Figure 11.12). The main responses arise at the wave peak frequency (especially for the DTU simulation) and the 1P excitation frequency. There are also important responses at the tower natural frequency (0.42Hz), 3P (0.6Hz) and the blade out of plane natural frequency (0.7Hz).
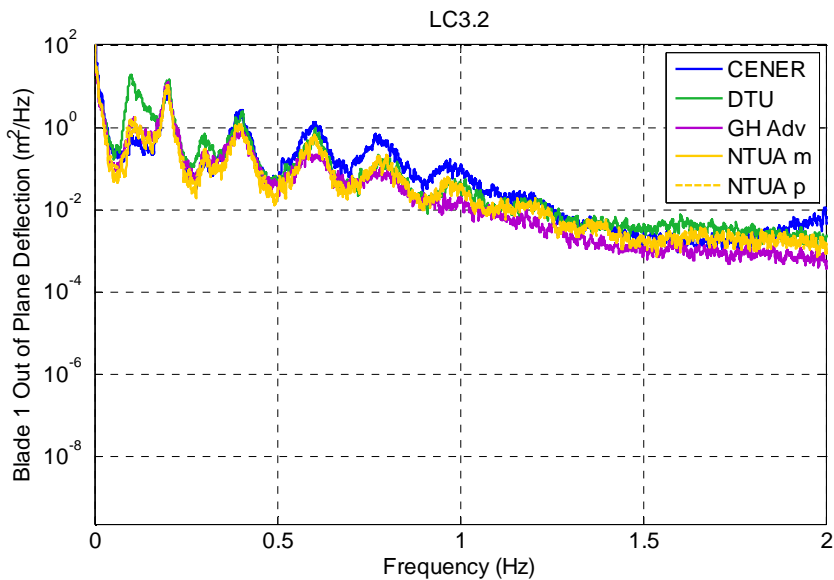
Figure 11.12: PSD of blade out of plane deflection in case 3.2

11.7 Summary of the Partners Participation on the OC4

In general, the results provided within OC4 by the different codes that are developed by the InnWind Task 4.2 partners show a good agreement and the differences in the simulations can be addressed by the different modelling theories implemented.

INNWIND.EU, D4.21, State-of-the-art and implementation of design tools for floating structures

The work developed during the IEA Annex 30 provided a very extensive validation of the codes. The comparison of the simulations and the discussion within the group allowed the developers to improve their tools, to detect bugs and to identify future lines of development and research.

11.8 References

[11.1] Goupee, A.J., Koo, B.J., Lamrakos, K.F. & Kimball, R. *"Offshore Wind Energy: Model Tests for Three Floating Wind Turbine Concepts"* In: Proceedings of the Offshore Technical Conference. Houston, TX, 2012.

[11.2] Jonkman, J. *"Definition of the Floating System for Phase IV of OC3"* National Renewable Energy Laboratory, 2010.

[11.3] Robertson, A., Jonkman, J., Musial, W., Vorpahl F. and Popko, W., *"Offshore Code Comparison Collaboration, Continuation: Phase II Results of a Floating Semisubmersible Wind System"* In: Proceedings of the EWEA Offshore 2013, Frankfurt.

INNWIND.EU, D4.21, State-of-the-art and implementation of design tools for floating structures

12 CONCLUSIONS

Different tools for the analysis and simulation of floating offshore wind turbines have been presented in this document. These tools are currently under development by the different participants in the task. The partners have documented the state of development of the codes, describing the fundamentals of the physical approach that have been applied, the current capabilities of the codes, the future lines of research and development and some cases of verification of the results against available data, together with a few examples of application of the codes to particular problems.

The nature of the software gathered in this report is diverse: some tools are integrated codes for the analysis of the whole floating wind turbine system and others are focuses on the mooring lines dynamics, the rotor aerodynamics or the platform hydrodynamics. In addition, the tools address the different modelling problems with different levels of complexity. For instance, the rotor aerodynamics is modelled with such different theories as BEM, free vortex wake or CFD and something similar happens with the platform hydrodynamics, where Morison equation, potential theory or CFD have been applied.

This report documents the state of development of the tools before starting the validation against experimental data. As have been shown in the report, the tools are in an advanced state of development and have already been verified. Thus, the experimental validation is the natural next step that will increase the confidence and reliability of the codes, providing to the designers the means to achieve more cost-effective designs.

The exercise that has been performed within this deliverable of describing the type of codes, the different problems analyzed and the different approaches will provide very valuable information for the definition of the test campaign that will be carried out in this task 4.2. This information will guide the design of the testing cases improving the effectiveness of the testing campaign in order to validate the codes.

The work developed in the IEA Annex 30 by the partners of the InnWind Task 4.2 has being summarized. It has been shown that the results provided within OC4 by the codes under development in InnWind showed a good agreement and the differences in the simulations can be addressed to the different modelling theories implemented. The work developed during the IEA Annex 30 provided a very extensive validation of the codes and was very useful for the improvement of the tools.

Finally, the different theories implemented and the diverse levels of complexity of the tools will provide interesting conclusions, when compared with experimental data, about the accuracy of the modelling approaches and points were further research and development is necessary.

INNWIND.EU, D4.21, State-of-the-art and implementation of design tools for floating structures